JPL Quarterly Technical Review

Volume 3 July 1973 Number 2

Contents

Bibliography of Current Reporting

JPL Quarterly Technical Review Volume 3, Number 2 July 1973

Index: computer applications and equipment, computer programs, control and guidance, electronic components and circuits, Mariner Jupiter/Saturn 1977 Project

The Development and Demonstration of Hybrid Programable Attitude Control Electronics

L. S. Smith and E. H. Kopf, Jr.

Guidance and Control Division

In the course of Extended Life Attitude Control System (ELACS) research sponsored by the NASA Office of Advanced Space Technology (Research Electronics), a Hybrid Programable Attitude Control Electronics (HYPACE) concept was developed and demonstrated. The wide variety of future planetary missions demanded a new control approach to accommodate the automatic fault tolerance and long-life requirements of such missions. HYPACE provides an adaptable, analog/digital design approach that permits preflight and in-flight accommodation of mission changes, component performance variations, spacecraft changes, etc., through programing. This enabled broad multimission flexibility of application in a cost-effective manner. Previously, flight control computers have not been flown on planetary missions because of weight and power problems. These problems were resolved in the design of HYPACE. The HYPACE design, which was demonstrated in breadboard form on a single-axis gas-bearing spacecraft simulation, uses a single control channel to perform the attitude control functions sequentially, thus significantly reducing the number of component parts over hard-wired designs. The success of this effort resulted in the concept being selected for the Mariner Jupiter/Saturn 1977 spacecraft application.

Introduction

Customarily, JPL-designed spacecraft attitude has been controlled by hard-wired analog techniques because of the need to achieve low weight and power usage. These techniques resulted in inflexible designs, sized to the mission-peculiar characteristics of each spacecraft. Hardware had to be resized and reconfigured to accommodate new missions, requiring costly and significant changes. With the advent of more complex missions such as outer planet flybys and orbiters, atmosphere probes, landers, sample and return, and comet or asteroid rendezvous, the need for mission-independent control techniques became more evident. For example, the vehicle configurations require a variety of propulsion systems such as solids, liquids, or electric propulsion, each requiring the implementation of unique control laws. This need set the stage for the design, breadboarding, and demonstration of the

Hybrid Programable Attitude Control Electronics (HYPACE), configured for a single-axis gas-bearing spacecraft simulator facility. The single-axis gas-bearing spacecraft simulator provided a unique test bed in that it is the closest possible hardware facsimile to an actual spacecraft. The task was accomplished under the sponsorship of a Research and Technology Operating Plan funded by NASA OAST entitled "Extended Life Attitude Control System (ELACS) for Unmanned Planetary Vehicles," during the fiscal years 1972 and 1973. The primary goal of the HYPACE task culminated in demonstrations of the workability and practicality of such a control system concept. In the achievement of this goal, a number of specific tasks were undertaken. The specific task requirements were as follows:

(1) Adapt an existing simulation facility to HYPACE requirements.

(2) Size and define the programmable processor speed, memory, and instrumentation capability.

(3) Design processor logical hardware for repertoire requirements.

(4) Develop a HYPACE software assembly program.

(5) Configure the control console to interface an input-output typewriter with HYPACE telemetry data.

(6) Develop a HYPACE software package to demonstrate the attitude control functions of a typical spacecraft mission.

(7) Configure a communication channel to handle off-table as well as on-table data.

(8) Interface the input sensing and output loads to the HYPACE data management system.

(9) Configure the control console to decommutate multiplexed direct access monitoring data from the table to the control console discrete displays.

(10) Configure the control console to communicate in spacecraft fashion from either manual switches, a card reader, and/or a typewriter.

HYPACE Description

The single-axis gas-bearing spacecraft simulator facility had been developed during a prior program for the development of a hard-wired processor (Refs. 1 and 2). In addition to the simulation platform, the following peripheral hardware was available: true position incremental encoder, solar simulator, dry nitrogen gas system, battery chargers, and reference autocollimator. Also acquired for the HYPACE buildup were an incremental gas-bearing gyro, a digital Sun sensor, a 180-deg Sun acquisition sensor, a reaction wheel, nickel cadmium batteries, and various power conditioners. (Had other peripheral hardware been available for integration with HYPACE, the configuration was adaptable to its incorporation.) Some of these items are shown in Fig. 1, in addition to the HYPACE memory, processor, and ancillary hardware. The simplified block diagram of Fig. 2 illustrates the functional interconnection of the various elements comprising the HYPACE test facility.

The memory is a commercially produced plated wire memory having 4096 words of 18-bit length. The processor and ancillary hardware was designed to use exclusively low-power transistor-transistor logic (TTL) to the medium-scale integration (MSI) level. The processor is serial-byte organized with 4-bit bytes and has an instruction repertoire of 32 instructions, of which 14 are indexible. An index register was incorporated in the design such that one software routine could be used for all three axes. The index register keeps track of the pertinent data block of the axis being processed. This approach greatly simplified the configuration and allowed a minimum memory size to accomplish three-axis control. The shift rate is 607.5 kHz, which yields an add instruction time of 28 μs. An interrupt responsive phasing sequence is incorporated with no established service priority. Each interrupt is fully serviced before return to normal processing or unmasking occurs.

The attitude control subsystem, while very analog in nature, must as well be responsive to and generate discrete single events (called flags). HYPACE was designed to fully satisfy this requirement. Four types of flags are handled by the design. The most basic single event is the loss of power. This event unconditionally freezes the system into an inactive mode so that no control functions can occur and the memory cannot be changed. Software routines are used to determine that such an event has occurred and bring the system back into an operational mode when power is again available.

Timing signals are flags to which HYPACE's activity can be slaved. These flags cause the processing to be interrupted so that a transfer occurs to another processing routine and the point of interruption is stored for later return. This flag activity causes an immediate masking so that no subsequent interrupt routine can be initiated until a return from the existing routine occurs. These interrupts are sorted by software steps to their respective routines.

The remaining two flag types are for software-monitored (or input) flags and software-generated (or output) flags. Input flags are stored when generated; subsequently under software control they are monitored for occurrence. Output flags are generated and terminated by software instructions. For added flexibility all flags are under software control such that they can be set to a desired state. One input flag has uniquely been used to allow software masking of the interrupts; consequently, some higher-priority event could be used to overcome a software interrupt mask. This HYPACE design has eight interrupt flags, 12 input flags and 20 output flags.

System Interfaces

The sensor and actuator hardware used with HYPACE (the design was configured to interface with anything available) is representative of both

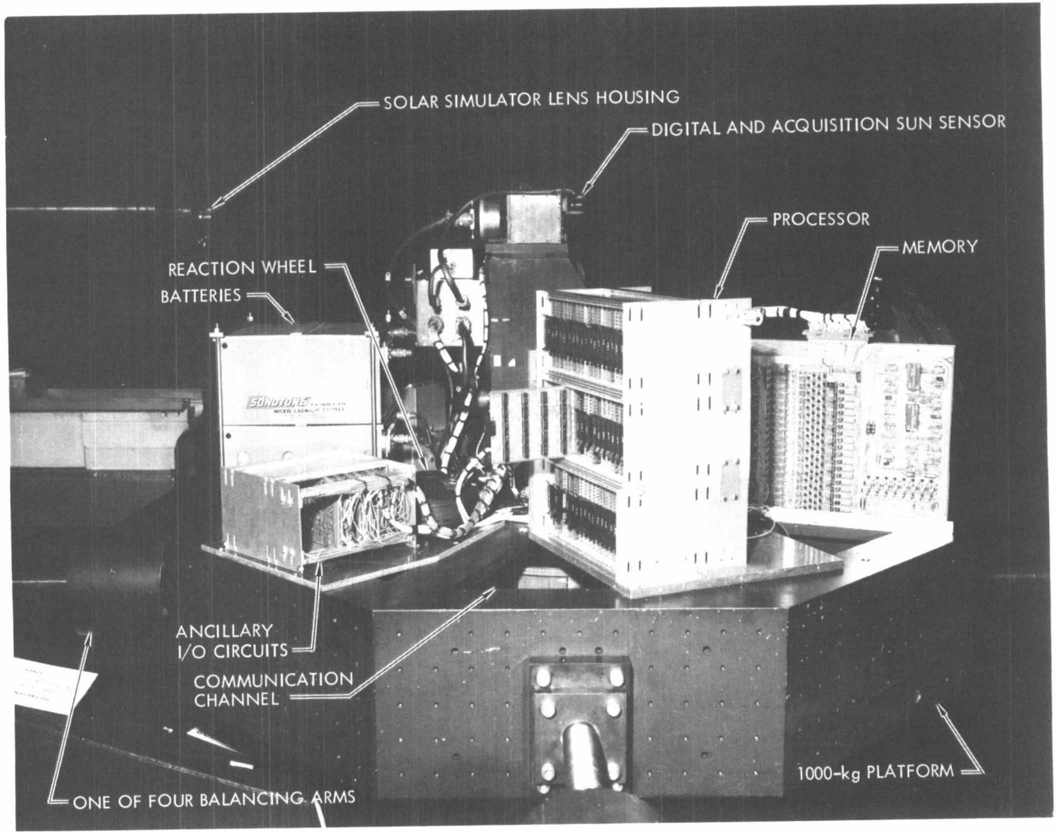

Fig. 1. Single-axis gas-bearing spacecraft simulator platform

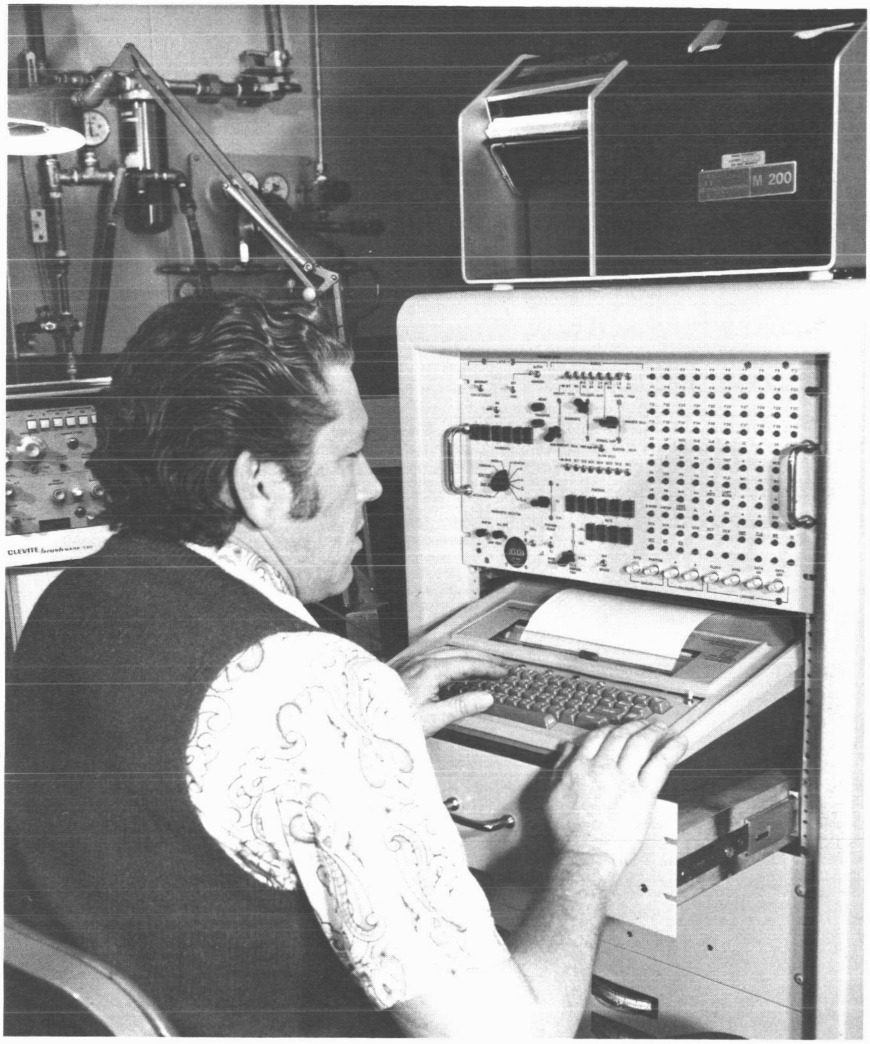

Fig. 2. HYPACE control console

analog and digital interface disciplines. An 8-bit grey coded digital Sun sensor is used to monitor platform motions as small as 0.025 deg over a range of ±3.2 deg. This Sun sensor's field-of-view (FOV) is centrally located in the centrally shadow-masked region of a cadmium sulfide cell pair 180-deg-FOV acquisition Sun sensor. An incremental gas bearing gyro is used which has 0.001 deg resolution. The actuators are a two-phase reaction wheel motor and two opposing dry nitrogen solenoid-actuated thrusters.

Facility Description

The single-axis simulator facility was designed as an attitude control test platform which accurately simulates the rigid-body actions and interactions of a real spacecraft. The gas bearing, designed for hydrostatic operation, is adequate for operation in a nonevacuated chamber (Ref. 3). The 150- to 3000-dyne-cm residual torque level achieved is within the limits of actual spacecraft environment. The HYPACE application communicates with remote support equipment over four 250-MHz bandwidth noncontacting channels in a manner simulating an actual spacecraft interface (Ref. 4). Power is provided by four 22-A-h, 24.5-V rechargeable nickel-cadmium batteries mounted on the platform.

Rotational motion of the platform is monitored by a quadrature incremental optical encoder mounted on the bottom end of the gas-bearing armature (Ref. 5). Decimal readouts of position and rate are available at the support equipment console, and analog signals of the same are available for XY or strip chart recording. Since platform motions are very difficult to visually monitor, a laser pointer was used, projecting a 12-m (40-ft) beam to a wall to amplify the motion. Platform rotation of 0.01 deg yields a laser spot movement of approximately 2.54 cm (1 in.) on the wall.

Integral to the gas-bearing stator is a solar simulator. This device provides a 12.7-cm-diam (5-in.-diam) collimated light beam that simulates the Sun as seen at Earth and, in steps, as seen as far as 30 AU. This allowed demonstrations to be conducted which were representative of environments encountered in the far reaches of the outer planets.

Peripheral support equipment unique to the gas-bearing platform comprises (1) battery chargers that can be used in lieu of batteries during static tests, (2) a booster pump that uses shop air power to boost the bearing dry nitrogen supply gauge pressure of 1.38×10^6 N/m^2 to 1.38×10^7 N/m^2 (200 to 2000 psi), thus filling four spherical chambers on the platform that supply the thrusters, and (3) a solenoid-actuated brake for stilling the platform motion when needed. Additionally, the platform has four threaded horizontal arms on two perpendicular axes which have weights that are used to balance the platform. When the platform is being balanced, the platform-stator structure is tilted 2 deg to amplify the unbalance torques.

The Control Console

The control console (Fig. 3) establishes the man-machine interface for operational procedures and diagnostic assessment of system performance. The control console design was configured to simulate the equivalent of a radio link with an actual spacecraft. Standard TTL devices to the MSI level were used in the console logic. The high speed of the data communication channels required the use of high-speed Schottky TTL devices in the console and table data circuits.

The card reader signals, typewriter keyboard signals, and console switch positions are conditioned by the console to a representative spacecraft command format. This data format is time-multiplexed to be coupled onto the table over two data channels and one reference channel. On the table, the multiplexed data is effectively decommutated to the proper format for HYPACE response. A third data channel on the table is used for off-table multiplexed data that contains telemetry and HYPACE direct-access monitoring data. This off-table data is decommutated into the console discrete displays and typewriter printout. Additional diagnostic circuits were designed into the HYPACE simulator complex to permit operator takeover of the HYPACE operation on an operator-actuated basis. This capability afforded any troubleshooting effort a very powerful tool.

Software Development

The software package developed to demonstrate the HYPACE system consists of about 1500 instructions and 600 words of data. A software digital equivalent of an analog estimator control algorithm was used in the foreground program for the attitude control functions of acquisition, cruise, commanded turn, and inertial hold. The foreground program was framed at 100-ms intervals and effectively was completed in 7 ms. The remaining time was dedicated to a background program that serviced housekeeping functions such as updating telemetry data, memory refresh, or noncritical interrupts.

Two documents that support the software phase of the effort have been released. The "HYPACE Processing Unit Reference Manual" describes the operation and organization of the processor (Ref. 6). The arithmetic, logic and input/output data management of the instruction repertoire are detailed to the level of an analyst/programmer's need. The second document, "HYPACE Assembly Language Assembler Reference Manual" (Ref. 7), describes how HYPACE software can be symbolically written to interface with a Univac 1108 program that has been designed to assemble a HYPACE program and punch cards in the HYPACE format. As formatted, a deck of less than 400 punched cards can fully load the 4096-word memory.

Demonstration Results

The HYPACE demonstration verified the adequacy of the prototype software package as well as the operable performance of the processor,

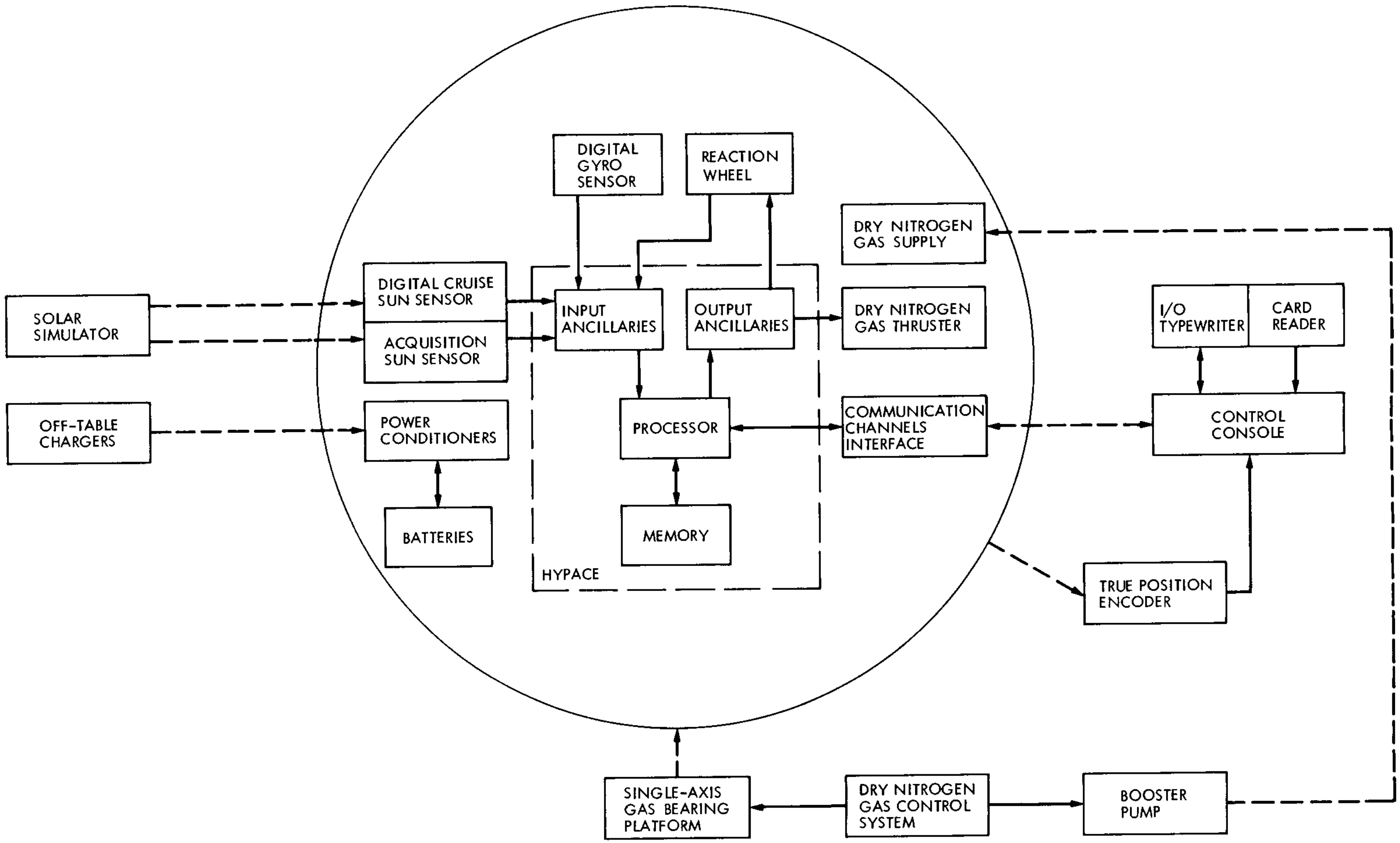

Fig. 3. Single-axis simulator HYPACE configuration

memory, and input/output circuits. The control console man–machine interfaces provided the operator with the interactive tool necessary to assess system performance. As an example, the subsystem would be remotely commanded to acquire the Sun. During the acquisition the operator could monitor relevant data being used by the processor, e.g., the acquisition Sun sensor signal or gyro readout, which allowed tracking of the software algorithm performance. This technique yielded excellent results. As an example, the acquisition rate as measured by the true position encoder readout and as indicated by the gyro readout agreed closely with the programmed rate of 0.16 degrees per second.

Although quantitative study and optimization of performance have not been accomplished to date, the qualitative results were a very satisfactory basis for performance assessment. These results proved the performance demanded of HYPACE for planetary missions had indeed been accomplished. The laser pointer when visually monitored yielded fine resolution that supported the assessment and demonstration of the system performance. Acquisition and commanded turn operations were executed and observed to have little or no overshoot. The fine deadband cruise and inertial hold operations were observed to maintain position within a 0.050-deg envelope that increased 10% during the reaction wheel software dumping routine. The corresponding wide deadband cruise and inertial hold operations yielded similar results with a 0.5-deg envelope. The wide deadband operation was designed to maintain attitude with gas jets only, thereby minimizing gas consumption and reducing reaction wheel bearing wear. This performance is similar to that planned for the Mariner Jupiter/Saturn mission.

The software package was also configured to cause automatic actions under certain adverse conditions. One demonstrated automatic action is the transfer from the acquisition to the cruise control algorithm. Here the acquisition algorithm rate and position estimates are software-monitored until they fall within prescribed limits, at which time the cruise algorithm is placed in control. A related action is the simulated turnoff of the gyro 45 s after cruise activation. Another demonstrated automatic software feature is the reverse of the above. Should the system be in the cruise or inertial hold modes and the estimates of rate and/or position exceed prescribed limits, the system will revert to an algorithm that is designed to optimally return to the point where the limits had been exceeded. This corresponds to a simulation of the spacecraft being struck by a high-speed particle, usually demonstrated by striking the table with one's hand. This software automatic response is vital to the control of the spacecraft because of the very long ground-link communication times of outer planet missions.

Relevant to the demonstration of the HYPACE concept was the troubleshooting buildup phase of the activity. During this activity, a quantitative assessment of the processor performance was aided by the processor itself. Repeated software routines were run that exercised a circuit or circuits repeatedly such that signals could be easily observed, measured, and/or coordinated with predicted results. A listing of these routines is beyond the scope of this article. It is sufficient to state that propagation delays, instruction times, memory contents, input/output interfaces, etc., were verified by this method.

Conclusions

The HYPACE support equipment and single-axis simulation facilities involved assembling approximately 1150 discrete components and 1200 integrated circuits. The effort up to the point of a fully operational system occupied a time span of approximately 14 months. Initial demonstrations yielded performance that exceeded expectations. The demonstrations confirmed the viability and practicality of the hardware and software designs. All requirements demanded of the development were met—low power, low weight, programability in a near-real simulation. As a direct result of the progress made on the ELACS program, the Mariner Jupiter/Saturn 1977 flight project selected the HYPACE concept for the attitude and articulation control subsystem baseline.

References

1. Smith, L. S., "Single-Axis Simulation Test Report," Engineering Memorandum 344-356, Jet Propulsion Laboratory, Pasadena, Calif., Aug. 16, 1971 (JPL internal document).
2. *Thermoelectric Outer Planets Spacecraft (TOPS) Advanced Systems Technology Project Final Report*, Technical Memorandum 33-589, Jet Propulsion Laboratory, Pasadena, Calif., Apr. 1, 1973.
3. Ferrera, J. D., and Perkins, G. S., "TOPS Attitude-Control Single-Axis Simulator," in *Supporting Research and Advanced Development*, Space Programs Summary 37-65, Vol. III, pp. 118–119, Jet Propulsion Laboratory, Pasadena, Calif., Oct. 31, 1970.
4. Smith, L. S., "TOPS Attitude-Control Single-Axis Simulator Command Telemetry Link," in *Supporting Research and Advanced Development*, Space Programs Summary 37-64, Vol. III, pp. 74–75, Jet Propulsion Laboratory, Pasadena, Calif., Aug. 31, 1970.
5. Goss, W. D., and Smith, L. S., "TOPS Attitude-Control Single-Axis Simulator True Position Encoder," in *Supporting Research and Advanced Development*, Space Programs Summary 37-65, Vol. III, pp. 119–121, Jet Propulsion Laboratory, Pasadena, Calif., Oct. 31, 1970.
6. Kopf, E. H., "The HYPACE Processing Unit," Engineering Memorandum 344-369, Jet Propulsion Laboratory, Pasadena, Calif., Feb. 2, 1972 (JPL internal document).
7. Kopf, E. H., "The HYPACE Assembly Language Reference Manual," Engineering Memorandum 344-374, Jet Propulsion Laboratory, Pasadena, Calif., Apr. 3, 1972 (JPL internal document).

JPL Quarterly Technical Review Volume 3, Number 2 July 1973

Index: computer applications and equipment, computer programs, mechanics, test facilities and equipment

Induced Shock Pulse Testing by Transient Waveform Control

B. K. Kim

Applied Mechanics Division

A method of synthesizing an arbitrarily shaped transient time pulse on vibration exciters is described. The transient waveform control technique is based on recent developments in digital time series analysis, the real-time FFT processor. A brief description of the theory, error estimates, and hardware/software implementation to the JPL Dynamic Environmental Testing Laboratory is presented.

Introduction

Induced environmental testing at JPL is primarily that of random noise, sinewave, and shock excitation. Subsystem shock tests are performed on electrodynamic shaker systems or on special-purpose shock testing machines. Generating a shock pulse on an electrodynamic shaker can be controlled to a given shock spectrum using a shock pulse synthesizer and shock spectrum analyzer. The main concern with this method is the process of obtaining the shock spectrum specification. The single-degree-of-freedom linear model assumption, proper Q assumption and damage potential with respect to the resonance behavior may be hard to justify for a given specimen. The other shock testing machines are controlled to a given time history. However, they are limited to specific time profiles such as terminal peak sawtooth, half-sine, square wave, etc. The results of the test using these special machines can, of course, be displayed in the form of a shock spectrum or a time history.

With this much background, it became increasingly desirable to be able to deliver arbitrarily shaped transient time pulse to a test specimen with good controllability and repeatability. With the advances of real-time fast Fourier transform (FFT) processors, it seemed natural to combine existing shaker systems with FFT processors (Ref. 1). In fact, recent experiments with digitally controlled random vibration testing have demonstrated the capabilities of coupling a FFT processor and a special-purpose minicomputer with existing shaker-amplifier systems (Refs. 2, 3). The present work of transient waveform control (TWC) focuses on an electrodynamic shaker as the means of excitation and controlling to a given time history waveform using a FFT processor and minicomputer system. The idea of waveform control is not new (Ref. 4). However, in the past it was performed with analog devices such as waveform synthesizers. This left the waveform control testing highly susceptible to human errors, poor controllability, and poor repeatability. The first implementation of TWC using digital devices was proposed by Favour, LeBrun and Young of Boeing in 1969 (Ref. 5).

The purpose of this paper is to describe the first successful implementation of TWC at JPL, utilizing the JPL experimental digital vibration control system (Fourier processor, minicomputer, and environmental laboratory amplifier and shaker systems). The physical layout of the hardware including the test article is shown on Fig. 1. A conversational TWC computer program was written in assembly language and is ready for real-time transient environmental shock testing. A description of the TWC JPL technique is presented below and an example test is discussed. A simplified flow chart of the software program is illustrated in Fig. 2.

Analysis

The main theory behind the TWC process is that of computing an instantaneous transfer function experimentally, assuming linearity of the system. It is most crucial to obtain a meaningful transfer function within the dynamic range of the digital equipment. In order to guarantee the full

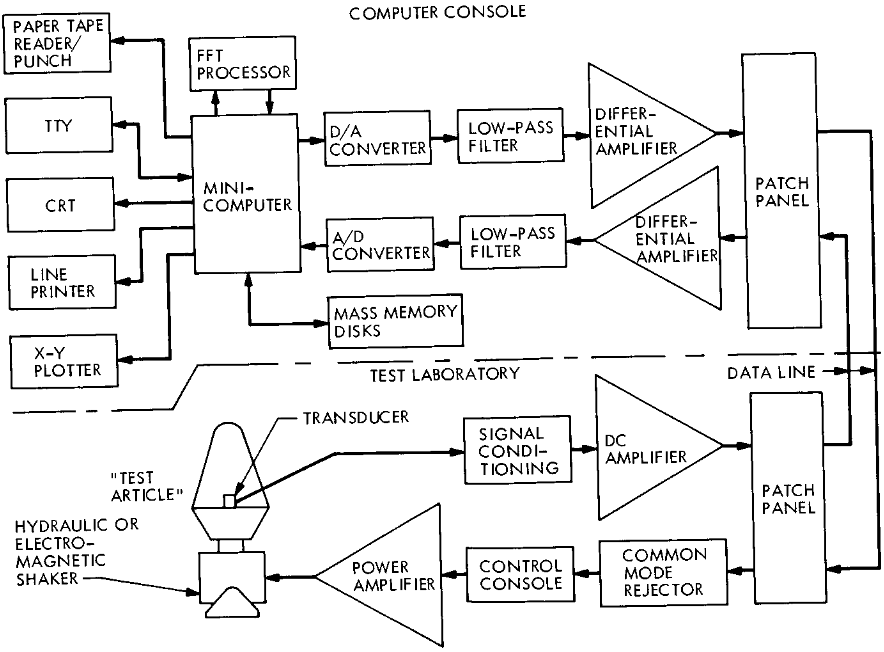

Fig. 1. Transient waveform control, functional hardware block diagram

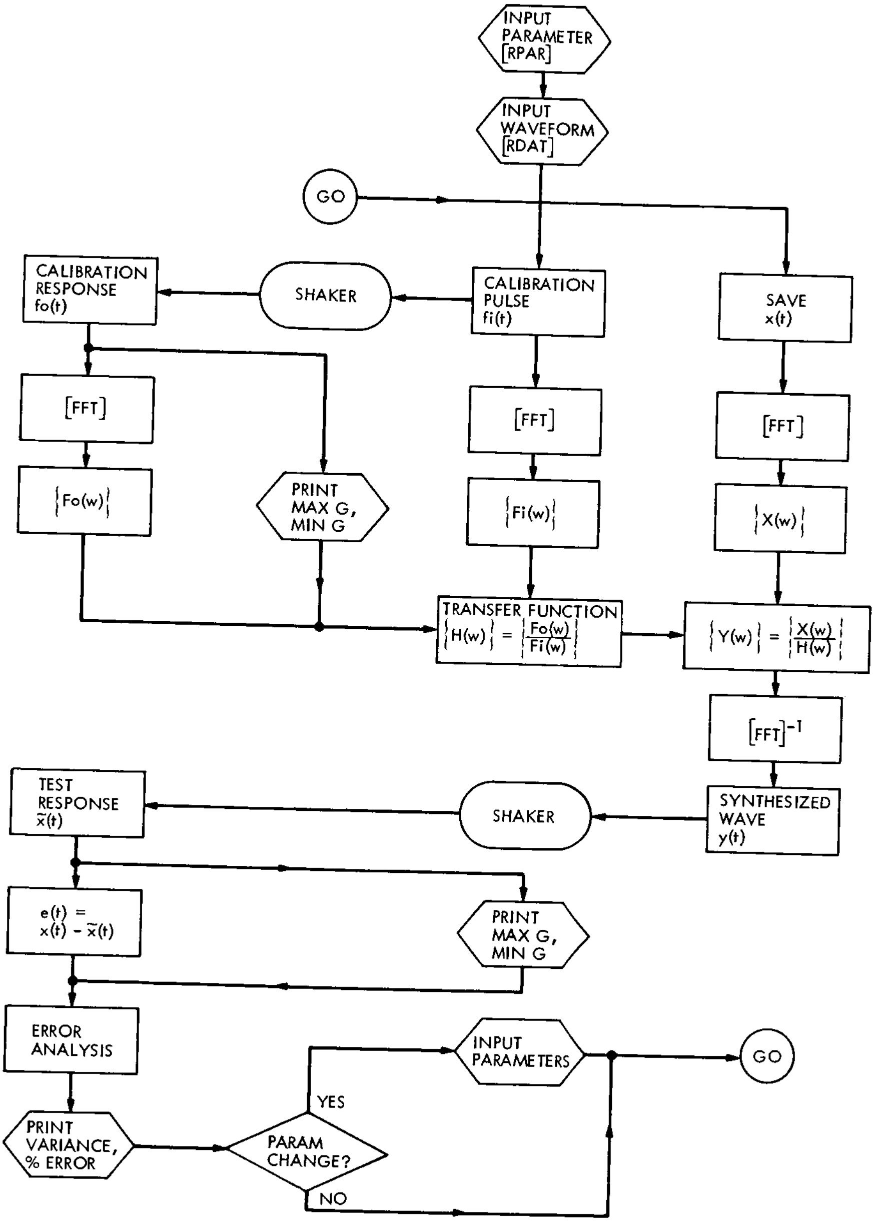

Fig. 2. Transient waveform control, software flow chart

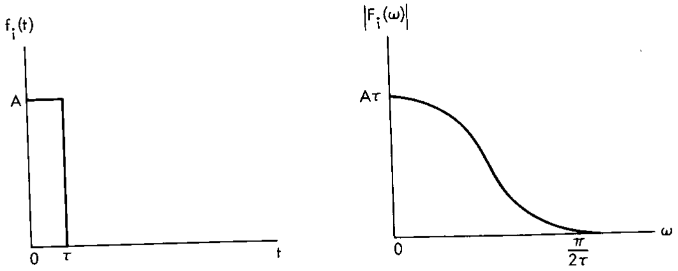

Fig. 3. Transform pair of the initial calibration pulse

frequency response of wide bandwidth, a delta function can be chosen for the initial calibration pulse $f_i(t)$. In reality, an ideal delta function is simulated by a finite amplitude square wave pulse with extremely short duration.

The direct Fourier transform of $f_i(t)$ yields $F_i(\omega)$:

$$\begin{aligned} F_i(\omega) &= \int_{-\infty}^{\infty} f_i(t)\, e^{-j\omega t}\, dt \\ &= A \int_0^{\tau} e^{-j\omega t}\, dt = \frac{A}{\omega}\left[\sin \omega\tau + j(\cos \omega\tau - 1)\right] \end{aligned} \tag{1}$$

and

$$|F_i(\omega)| = \frac{A}{\omega}\sqrt{2(1 - \cos \omega\tau)} \tag{2}$$

The transform pair, functions $f_i(t)$ and $|F_i(\omega)|$, is shown in Fig. 3. If τ is selected as one sample period of the D/A converter, then $\pi/2\tau$ is the total bandwidth of $F_i(\omega)$. The choice of a delta function as the calibration pulse is not unique, although it is found to be most convenient for digital controllability.

The calibration pulse $f_i(t)$ is transmitted to the shaker through the D/A converter, and the test specimen response signal $f_0(t)$ is detected by a transducer and stored in the computer memory through the A/D converter (refer to Fig. 1). A real-time Fourier transform is performed on $f_i(t)$ and $f_0(t)$.

$$\begin{aligned} F_i(\omega) &= \mathcal{F}[f_i(t)] \\ F_0(\omega) &= \mathcal{F}[f_0(t)] \end{aligned} \tag{3}$$

where $\mathcal{F}$ is the Fourier transform operator.

Then the transfer function is obtained through complex division,

$$H(\omega) = \frac{F_0(\omega)}{F_i(\omega)} \tag{4}$$

Equation (4) appears to be straightforward algebra, but it requires particular care in practice. First, one must send out $f_i(t)$ such that the physical system will produce a healthy frequency response in the bandwidth of the desired transient waveform. This requires the understanding of the physical limitations of the shaker-amplifier system. To point out this important fact, the vibration nomograph of Fig. 4 is presented. It is clear that one must analyze the desired test pulse waveform $x(t)$ beforehand to obtain its frequency bandwidth, peak acceleration, velocity, and displacement levels such that all the requirements fit within the shaker limitation polygon shown in Fig. 4. Note that all the electrodynamic shakers behave like high-pass filters up to 3000 Hz, while the hydraulic shaker behaves like a low-pass filter. Second, the complex division of Eq. (4) must be done within the dynamic range of the digital machinery. The JPL Environmental and Dynamic Testing Section FFT processor has only an 8-bit word size, which gives a theoretical dynamic range of 36 dB. This turns out to be a crucial limitation whenever the transfer function possesses sharp resonance characteristics.

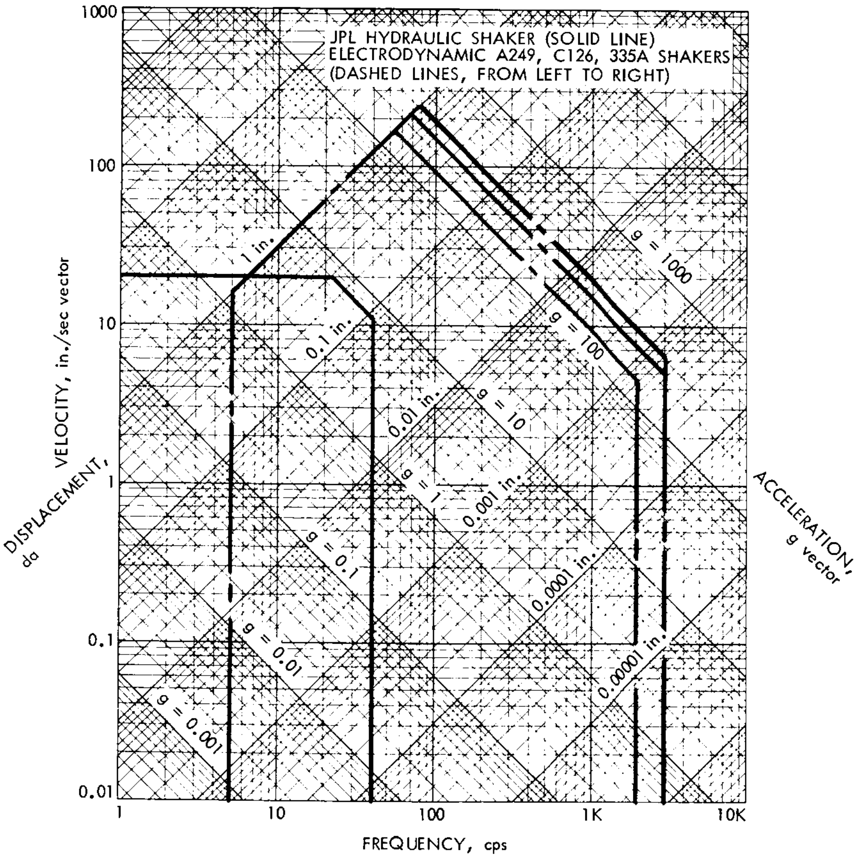

Fig. 4. Shaker limitations, transient peak

Once $H(\omega)$ is accurately determined, the required input waveform $y(t)$ is synthesized in order to achieve the desired waveform $x(t)$ at a specified location on the test specimen. The Fourier transform of the required transient wave $y(t)$ is

$$Y(\omega) = \frac{X(\omega)}{H(\omega)} \tag{5}$$

where $X(\omega) = \mathcal{F}[x(t)]$.

Then

$$y(t) = \mathcal{F}^{-1}[Y(\omega)] \tag{6}$$

All the frequency functions are complex functions; thus all the Fourier transform pairs constitute one-to-one invertible mapping. This eliminates the arbitrary phase assumptions which are associated with test specifications given as frequency spectra.

Error Tolerances

Computational roundoff errors, truncation errors, and physical nonlinearity errors will occur in practice, and it is important to obtain quantitative information on the relative magnitude of the error; that is, the required function $y(t)$ will not exactly yield the desired response $x(t)$.

Let $x(t)$ be the specimen response signal as $y(t)$ is transmitted to the shaker. The error signal $e(t)$ can be defined at each discrete point i in time as

$$e_i = x_i - \bar{x}_i, \qquad i = 1, 2, \cdots, N \tag{7}$$

$$N = \text{digital frame size}$$

The error can be given as statistical quantities, i.e., a mean and a variance. The mean of the specified waveform is

$$m_x = \frac{1}{N} \sum_{i=1}^{N} x_i \tag{8}$$

The mean of the resulting error is

$$m_e = \frac{1}{N} \sum_{i=1}^{N} e_i \tag{9}$$

The associated variances are

$$\sigma_x^2 = \frac{1}{N-1} \sum_{i=1}^{N} (x_i - m_x)^2 \tag{10}$$

and

$$\sigma_e^2 = \frac{1}{N-1} \sum_{i=1}^{N} (e_i - m_e)^2 \tag{11}$$

Thus a measure of the error in time domain can be defined as

$$\text{percent variance error} = 100 \times \sigma_e^2/\sigma_x^2 \tag{12}$$

For typical transient pulses generated on electrodynamic shakers, the percent variance errors are in the neighborhood of 10%, and this is considered acceptable. TWC allows for improved control tolerances. This means that acceptable errors and tolerances can be realistically specified for this type of shock testing.

In a typical shock test specification, the time history tolerances are specified for its peak amplitude and duration. International standards set by the International Electrotechnical Commission specify the peak amplitude tolerances of ±15% on the terminal peak sawtooth pulse (Ref. 6), whereas the JPL specification calls for ±10% peak amplitude tolerances (Ref. 7). The waveforms synthesized by the TWC method exhibit the peak amplitude tolerances well within the JPL specification. The accuracy can be improved further when the dynamic range of the FFT processor is increased to a 16-bit word size.

Example

An example test run was made using a Ling 335A electrodynamic shaker driven by a 175-KVA amplifier. The shaker was horizontally positioned using a slip plate riding on an oil film slip table. A Viking Orbiter 1975 bay fixture was attached to the slip plate. The bay fixture was the test specimen. The control accelerometer was mounted on the bay fixture at a specified location, and an arbitrary transient waveform shock pulse $x(t)$ was specified as the desired specimen response at the mounting point of the accelerometer. The idea of the experiment was to synthesize a transient waveform $y(t)$ such that when this pulse was transmitted through the amplifier-shaker system and test item, the transfer function $H(\omega)$ of the total system would modify $y(t)$ in such a manner as to produce $x(t)$, the desired response.

The digitized waveform specification $x(t)$ is shown in Fig. 5; 500 discrete points define $x(t)$ in digitized form. The transient waveform $x(t)$ was specified as a 50-*g* peak acceleration with a duration of 500 ms.

The Fourier transform of $x(t)$ was performed, resulting in the real and imaginary parts of the frequency function $X(\omega)$ as indicated in Figs. 6 and 7, respectively. The frequency function shown by this analysis indicated that the frequency content was about 100 Hz.

A delta function was generated by the test system in such a manner as to result in a transfer function $H(\omega)$ of the total system to a frequency bandwidth of 500 Hz. Figures 8, 9 and 10 illustrate the system transfer function.

Since $X(\omega)$ and $H(\omega)$ were known, it was then possible to obtain $Y(\omega)$ from Eq. (5). The test equipment hardware and software algorithm were then able

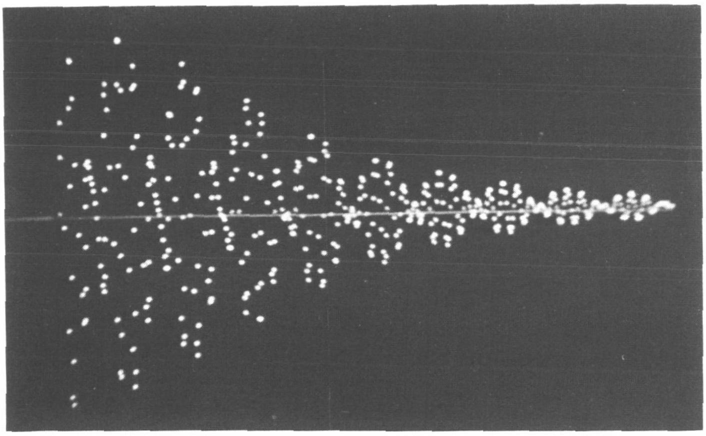

Fig. 5. Desired digitized waveform specification x(t): duration = 500 ms; peak amplitude = 50 g

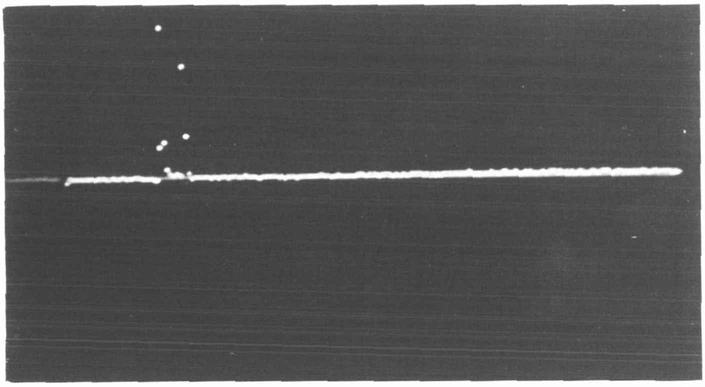

Fig. 6. Real part of $\mathcal{F}[x(t)]$ Re $X(\omega)$: frequency bandwidth = 500 Hz; frequency resolution = 2 Hz

to take the inverse Fourier transform of $Y(\omega)$ to obtain $y(t)$. Then $y(t)$ (Fig. 11) was transmitted to the test specimen through the test system. This resulted in the response $x(t)$ as seen in Fig. 12. It can be seen that Fig. 12, $x(t)$, and Fig. 5, $x(t)$, are extremely close in appearance. A special algorithm in the software program computed the error as seen in Fig. 13. The percent variance between $x(t)$ and $e(t)$ is given by the program as 9.3%, an acceptable error.

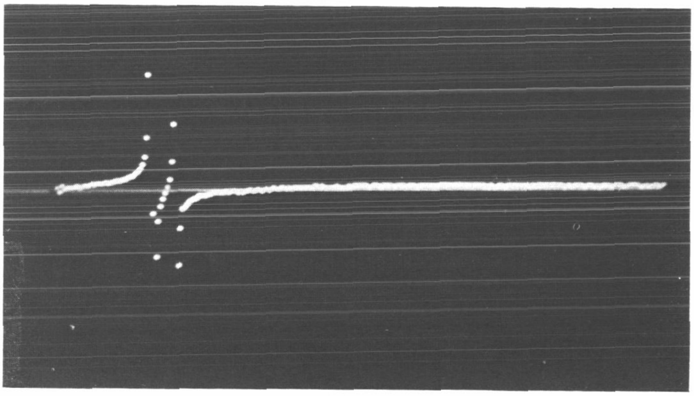

Fig. 7. Imaginary part of $\mathcal{F}[x(t)]$, Im $X(\omega)$

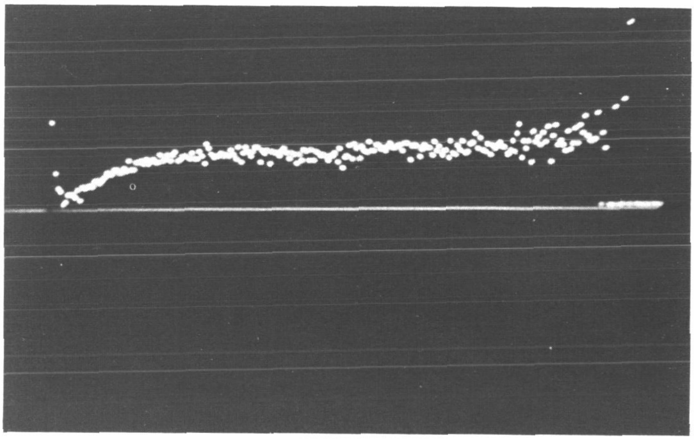

Fig. 8. Transfer function $|H(\omega)|$: frequency bandwidth = 500 Hz; frequency resolution = 2 Hz

Summary

Transient waveform control has been implemented at JPL by utilizing the digitally controlled vibration hardware. The TWC technique is demonstrated to be controllable to an arbitrary transient profile and repeatable to the JPL tolerances at least to the known limitations of the hardware. The main argument for this technique is that of closer realism in the vibration testing, providing that a typical time history transient waveform can be defined for a physically transient phenomenon. This method of testing will complement and improve the realism in a conventional shock spectrum testing as well as sine sweep test specifications, which are typically based on some transient phenomena.

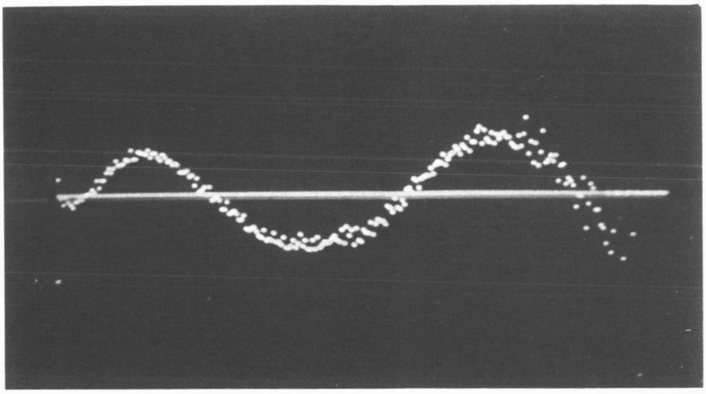

Fig. 9. Real part of the transfer function Re $H(\omega)$

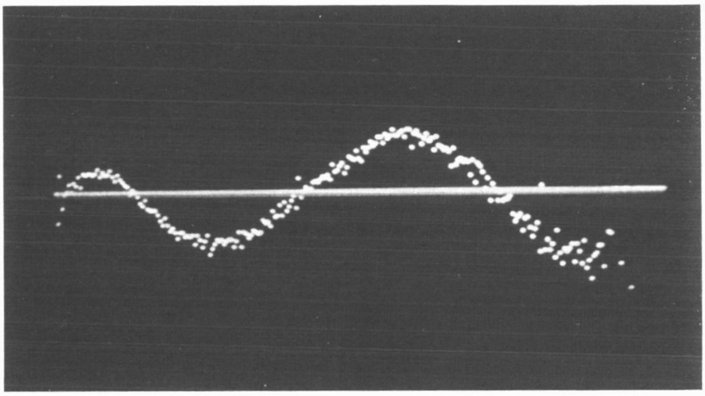

Fig. 10. Imaginary part of the transfer function Im $H(\omega)$

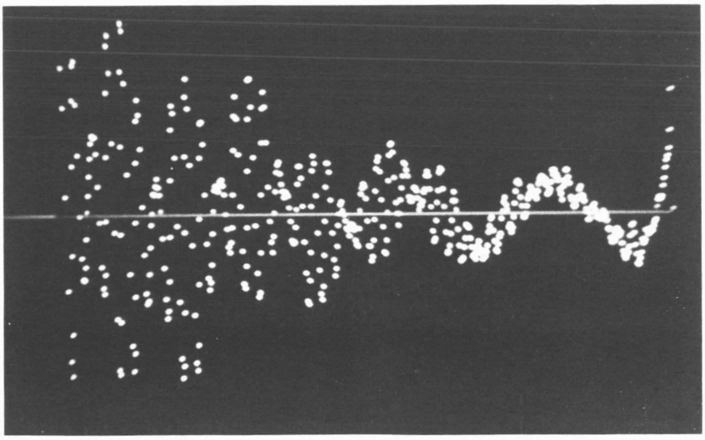

Fig. 11. Synthesized waveform $y(t)$: $y(t) = \mathcal{F}^{1}[X(\omega)/H(\omega)]$

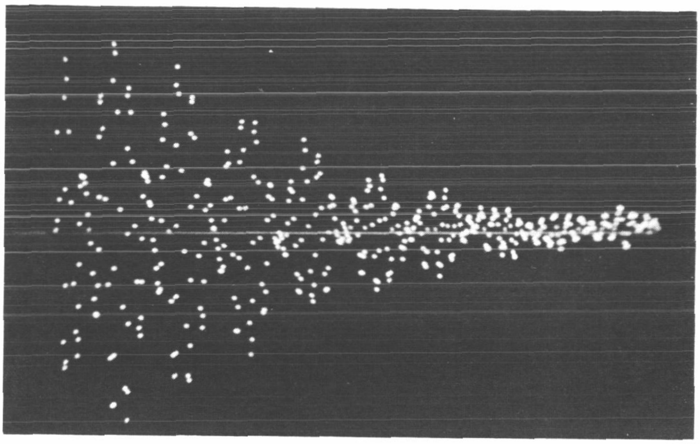

Fig. 12. Achieved specimen response x(t): duration = 500 ms; peak amplitude = 52.3 g

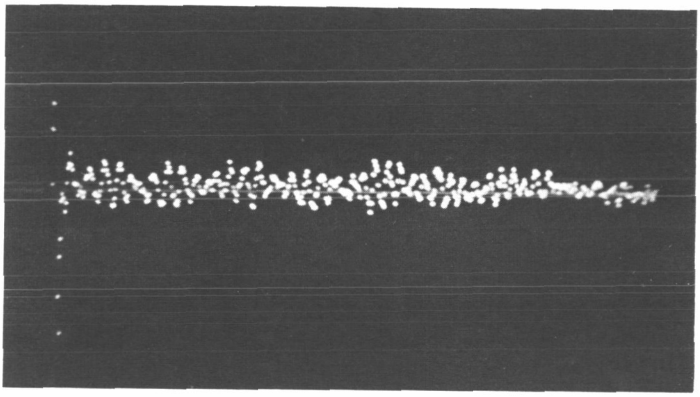

Fig. 13. Error e(t) = x(t) - x(t): percent variance error = 9.3%

References

1. Chapman, C.P., Shipley, J., and Heizman, C.L., "A Digitally Controlled Vibration or Acoustic Testing System," *Institute of Environmental Sciences 1969 Proceedings*, pp. 387 - 409, Institute of Environmental Sciences, Mt. Prospect, Illinois.

2. Sotomayor, B.R., "Software Requirements for Computer Control of Random Noise Vibration Tests," *Institute of Environmental Sciences*

1971 Proceedings, pp. 145 – 155, Institute of Environmental Sciences, Mt. Prospect, Illinois.

3. Chapman, C.P., "Computer-Controlled Environmental Test Systems: Criteria for Selection, Installation, and Maintenance," *Society of Automotive Engineers*, Paper 720819, New York, 1972.

4. Trubert, M.R., *A Fourier Transform Technique for the Prediction of Torsional Transients for a Spacecraft from Flight Data of Another Spacecraft Using the Same Booster*, Technical Memorandum 33-350, Jet Propulsion Laboratory, Pasadena, Calif., Oct. 15, 1967.

5. Favour, J.D., LeBrun, J.M., and Young, J.P., "Transient Waveform Control of Electromagnetic Test Equipment," *40th Shock and Vibration Bulletin*, Part 2, December 1969.

6. Broch, J.T., *Mechanical Vibration and Shock Measurements*, pp. 210 – 218, Bruel & Kjaer Publications, Naerum, Denmark, 1972.

7. Inouye, G., "Type Approval and Flight Acceptance Test Requirements and Preacceptance Test Limits, Mariner Mars 1971 Flight Equipment General Specification," Environmental Test Specification TS504550A (an internal document), Jet Propulsion Laboratory, Pasadena, Calif., Aug. 11, 1969.

JPL Quarterly Technical Review Volume 3, Number 2 July 1973

Index: antennas and transmission
lines, Mariner Venus/Mercury 1973
Project, wave propagation

NASA/JPL Deep Space Network 64-Meter-Diameter Antenna Dual-Frequency Feed System

P. D. Potter

Telecommunications Division

To support the Mariner 1973 X-band experiment, it was necessary to implement a dual-frequency microwave feed system for the Cassegrainian-fed DSS 14 64-m antenna. This system must be capable of simultaneous low noise reception at S- and X-bands and high-power transmission at S-band. This article describes the design and measured performance of the DSS 14 reflex feed system.

To support the Mariner 1973 X-band experiment, it was necessary to implement a dual-frequency microwave feed system for the Cassegrainian-fed DSS 14 64-m antenna. This system must be capable of simultaneous low noise reception at S- and X-bands and high-power transmission at S-band. To fulfill this requirement, a particularly attractive approach, the reflex feed system, was implemented. By a system of two reflectors, one of which is dichroic, the effective S-band feed phase center is translated from its normal position in the S-band feedhorn to a new point which very nearly coincides with the X-band feedhorn phase center. Thus, during simultaneous S- and X-band operation, the antenna subreflector optics are aligned with the X-band feedcone position.

A cross-sectional view of the reflex feed system geometry is shown to scale in Fig. 1. The system is comprised of four basic components: the S-band feedhorn centrally located in its support structure (feedcone), an ellipsoidal reflector, a planar dichroic reflector, and the X-band feedhorn centrally located in its feedcone. By reciprocity, the operation of the reflex feed is the same in the receiving mode as in the transmitting mode; for simplicity, Fig. 1 shows only the transmitting mode. For S-band operation, from a geometrical optics standpoint, radiated energy from one of the ellipsoid foci f_1 is focused to the point f_2. As shown in Fig. 1, however, the system is not large compared to a wavelength. Because of this consideration and the fact that the S-band feedhorn does not represent a point source, the radiated energy from the ellipsoid is actually found to focus to a small region centered at the point C. This energy is then redirected by the planar reflector to the antenna subreflector. By the principle of images, this redirected radiation appears to emanate from the point F_X, which is the far-field phase center of the X-band feedhorn and also coincides with one of the subreflector foci. To permit simultaneous X-band operation, the central region of the planar reflector is perforated with an array of X-band resonant apertures, thereby making the reflector essentially transparent to X-band but reflective to S-band.

Various practical considerations highly constrain the geometry of the reflex feed system and, as a result, the ellipsoid had to be placed in the near-field region of the S-band feedhorn. Additionally, the S-band feedhorn was constrained to be the existing design. As a result of these constraints it was necessary to analytically determine the scattering properties of the ellipsoidal reflector in its actual location, as a function of its surface design parameters. Fortunately, a practical and accurate technique for doing such calculations had recently been devised and implemented by Arthur Ludwig of the Jet Propulsion Laboratory (Ref. 1). A slightly modified version of Ludwig's computer program was utilized to calculate the far-field radiation patterns of the S-band horn and ellipsoidal reflector combination.

The Ludwig scattering program was thus used to study and optimize the ellipsoid geometry in order to produce a scattered radiation pattern very similar to the radiation pattern of the horn by itself. The horn pattern had

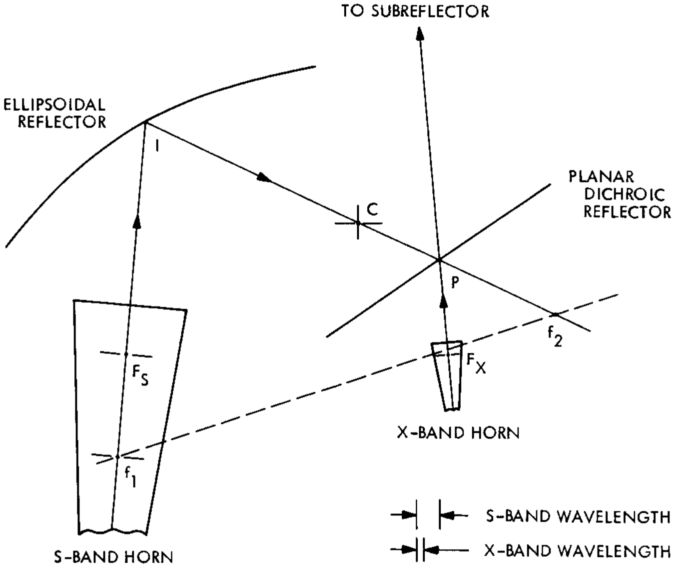

Fig. 1. Reflex feed geometry

been previously optimized for correct subreflector illumination. The phase of the ellipsoid scattered fields was used to locate the point C (Fig. 1) for a practical overall geometry.

Since the reflex feed design was based on a computer program which was novel in some respects, it was necessary to experimentally validate the design by scale model testing. A scale model ellipsoid was tested in the JPL Mesa Antenna Range anechoic chamber. Scale model patterns were also taken of the complete feed including the flat plate (planar reflector). The agreement between measured and computed radiation patterns was virtually perfect and the finite-size flat plate was found to behave in a completely optical manner, as expected.

Completion of the reflex feed installation into the 64-m antenna was accomplished on January 24, 1973. The system performance was evaluated during the period of January 25, 1973, through January 30, 1973. Figure 2 shows the simultaneous S- and X-band antenna response.

For purposes of the Mariner 1973 X-band experiment, the DSS 14 prototype reflex dichroic S/X feed system is entirely adequate. Prime S-band system gain and system noise temperatures are within 0.03 dB and 2.0 K of the original nonreflex performance (noise temperature improvement). The experimental X-band system is within 0.10 dB and 2.0 K of the original nonreflex performance (the X-band numbers are degradations). Coincidence of all four possible beams (two nonreflex and two reflex) has been established with negligible error and is adequate.

Reference

1. Ludwig, A. C., *Calculation of Scattered Patterns from Asymmetrical Reflectors*, Technical Report 32-1430, Jet Propulsion Laboratory, Pasadena, Calif., Feb. 15, 1970.

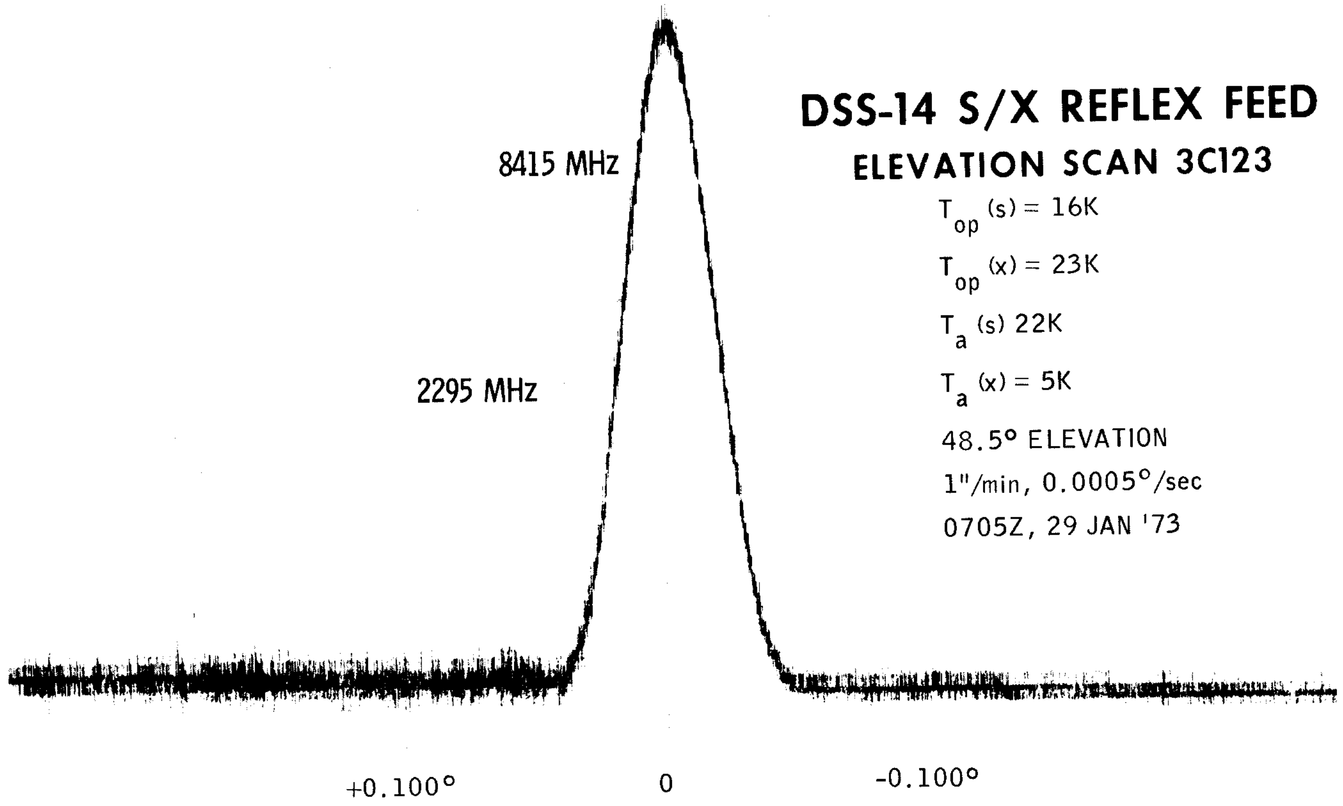

Fig. 2. DSS 14 S/X reflex feed elevation scan

JPL Quarterly Technical Review Volume 3, Number 2 July 1973

Index: optics, photography, temperature control

A Silicon Vidicon Camera for Slow Scan Operation

W. M. Porter

Space Sciences Division

A silicon vidicon camera has been designed, built, and tested to determine its potential for use aboard future Mariner spacecraft. Slow scan operation is made possible by cooling the vidicon to -40°C. Cooling is achieved by a simple thermal conduction path between the vidicon and a radiator mounted on top of the camera head. The camera has been successfully operated under simulated space flight conditions and has survived vibration designed to simulate the launch of a Mariner spacecraft. A description of the camera and its operation along with the results of the testing is presented.

Introduction

Future Mariner missions may require cameras with increased sensitivity and spectral response over those that have been flown aboard Mariner spacecraft to date. Recently developed silicon vidicons may provide the basis for a new high-performance camera. These vidicons differ from those used in the current Mariner camera in that the silicon vidicon uses a target made up of a silicon diode array rather than amorphous selenium-sulfur. The use of a silicon vidicon camera would result in performance improvements over existing Mariner cameras in both sensitivity and spectral response.

Unfortunately, the silicon vidicon is not without its problems. Leakage current in the diode array also called dark current is substantial at room temperature and limits the usable frame time to a few seconds or less. For a silicon camera to be compatible with Mariner technology, its frame time must correspond to Mariner data handling rates. The frame time, for a picture of 500 lines by 500 elements, is on the order of 20 seconds. An even larger format with a correspondingly longer frame time would be preferred, as this format represents what is minimally acceptable.

The dark current problem associated with the silicon vidicon can be eliminated by cooling the vidicon during operation. The silicon target's dark current is a function of its temperature, and at a sufficiently low temperature, −40°C in the case of a 20-s frame time, satisfactory slow scan operation can be obtained.

To determine how much of a problem this presents and the feasibility of operating a silicon camera on board a Mariner spacecraft, a camera (Fig. 1) was designed and built. The camera was designed to include provision for cooling, not only in space, but also on the ground to allow for testing and calibration. This article describes the camera structural and thermal design and the results of environmental testing to verify the design.

Camera Construction

The camera design was intended to be as close to a flight configuration as possible and to be compatible with Mariner electronics. Pertinent specifications for the camera appear in Table 1. As designed, the silicon vidicon camera is somewhat larger and heavier than is desirable for spacecraft application. This is mostly due to the large coil required by the silicon vidicon for good performance. A smaller coil can be used but at the expense of the picture quality. Resolution in the corners of the picture and shading performance would suffer (shading is a measure of the photometric uniformity of the camera).

The camera was designed with the goal of keeping the cooling system as simple as possible. This precluded the use of such items as heat pipes or fluid

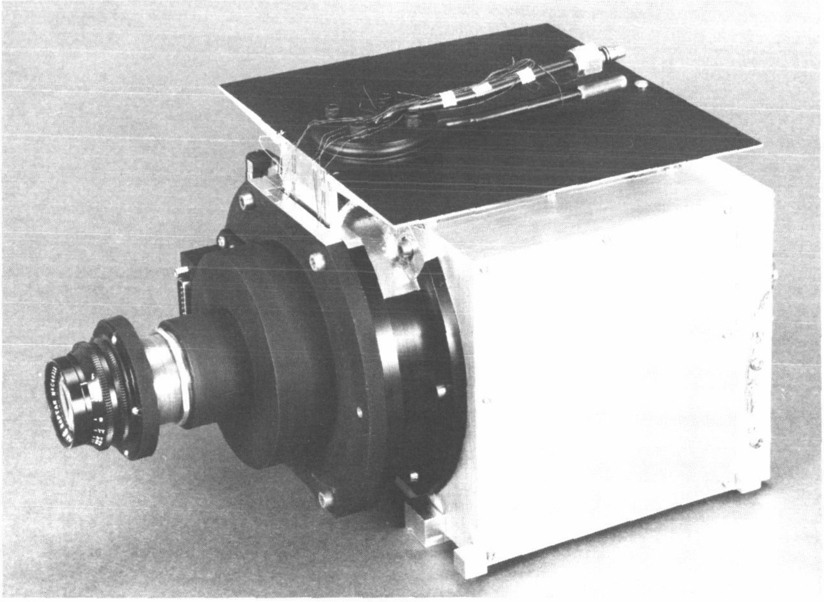

Fig. 1. Silicon camera with test optics mounted (shown with thermocouples attached). The plumbing on top of the radiator is the LN_2 heat exchanger which is used for bench operation

Table 1. Silicon camera specifications

Dimensions[a]	20 × 20 × 19 cm
Weight[a]	6.8 kg
Ambient temperature range for operation	−20 to +35°C
Frame time	20 s
Format	500 lines × 538 pixels
Vidicon temperature:	
Flight conditions	$-70 \leq T \leq -40$°C
Bench operation	−40°C

[a]Camera head without optics.

loops. Instead, the design provides a simple conduction path between the elements to be cooled and a radiator. The design does not include any form of thermal control for maintaining the vidicon at a constant temperature. Instead, the camera was designed to keep the vidicon at -40°C or colder for any foreseen combination of ambient temperature and viewing of the spacecraft by the camera head radiator. This is possible because the silicon vidicon signal current (and hence the camera calibration) is not a significant function of temperature.

The initial concept for building the camera was to support the vidicon by the coils and then cool the entire camera. This approach was determined to be impractical because of the radiator size (estimated to be in excess of 775 cm^2) which would be necessary to cool the entire structure. The concept which was used is to cool only the vidicon, isolating it from the surrounding coils and camera head structure.

The method by which the vidicon is cooled within the camera head can be seen in Fig. 2 (which for clarity omits the shutter). The vidicon is isolated from the deflection coil by virtue of the fact that it is a 25 mm vidicon and the inside diameter of the coil is 37 mm. This is done to avoid the necessity of cooling the coil. Radiative heat transfer between the coil and vidicon is minimized by the use of a thermal blanket between the two.

The design provides for supporting the vidicon by a beryllium oxide sleeve as shown in Fig. 3. The vidicon which is used is a special ruggedized version in a ceramic envelope. In addition to supporting the vidicon, the sleeve serves to conduct heat from it. Beryllium oxide was chosen because of its thermal conductivity and because metal cannot be located near the vidicon target. The vidicon is bonded to the sleeve with a low outgassing silicon rubber adhesive which remains pliant at the low temperatures involved. The adhesive used was General Electric's RTV 566. Before the adhesive was applied, the surfaces to be bonded were treated with General Electric's SS4155 RTV primer.

Bonded on one end of the beryllium oxide sleeve with the same adhesive is a molybdenum flange. This, in turn, is bolted to an aluminum front plate (Fig. 4). Besides serving to attach the vidicon and sleeve assembly to the front plate, the flange is used to produce a good thermal bond to it without

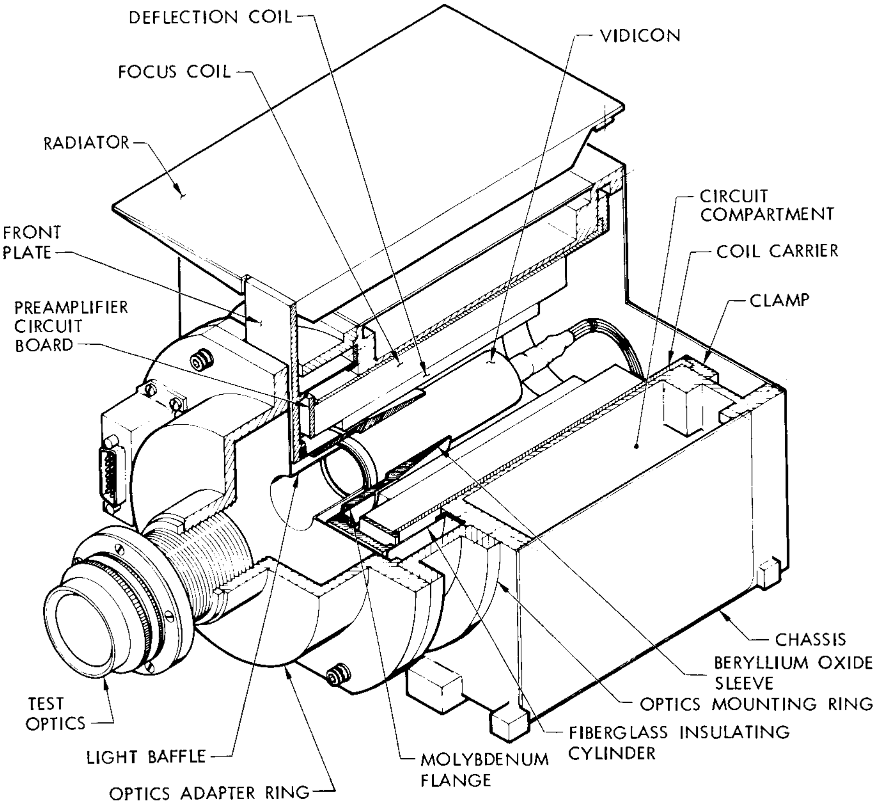

Fig. 2. Silicon vidicon camera

the use of thermal joint compounds. Thermal joint compounds in the vicinity of the vidicon were considered undesirable because of the possibility that they would outgas and that the material would condense onto the cold vidicon faceplate. The flange fits snugly into a recess in the plate. As the front plate cools, it shrinks at a much faster rate than the flange because it has a much larger temperature coefficient of expansion. This shrinkage produces a very tight grip on the flange which, in turn, gives a good thermal conductance across the joint. The flange is necessary, because attempting to clamp the beryllium oxide sleeve directly in this manner would result in its being crushed. Molybdenum was chosen for its temperature coefficient of expansion, which is a reasonable match to that of beryllium oxide. In addition, its thermal conductivity and strength are good.

The aluminum front plate which conducts heat from the vidicon assembly to the radiator serves to support both the vidicon assembly and the front of the radiator. The front plate is isolated from the camera head chassis through a cylindrical fiberglass insulator. Further isolation from the chassis and from the optics is obtained by the use of thermal blankets on either side

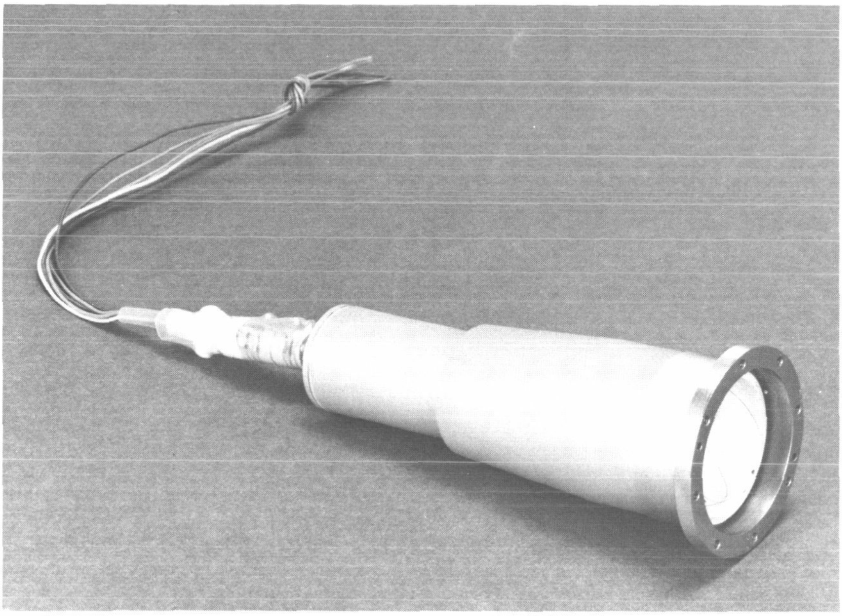

Fig. 3. Vidicon and beryllium oxide sleeve. The wires which appear at the front are the target and G4 leads; both are 0.013-mm-diameter stainless-steel wires to minimize heat transfer into the tube

of the front plate. The fiberglass cylinder, which has a wall thickness of only 0.64 mm, is loaded through a metal flange at either end. The fiberglass cylinder is aluminized to minimize heat leaks into it.

The radiator is supported at the front by the front plate and at the back by a fiberglass bracket. This bracket is designed to be stiff along the lateral axes of the camera. Longitudinal stiffness is provided by the front support. The size of the radiator (355 cm^2) was determined by a thermal analysis which considered heat leaks into the cold system through the various insulators and by radiation as well as by the fact that the radiator partially views the spacecraft.

Bench operation is obtained by attaching a heat exchanger to the radiator and evaporating liquid nitrogen in it. To eliminate the giant heat leak presented by the radiator while operating in this mode, the radiator is enclosed in a block of plastic foam. The other heat leaks produced by operating a system designed for vacuum operation in air are simply overwhelmed by evaporating sufficient liquid nitrogen. To prevent the vidicon and other cold camera parts from icing up, the camera is purged with dry nitrogen during bench operation.

Testing and Results

The reason for building the silicon vidicon camera was to determine its suitability for use aboard a spacecraft. For this reason, testing of the camera

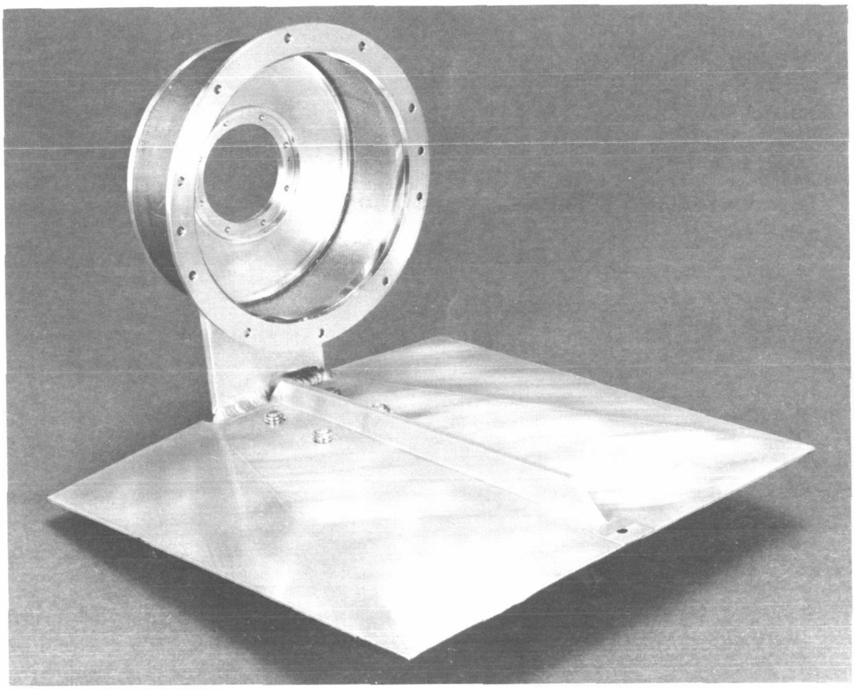

Fig. 4. Front plate and radiator assembly with fiberglass insulating cylinder attached

concentrated on its ability to operate under space flight conditions and to survive a rocket launch. No serious effort was undertaken to evaluate the quality of its pictures since the vidicon was evaluated separately under another program.

The first test performed on the camera was to verify its ability to operate on the bench. This was done by evaporating LN_2 in the heat exchanger attached to the radiator, as shown in Fig. 1. The radiator was covered with 2.5 cm of polystyrene foam, and the camera was purged with dry nitrogen.

No trouble was encountered in lowering the faceplate of the vidicon to -40°C. Cooling the vidicon down from room temperature to -40°C was found to take about one hour. The faceplate temperature was measured because of the impossibility of attaching a thermocouple to the target. Prior tests with the vidicon during its development showed the faceplate temperature to be quite representative of the target temperature. Satisfactory pictures were obtained during bench operation, indicating that the target was indeed near -40°C. Additionally, the quality of the pictures did not suffer from thermal gradients across the target, indicating that temperature gradients across the target are less than 2°C during operation.

Some of the aluminization applied for thermal control in the camera was tarnished during bench operation. This could be avoided by the use of a protective coating or by using gold instead of aluminum. After the camera was bench-tested, during which time it was aligned and electronically focused, it was put into a thermal vacuum chamber to test its operation under simulated space conditions. One problem associated with cooling had been anticipated and was compensated for prior to the start of thermal vacuum testing. Analysis showed that the relative motion between the vidicon and the lens would be 0.13 mm as the camera was cooled. This is due to the contraction of various camera head parts with the changing temperature and will produce a change in optical focus. It was determined that setting the 135-mm test lens slower than f13 would insure maintaining an adequate optical focus. To further insure no problem of this sort, the lens was set at f32 during the thermal vacuum tests. This problem would be designed out in a true flight instrument. Instead of an aluminum lens support, a compensating composite support would be used.

For the thermal vacuum testing, the camera was mounted in the chamber on a temperature-controlled plate to simulate mounting to a spacecraft. Tests were run with the plate at the designed for ambient temperature extremes +35 and -20°C. During the tests, the camera was wrapped in a thermal blanket with just the radiator and lens exposed. Cooling was achieved by chilling the inside walls of the chamber with LN_2. No attempt was made initially to simulate the worst case combination of heat leaks and partial viewing of the spacecraft by the radiator.

The first test in thermal vacuum was run with the mounting plate at +35°C. This resulted in a vidicon faceplate temperature of -58°C against a designed for temperature of -40°C and a predicted temperature of -65°C for the conditions actually simulated. Subsequent analysis of the temperature data taken shows the heat leak into the camera front plate to be larger than predicted.

The initial thermal design for the camera predicted a minimum temperature of -70°C for the vidicon faceplate. Because the structural design did not consider a lower temperature than this, part of the radiator was masked off before testing continued. This was done as a precaution against overstressing the vidicon or its supporting structure. On the basis of the data taken, all but 130 cm^2 of the radiator was covered with aluminum tape to hold the vidicon to a predicted temperature of -61°C.

After masking off part of the radiator, a second test was run with the mounting plate at -20°C. The vidicon faceplate reached a temperature of -60°C. Temperature gradients across the various parts of the camera reasonably matched those predicted by the computer model used during the design of the camera. Significant gradients are tabulated in Table 2. The gradients indicated better performance then expected for the silicon rubber bonds.

Although the minimum design temperature for the vidicon was not reached during the thermal vacuum tests, the vidicon assembly was tested to this temperature in a cold chamber. No damage to the part resulted.

It is interesting to note that scarcely any evidence of outgassing was noticed in pumping down the chamber—indicating that the adhesives, fiberglass, and potting compounds used in the camera were indeed clean.

After the thermal vacuum tests, the camera was subjected to a forced vibration test. The object of this test was to determine if the camera could survive a rocket launch. Since the camera was not designed for use aboard any particular spacecraft, a test program was designed which is a conservative composite of previous and anticipated Mariner launches.

Testing consisted of shaking the camera along all three axes: first in a 0.5 g rms sine sweep from 30 to 2000 Hz at 2 oct/min, and following this, at the flight acceptance and type approval levels shown in Figs. 5 and 6. The flight assurance test is conducted at the level of vibration actually expected during launch. It is used to verify that the object being tested could actually survive the launch. The test assurance test levels are higher than those expected during launch and are used to prove the design of the object being tested. In both cases, the sine sweep preceded the random vibration test. All three axes were tested at the FA levels before proceeding to the TA levels.

The camera survived all vibration testing intact except that the rear fiberglass support for the radiator broke during testing at the TA levels. This was considered to be of little consequence as this part could easily be made stronger without compromising the overall design. Some metallic particles were observed on the target after testing. However, these particles were also found on the targets of other vidicons and appear to be a result of the manufacturing process. They did not appear in pictures taken by the camera before or after testing.

The camera design was based on the vidicon seeing 300 g at its center of gravity or about 450 g at its base. The accelerations measured at the base of

Table 2. Camera head thermal gradients

Gradient[a]	Predict, °C	Observed, °C
Vidicon to beryllium oxide sleeve	3.3	0.55
Beryllium oxide sleeve to aluminum front plate	2.2	1.6
Aluminum front plate to warm chassis	55	51

[a] Refer to Fig. 2.

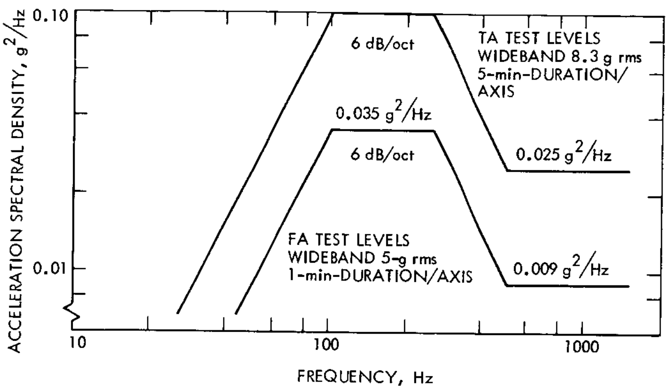

Fig. 5. Flight acceptance and type approval random vibration test levels

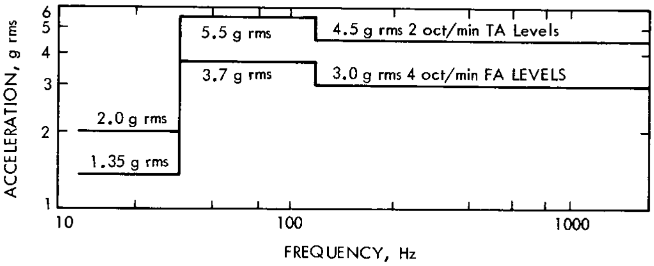

Fig. 6. Flight acceptance and type approval sine vibration test levels

the tube for the various tests are tabulated in Table 3. They are well below the design limit.

Conclusions

On the basis of the data taken, both the thermal and structural designs can be considered satisfactory. The rear radiator support needs strengthening, but this can be done without compromising either the thermal or mechanical designs. Elimination of the abnormal heat leak discovered during testing should be attempted in the interest of improving performance. It may also be desirable to provide additional damping for the vidicon assembly to lower the acceleration levels seen by it, although this would result in another heat leak. In all, the design appears suitable for use aboard a Mariner spacecraft.

Acknowledgements

Joseph L. Gertz was responsible for the concept used in building the camera. Robert Bamford and Walter Petrick developed the structural and thermal designs of the camera.

Table 3. Accelerations measured at vidicon base

Input to camera			Peak acceleration at base		
Test	Level	Axis excited	x axis	y axis	z axis
Low level	.5 g rms	x	50 g	36 g	27 g
		y	24	29	3
		z	8	17	36
Flight acceptance	3.75 g rms	x	152	100	34
		y	104	176	32
		z	48	140	200
	Random	x	192	112	28
		y	96	144	30
		z	40	100	192
Type approval	5.5 g rms	x	240	120	56
		y	112	150	32
		z	70	140	240
	Random	x	300	120	68
		y	96	190	48
		x	72	160	250

Orientation: x is the vertical axis.
y is the horizontal axis.
z is the longitudinal axis.

JPL Quarterly Technical Review Volume 3, Number 2 July 1973

Index: Mariner Jupiter/Saturn 1977 Project, solar phenomena, spacecraft environments and shielding

Probabilities for the Peak Flux and Fluence of Energetic Solar Protons Incident on Interplanetary Spacecraft

N. Divine

Project Engineering Division

Energetic protons injected into interplanetary space in solar particle events can interfere with spacecraft operations and experiments and can cause permanent degradation of some components. For future long-term interplanetary and planetary missions, techniques have been developed which use solar particle event data from 1956 through 1970 to predict the probability of exceeding any value of peak proton intensity or mission proton fluence. Dependences on proton energy (near 10 to 100 MeV), heliocentric distance, and phase of the solar cycle are included. The techniques are described and applied to the Mariner Jupiter/Saturn 1977 mission.

Introduction

Occasionally, protons with kinetic energies of the order of 10 to 100 MeV are present in interplanetary space following acceleration near the Sun. In some events, peak fluxes of these protons are severe enough to cause interference or malfunction in spacecraft science experiments or electronic subsystems, and for long-duration interplanetary missions permanent degradation can result from the accumulated fluence of such particles. To permit cost-effective countermeasures in spacecraft and mission design, a thorough, probabilistic description, continuous in particle energy, peak intensity, and fluence applicable to any interplanetary mission, is needed for this sporadic environment.

Observations

The presence of energetic solar particles near the Earth has been inferred from various ground-based instruments, notably neutron monitors, ionization chambers, and riometers, and from charged particle detectors carried in balloons, aircraft, and Earth satellites. The data so acquired, however, include modifications which result from particle interactions with the Earth's magnetosphere and atmosphere. More direct data are fortunately available from charged particle detectors on Earth-orbiting satellites with apogees outside the magnetosphere and on interplanetary spacecraft, notably IMP and Pioneer. Although some protons in the energy range of interest are commonly present (of both galactic and solar origin), flux enhancements of several orders of magnitude occur in relatively distinct events at very irregular intervals. In some months, for example, no events are detected, but in others as many as six occur, such that an average rate of occurrence is of the order of one event per month.

During such an event, particle intensities at and above some particular energy follow a rapid rise (commonly a few hours) and a slower decrease and disappearance (several days). The time profiles and the development of the spectra are characteristic both of the individual event and of the detector trajectory, displaying great variety (Ref. 1). The integration of the intensity over solid angle and over the duration of the event leads to values for the fluence at various proton energies. Recurrences of proton detection about 27 days (one solar rotation) following the original event have also been observed, but the recurrent intensities are orders of magnitude smaller than the original ones.

The angular distributions derived from charged particle telescope data are strongly variable as well, as summarized, for example, by McCracken et al. (Ref. 2). The anisotropy commonly ranges between 0.2 and 0.5 early in an event, with the variable direction of maximum intensity often parallel to the interplanetary magnetic field. Later in the event (say, after the peak intensity), the anisotropy is commonly smaller (e.g., 0.1), indicating a more nearly isotropic intensity. Because the dependence of the intensity on direction is so variable, the intensities are so variable in time, and the events are so sporadic, it is not worthwhile to include directional effects directly into an engineering model, their variations being masked by other uncertainties.

Theory

Several authors have discussed mechanisms for processes near the Sun which result in particle acceleration, storage, injection, and/or leakage. The application of the results of such theories for the origin of solar particles is limited by the major modifications in particle populations which result from various mechanisms of particle transport in interplanetary space. These mechanisms include convection, adiabatic deceleration, anisotropic diffusion, interaction with a diffusion region external boundary, and possibly others. Their theoretical treatment is commonly handled using a Fokker–Planck equation, and the complexity of the relationships among position, time, energy, intensity, fluence, and various input parameters (e.g., in the diffusion coefficients, and boundary conditions) suggests that numerical solutions are appropriate. Aspects of such theories, their development in the literature, their numerical solutions, and comparisons with the observations have been published by Englade (Ref. 3) and Webb and Quenby (Ref. 4), among others.

Both the complexity of the theory and the individuality of particular events suggest that the successes of the theoretical and numerical treatments are not suitable for the overall engineering descriptions needed here. For this purpose, we concentrate on the peak intensity and fluence for an event as functions of energy and heliocentric distance, ignoring the time profile, and angular and heliocentric longitude dependences. Average energy spectra, at least near the Earth's orbit, can be obtained from spacecraft data which cover numerous events, but only a few events have been observed at widely separated positions so that inferences about position dependences are confused by the individuality of the events observed. Further, the position dependences may be different at different energies, as the relevant transport mechanisms assume different relative importances.

To provide a suitably simple model, three ad hoc assumptions, only loosely tied to the results of the theoretical treatments, are adopted here. First, particle acceleration and loss in interplanetary space are ignored, so that energy spectra are independent of position. Second, any angular spreading of the particles (as they move a distance S from the Sun) is ignored, so that, to avoid long-term changes in the particle content of interplanetary space, a fluence proportional to S^{-2} applies to events on the average. Third, to simulate the fact that diffusion in the general direction of the particle trajectory is more rapid than perpendicular diffusion, the radial extent of a group of particles is taken as proportional to S, such that the peak intensity is proportional to S^{-3} (inversely proportional to the volume occupied by the particles) for events on the average. Some alternative, energy-dependent relations and further references are discussed by Thomas (Ref. 5) and by Haffner (Ref. 6).

Correlations and Predictions

The association of solar particle events with solar flares and other manifestations of solar activity has prompted searches for correlations of event severity and/or rate (or probability) of occurrence with other indices of solar activity, notably sunspot number. For this purpose, tables are needed that summarize data from many events on a common basis, and the most useful summaries are those which provide the peak intensity and the fluence of protons above various energy values for each event exceeding some threshold. For cycle 20, between 1964 and the present, such a tabulation is provided by Atwell (Ref. 7) from spacecraft experiments (IMP and Explorer) exclusively. For cycle 19, between 1954 and 1964, a tabulation is provided by Weddell and Haffner (Ref. 8), which extends the ground-based, balloon, and satellite data compiled by Webber (Ref. 9) through 1963. Prior to cycle 19, insufficient data on solar protons are available for useful analysis.

Some of the above data compilations (and others) include various other facets of solar activity, e.g., observed details of associated sunspots, flares, plages, and RF bursts. Correlations of such data with solar particle event observations permit short-term predictions of solar particles on time scales from weeks to hours in advance, with modest accuracy. Such predictions are useful in spacecraft operations (Ref. 10), but for spacecraft (and mission) design purposes long-term predictions are needed. The available techniques quantify the correlations of event probability of occurrence and severity with solar activity and use the results for prediction purposes. Leading proponents of these techniques are Burrell (Ref. 11), Dollman and Bechtelheimer (Ref. 12), Roberts (Ref. 13), Thomas (Ref. 5), Wilson (Ref. 14), and Yucker (Ref. 15). The predictions serve specific purposes, particularly including calculations of radiation dose for manned missions, but are based entirely on data from solar particle events in cycle 19 and are restricted to the vicinity of the Earth's orbit (except for those in Refs. 5 and 15). Certain features from Refs. 5 and 15 have been included in the following development of a new and complete probabilistic description, notably a correlation of particle activity with sunspot number. The new prediction technique also includes the following features: solar particle event data from both cycles 19 and 20; continuous (rather than discrete) values for energy, intensity, fluence, and probability; and a formulation which permits applicability to interplanetary missions with arbitrary time profiles of heliocentric distance.

Reduction of Proton Data

The data tabulations discussed above provide peak intensities and fluences above three energies for 67 events between June 1, 1956, and September 30, 1964 (during cycle 19), and 38 events between April 1, 1967, and March 31, 1970 (during cycle 20). To construct the new model for probabilities of event occurrence, peak intensity, and fluence, these data were divided into six time intervals, each containing about 18 events, and for each interval a fluence plot and a peak intensity plot similar to that shown in Fig. 1 were made. The average sunspot number R_z was calculated for each such interval from data published regularly in *Solar Geophysical Data*, Part I, and intervals with similar average sunspot numbers were combined, yielding three plots, of which Fig. 1 is a sample; this was possible because the original plots with comparable sunspot numbers were very similar, even those from different solar cycles. Most of the 315 entries for the numbers $N(I)$ of events vs peak intensity I (with energy $> E$) could be approximated to within $[N(I)]^{1/2}$ by the numerical formula

$$N(I) = \sum C \exp\left[-3.69\left(S^3 I E^{1.55}/1.56 \times 10^9\right)^{\gamma_1}\right] \qquad (1)$$

The units for S are AU, those for I are $m^{-2}\ s^{-1}\ sr^{-1}$, and those for E are MeV, the summation extends over the months in the interval, and C and γ_1 are given by

$$C = \text{smaller of } [1.0, (1/6) \exp(R_z/42)] \text{ per month} \qquad (2)$$

and by

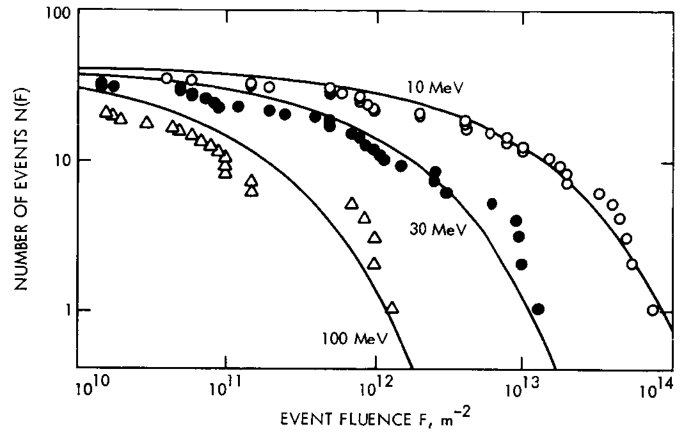

Fig. 1. Data and predictions for solar particle events with fluence exceeding F, for protons above three energies, for the interval June 1956 through October 1959

$$\gamma_1 = \text{larger of } [(468 - R_z)/1450, (R_z - 36)/275] \tag{3}$$

Similarly, it was possible to approximate 210 of the 315 entries for the number $N(F)$ of events vs fluence F to within $[N(F)]^{1/2}$ by the numerical formula

$$N(F) = \sum C \exp\left[-3.85\left(S^2FE^{1.87}/6.94\times 10^{15}\right)^{\gamma_2}\right] \tag{4}$$

where C is given by Eq. (2) and γ_2 by

$$\gamma_2 = \text{larger of } [(289 - R_z)/819, (R_z - 50)/243] \tag{5}$$

Expected numbers of events at several energies and fluences, calculated using Eq. (4), for the sample interval at the Earth, are included in Fig. 1 for comparison with the original data.

Long-Term Probabilities

The sporadic occurrence of solar particle events suggests that the Poisson distribution may be used for long-term prediction, even though, strictly, a uniform probability of occurrence does not pertain. This approach leads to an expression for the probability that the peak intensity I will be exceeded in the form

$$P(I) = 1 - \exp[-N(I)] \tag{6}$$

Here we have assumed that Eq. (1) for $N(I)$ can be used to predict the mean number of events in a time interval, and that the observed event rates in the base time intervals are means for the particular conditions, as described by the sunspot number.

The expression (comparable to Eq. 6) for the fluence probability is much more complex, because every event contributes to the fluence. (For the peak intensity, only the severest event at the energy of interest contributes.) An expression for the probability that the fluence F will be exceeded can be derived in the form

$$P(F) = \sum_{l=1}^{\infty} \left\{ 1 - [\exp(-N_o)] \sum_{k=0}^{l-1} N_o^k/k! \right\} D_l(F) \tag{7}$$

where

$$N_o = N(F) \text{ at } F = 0 \tag{8}$$

$$D_1(F) = N(F)/N_o \tag{9}$$

and

$$D_l(F) = N_o^{-1} \int_0^F [-dN(x)/dx] \, D_{l-1}(F-x) \, dx \tag{10}$$

This last expression must be evaluated for a sufficient number of terms—usually terms for which $l \geq (N_0 + 20)$ contribute less than 10^{-4} to $P(F)$. Equations (7) through (10) are comparable to expressions derived by Yucker (Ref. 15), where sums are presented for $[1 - P(F)]$.

The expressions presented above permit calculations to be performed for any mission and/or time interval if the actual smoothed or predicted sunspot number R_z is available. Values for R_z specified in *Solar Geophysical Data*, Part I, are appropriate here, and mean cycle values may be used beyond the limit of the tabulation provided there. The formulation is continuous in E, I, F and probability, and yields reasonable results in the ranges

$$30 \leq R_z \leq 180, \quad 10 \leq E \leq 100 \text{ MeV}, \quad 10^3 \leq I \leq 4 \times 10^7 \text{ m}^{-2} \text{ s}^{-1} \text{ sr}^{-1}$$

and

$$10^{10} \leq F \leq 10^{14} \text{ m}^{-2}$$

These are the ranges of the data used in the fitting procedures. For values beyond these ranges, the formulation is probably reasonable as long extrapolations to extremes such as

$$R_z \geq 250, \quad I \geq 10^9 \text{ m}^{-2} \text{ s}^{-1} \text{ sr}^{-1}, \quad \text{or} \quad F \geq 10^{15} \text{ m}^{-2}$$

are avoided.

Sample results, generated by a computer program which evaluates the quantities appearing in Eqs. (1) through (10), are shown in Fig. 2 for the Mariner Jupiter/Saturn 1977 (MJS'77) mission (JST trajectory). Fluence probabilities from Eq. (7) are shown for three energy values. Comparable calculations can be completed for peak intensities and mission fluences for any interplanetary mission.

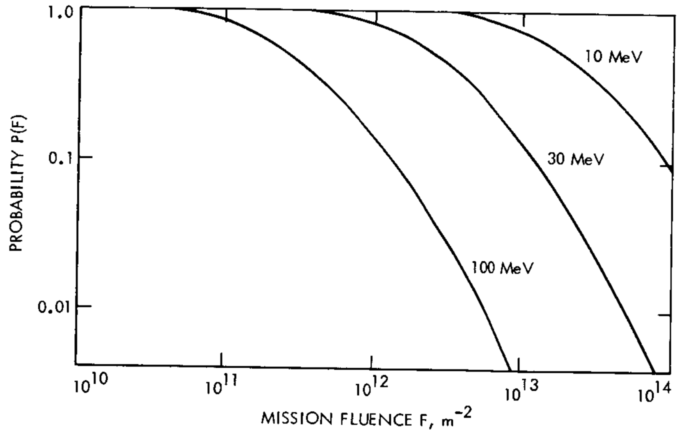

Fig. 2. Prediction of probabilities for mission fluence exceeding F, for solar protons above three energies, for the MJS'77 mission (JST trajectory)

References

1. McDonald, F. B., *Solar Proton Manual*, NASA TR R-169. National Aeronautics and Space Administration, Washington, 1963.
2. McCracken, K. G., Rao, U. R., and Ness, N. F., "Interrelationship of Cosmic-Ray Anisotropies and the Interplanetary Magnetic Field," *J. Geophys. Res.*, Vol. 73, No. 13, pp. 4159–4166, 1968.
3. Englade, R. C., "A Computational Model for Solar Flare Particle Propagation," *J. Geophys. Res.*, Vol. 76, No. 4, pp. 768–791, 1971.
4. Webb, S., and Quenby, J. J., "Numerical Studies of the Transport of Solar Protons in Interplanetary Space," *Planet. Space Sci.*, Vol. 21, No. 1, pp. 23–42, 1973.
5. Thomas, J. R., "Mariner Venus-Mercury 1973 Mission Solar Proton Environment: Fluence and Dose," in *JPL Quarterly Technical Review*, Vol. 2, No. 1, pp. 12–28, Jet Propulsion Laboratory, Pasadena, Calif., 1972.
6. Haffner, J. W., "Time Behavior of Solar Flare Particles to 5 AU," in *Proceedings of the National Symposium on Natural and Manmade*

Radiation in Space, NASA TM X-2440, pp. 336–344. National Aeronautics and Space Administration, Washington, 1972.

7. Atwell, W., "The Significant Solar Proton Events in the 20th Solar Cycle for the Period October 1964 to March 1970," in *Proceedings of the National Symposium on Natural and Manmade Radiation in Space*, NASA TM X-2440, pp. 329–335. National Aeronautics and Space Administration, Washington, 1972.
8. Weddell, J. B., and Haffner, J. W., *Statistical Evaluation of Proton Radiation from Solar Flares*, SID 66-421. North American Aviation, Inc., Downey, Calif., 1966.
9. Webber, W. R., *An Evaluation of the Radiation Hazard Due to Solar Particle Events*, D2-90469. The Boeing Company, Seattle, Wash., 1963.
10. Gonzalez, C. C., and Divita, E. L., *Solar Proton Forecast System and Procedures Used During the Mariner V Mission*, Technical Report 32-1303. Jet Propulsion Laboratory, Pasadena, Calif., 1968.
11. Burrell, M. O., "The Risk of Solar Proton Events to Space Missions," in *Proceedings of the National Symposium on Natural and Manmade Radiation in Space*, NASA TM X-2440, pp. 310–323. National Aeronautics and Space Administration, Washington, 1972.
12. Dollman, T. S., and Bechtelheimer, A. T., "Construction of Probability Envelopes of Flux-Energy Spectrum for Solar Proton Events," NASA TM X-53647, pp. 110–113. National Aeronautics and Space Administration, Washington, 1967.
13. Roberts, W. T., *Probabilities of Solar Flare Occurrence*, NASA TM X-53463. National Aeronautics and Space Administration, Washington, 1966.
14. Wilson, J. W., "Solar Radiation Hazard for Mars Orbiter," Internal Memorandum, Langley Research Center, Hampton, Va., 1971.
15. Yucker, W. B., "Solar Cosmic Ray Hazard to Interplanetary and Earth-Orbital Space Travel," in *Proceedings of the National Symposium on Natural and Manmade Radiation in Space*, NASA TM X-2440, pp. 345–355. National Aeronautics and Space Administration, Washington, 1972.

JPL Quarterly Technical Review Volume 3, Number 2 July 1973

Index: liquid propulsion, pyrotechnics, solid propulsion, test facilities and equipment

Development of Propulsion for High-Atmospheric-Pressure or Dense Environments

G. Varsi, L. H. Back, and W. L. Dowler

Propulsion Division

The development of a propulsion system that employs a detonating propellant is described, and the need for such a system and its use in certain planetary atmospheres are demonstrated. A theoretical formulation of the relevant gas-dynamic processes has been developed, and a related series of experimental tests have been pursued.

Introduction

Surface and near-surface[1] exploration of planets having hot, dense atmospheres (e.g., Jupiter, Saturn, Venus) will pose new requirements in the design of spacecraft, including their propulsive arrangements (Ref. 1-3).

Atmospheric mobility will be needed to gather samples in the atmosphere or on the surface and return them to Earth, where detailed and comprehensive analyses can be accomplished. In certain cases (e.g., Jupiter), where the difficulty in establishing a telecommunication link of sufficient power to overcome the high absorption coefficient of the atmosphere is almost insuperable, the return of samples becomes the only way to acquire the desired information—and is certainly a more attractive one than the alternative of setting up reliable, repeating stations at different altitudes (Ref. 4).

Design Requirements and Proposed Solution

The design requirements for a propulsion system to be used in the exploration of planets with hot, dense atmospheres can be summarized as follows:

---

[1] It is recognized that the large outer planets may not have "surfaces" in the same sense as the Earth or the terrestrial planets.

(1) Thrust-to-weight ratio: a high value to permit effective operation in the planetary gravitational field. (Gravity on the surface of Venus is approximately the same as on Earth; on Jupiter it is about 2.5 times that on Earth.)

(2) Performance: a specific impulse relatively independent of ambient pressure up to several hundred bars for effective operation at different altitudes and in a variety of planetary explorations[2]. This requirement is not satisfied by conventional chemical rockets, the performance of which depends on the ratio between the combustion chamber pressure and the outside ambient pressure. Typically, the specific impulse is halved when the ambient pressure reaches a few bars.

(3) Structural compactness: ability to withstand severe entry conditions. For Jupiter, for example, it is estimated that between 30 and 40% of the spacecraft mass will be lost by ablation during entry. This requirement tends to rule out aerodynamic devices such as propellers and air foils that by nature cannot be compact and are very difficult to make deployable or unfoldable.

(4) Mechanical simplicity: good reliability in severely adverse conditions (e.g., temperatures of several hundred degrees centigrade).

A promising solution presently pursued at the Jet Propulsion Laboratory employs a detonating propellant fired in a pulse mode. Typical pressures for a detonation propagating in a solid or liquid range between 20 and 200 kbars, so that ambient pressures of a few hundred bars or even a few kilobars will not appreciably affect the process. However, because of the pulsing mode of operation, such high pressures do not have to be contained statically as in the chamber of a conventional motor rocket. Rather, only the forward impulse must be received by the motor, and since the material behavior for impulsive loading of a few microseconds' duration is much different from that for static loading, structures can be designed to exploit a more favorable material response.

Regulation of average thrust can be obtained over a wide range by either controlling the size of the charges or varying the frequency of the firings (or both). Several mechanizations are possible to provide repetitive firings; because of its nature, all physical realizations of the process are rugged and well suited for a severe environment such as a Jupiter entry.

Analysis

A detonating propulsion engine can be analyzed in first approximation by schematizing it, as shown in Fig. 1. Here a rigid conical nozzle is at rest in an

---

[2] The pressure on the surface of Venus is of the order of 100 bars and is greater than 1 bar up to an altitude of about 50 km. While no surface has been established for Jupiter, it has been calculated that more than 99.5% of the mass of its atmosphere is at a pressure greater than 1 bar.

ideal gas when a mass m_e of high explosive releases an amount E of thermochemical energy instantaneously at the apex A. It is useful first to consider the upper bound for the performance of such a system. If it is assumed that the mass m_a of gases in the nozzle is negligible (or that operation occurs in vacuum), the performance upper bound as measured by the specific impulse I_{sp} is obtained by converting all the thermochemical energy E into kinetic energy of the mass (m_e) of the detonation products. One then has (in traditional units)

$$I_{sp} = \frac{(2E/m_e)^{1/2}}{g_0} \tag{1}$$

where g_0 = standard acceleration of gravity (9.8065 ms^{-2}) independent of $\mu = m_a/m_e$ for $\mu \ll 1$. In the other extreme case, when $\mu \gg 1$, one assumes that E is also totally converted into kinetic energy, but then the mass that leaves the nozzle is $m_a + m_e = m_e(\mu + 1) \cong m_e\mu$. Thus,

$$I_{sp} \cong \mu^{1/2} \frac{(2E/m_e)^{1/2}}{g_0} \tag{2}$$

Equations (1) and (2) are displayed in Fig. 2 as a dashed line for a typical explosive. While these are unattainable upper limits, they show the gain in performance to be expected when the ambient pressure, and therefore μ, increases. Numerous losses reduce the increase considerably but do not cancel it, as the subsequent analysis and experiments show.

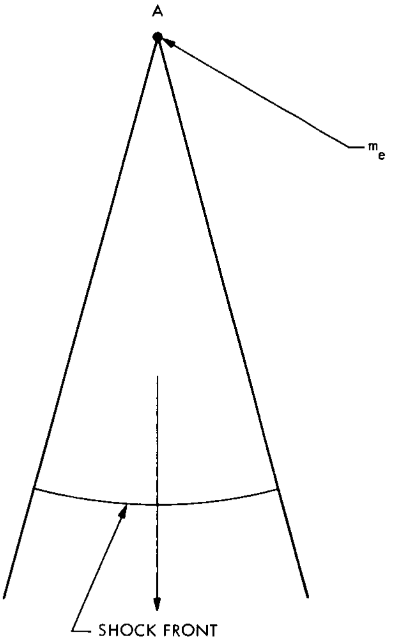

Fig. 1. Detonation propulsion nozzle

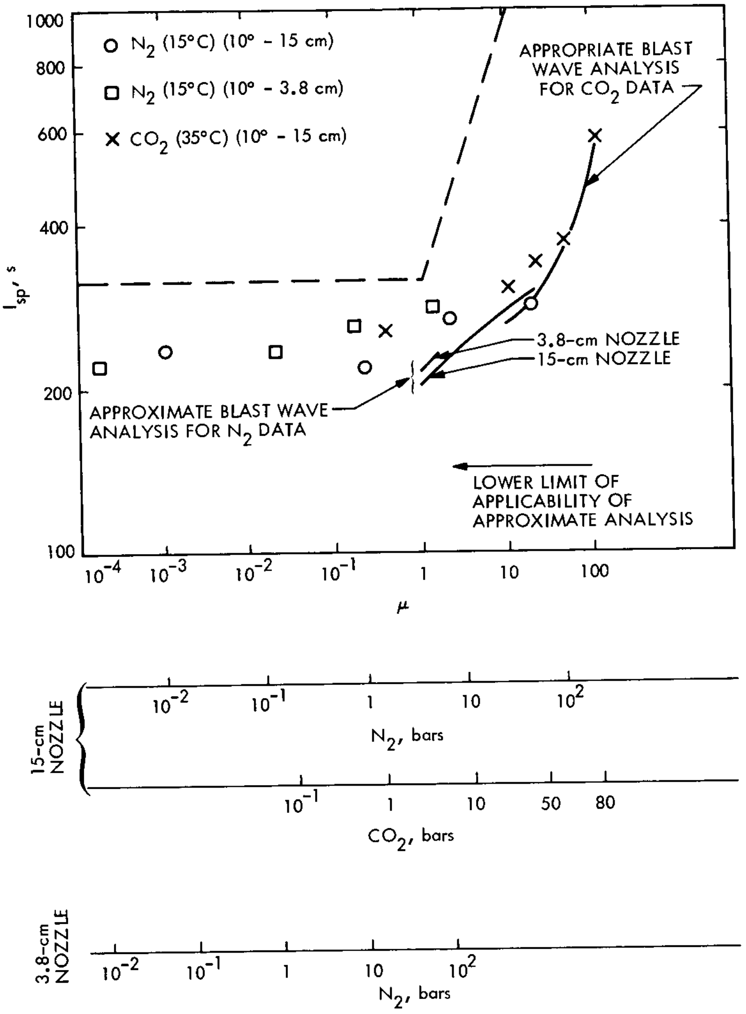

Fig. 2. Theoretical and experimental performance

An approximate description of the flow field suitable for analyzing some of the relevant aspects of the phenomenon when $\mu \gg 1$ can be obtained by writing the traditional jump conditions across the shock front that propagates through the nozzle, coupled with a closure condition involving the energy E. The peak pressure $P_{\max}$ across the shock is given in many textbooks; for example, in the case of a strong shock Ref. 5 (p. 217) gives

$$P_{\max} = \frac{8}{25}(\gamma + 1)^{-1} \alpha^{-2/5} \rho_1^{3/5} E_0^{2/5} t^{-6/5} (4\pi)^{2/5} \tag{3}$$

where

γ = ratio of the specific heats

ρ_1 = density of the undisturbed gas

t = time

$E_0 = E/\omega$ = energy released per unit of solid angle

α = a function of γ: $\alpha(1.4) = 0.851$

Similarly, the position of a strong shock is given as

$$R_s = (4\pi)^{1/5} \alpha^{-1/5} E_0^{1/5} \rho_1^{-1/5} t^{2/5} \tag{4}$$

and the pressure P is tabulated as a function of P_{max} and the previous parameters. Finally, by integration of the pressure over the nozzle wall during the flow period, one obtains the specific impulse. (See Ref. 6 for suitable approximations that account for the finite back pressure, and Fig. 2.)

Experiments

A series of experiments were conducted to demonstrate the feasibility of the concept and the performance of such a system, especially under high-pressure conditions. Figure 3 shows the experimental device used to measure impulse delivered by the detonating charge. The structure is built entirely of aluminum, with the exception of the central plug behind the explosive charge, which is made of 4130 heat-treated steel. Teflon bushings minimize friction against the guy wires. A payload of lead spheres is used to vary the total mass of the device so that its velocity is low and the excursion within the limits of the surrounding equipment. All the tests reported in Table 1 and illustrated in Fig. 2 were conducted in a steel tank, where the maximum excursion of the sled was about 25 cm. The impulse was determined by measuring the vertical distance traveled by the sled as indicated by a steel spring marker. The bottom of the cylindrical tank (diameter = 40 cm, length = 70 cm) was covered with a 25-cm-thick layer of number 00 steel wool to reduce the strength of a reflected shock wave. Experimental verification has shown that under the conditions of the tests (where a distance of 30 cm existed between the steel wool absorber and the exit plane of the nozzle), the impulse imparted by the reflected shock wave is within the repeatability of the measurement ($\cong$3%) and therefore negligible.

The configuration of the detonating charge used in all the tests is shown in Fig. 4. The plastic explosive contains 85% PETN (pentaerythritol tetranitrate) and 15% wax, and it is sold commercially as "Deta sheet" by the manufacturer, E. I. Du Pont Co., Wilmington, Del. The charge was detonated with a Space Ordnance Systems, Inc., microdetonator containing 32 mg of explosive. The mass of the charge itself was 1.5 g, so that the total

Table 1. Specific impulse, N-s/kg[a]

Pressure, bars	Dry nitrogen at 20°C		Dry carbon dioxide at 20°C, 15-cm nozzle[b]
	15-cm nozzle[b]	3.8-cm nozzle[b]	
10^{-2}	2314 (236)	2177 (222)	
1	2147 (219)	2324 (237)	2501 (255)
8.2	2648 (270)	2550 (260)	
25			3011 (307)
47			3315 (338)
68	2844 (290)	2765 (282)	
69			3707 (378)
83			5678 (579)

[a] Numbers in parentheses show specific impulse in seconds.

[b] Nozzle half-angle = 10 deg.

mass of explosive for each firing was 1.532 g. The specific impulses reported were obtained by dividing the impulse by 1.532 g.

The experimental results confirm the theoretical prediction of good performance in high-pressure or dense environments. As shown in Fig. 2 and Table 1, the specific impulses are in the range of 200 to 600 s, and both theory and experiments indicate the strong effect of high external pressure.

Additional experimentation performed after gathering the results reported above as well as the initial conceptual designs indicate that an attractive way to accomplish repetitive detonations is to employ a fluid high explosive initiated by a laser. A series of tests that use laser pulses with different characteristics as well as different explosives and hardware configurations for the protection of the frame structure and of the laser itself have shown much promise of leading to a realistic system integration. A further improvement in specific impulse is expected when the nozzle filling operation, after each pulse, is perfected so that the momentum loss during back filling is minimized.

Conclusions

It is apparent that the analysis and the results obtained to date in this work place the concept of a detonating propellant in a competitive position for propulsion in any spacecraft that is designed to operate, even to a limited extent, in a planetary atmosphere. Furthermore, the arguments presented in

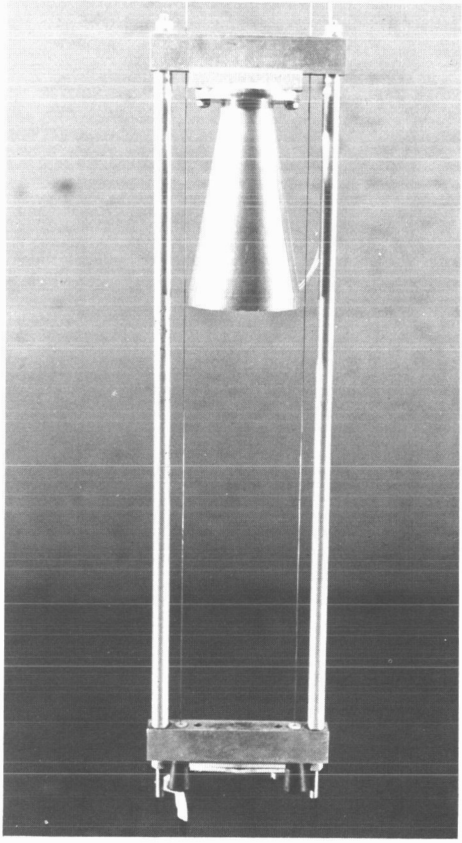

Fig. 3. Experimental device

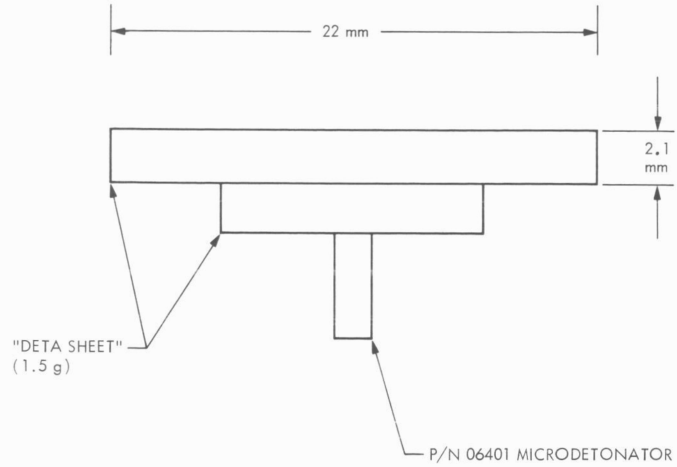

Fig. 4. Explosive configuration

the Introduction show that the acquisition of significant information about a large class of planets requires that the spacecraft penetrate the atmosphere. This makes a detonation motor a likely candidate for the propulsion systems of future spacecraft.

References

1. *Briefing to Advanced Propulsion Comparison Steering Committee, NASA*, Document No. 701-138, Jet Propulsion Laboratory, Pasadena, Calif., March 1, 1972 (JPL internal document).
2. *Venus Strategy for Exploration*, Report of a Study by the Space Science Board to the National Academy of Sciences, National Aeronautics and Space Administration, Washington, June 1970.
3. Sagan, C., "On the Origin and Planetary Distribution of Life," *Rad. Res.*, Vol. 15, 1961, pp. 174–192.
4. *Jupiter Atmospheric Entry Mission Study*, MCR-71-1, Martin Marietta Corp., Denver Division, Denver, Colo., 1971.
5. Sedov, L., *Similarity and Dimensional Methods in Mechanics*, Academic Press, London, 1959.
6. Back, L., Private communication based on unpublished results.

JPL Quarterly Technical Review Volume 3, Number 2, July 1973

Index: chemistry, fluid mechanics,
solid propulsion, thermodynamics

A New Look at AP/Composite Propellant Combustion

R. N. Kumar

California Institute of Technology[1]

This article presents some theoretical studies on the time-independent and oscillatory combustion of nonmetallized ammonium perchlorate (AP)/composite propellants. The study has for its aim a coherent and unified interpretation of the voluminous data available from experiments related to propellant combustion. Three fundamental hypotheses are introduced: the extent of propellant degradation at the vaporization step has to be specified through a scientific criterion; the condensed-phase degradation reaction of ammonium perchlorate to a vaporizable state is the overall rate-limiting step; gas-phase combustion rate is controlled by the mixing rate of fuel and oxidizer vapors. In the treatment of oscillatory combustion, the assumption of quasi-steady fluctuations in the gas phase is used to supplement these hypotheses. This study successfully predicts several experimental observations including a few that were inconsistent with previous theoretical results.

Introduction

Despite extensive applications that solid propellant rockets find, a theoretical understanding of the fundamental combustion processes has eluded researchers. Consequently, the performance predictions depend almost totally on empirical information whose limitations are always clear. However, a thorough theoretical study must necessarily start at the fundamental level, and hence on extremely simple propellant formulations that are far removed from the state-of-the-art technology. This apparent absence of immediate applications has provided very little incentive for fundamental theoretical studies. The extremely complex nature of the problem itself has undoubtedly aggravated this situation to a large extent.

In the present work, a study is made of ammonium perchlorate (AP), nonmetallized composite propellants. The objective is to identify the fundamental processes that are likely to be common to a variety of propellants and propellant applications. The motivation for the present

---

[1] Daniel and Florence Guggenheim Jet Propulsion Center

work comes from the observation that under normal conditions, the rate processes in the gas phase are likely to be much faster than those in the condensed phase. The present work differs from those available in the literature in three important aspects. The chemical kinetic degradation reactions in the condensed phase are explicitly included in the analytical treatment. The importance of a scientific criterion in specifying the extent of propellant degradation before vaporization is stressed, and it is shown that the usual arbitrariness is removed by applying the vapor pressure equilibrium criterion at the propellant surface. Lastly, the gas-phase chemical reactions are treated as wholly controlled by pressure-independent molecular mixing processes. It is found that the study predicts several of the features observed in AP/propellant combustion. Empiricism has been restricted to physical quantities whose values have been the subject of reasonable estimates in the past, and whose values should be within the grasp of experimental effort in the near future. The present work, which is best regarded as a feasibility study of research on a new path, has yielded very encouraging results in comparison with available experimental data. The same theory has, in addition, proved valuable in guiding and interpreting current experimental work (Ref. 1).

Physical Considerations

The fundamental physical structure of the present work is briefly discussed in this section.

It is of interest to know the mean molecular weight of the species leaving the propellant surface. This information is directly related to the extent of propellant degradation at the vaporization step, which, in turn, specifies the regression rate. In the combustion of AP/composites, the spectrum of possible species allowed by the chemical nature of the propellant is very rich. The mean molecular weight is an average over all of the species. However, by requiring that the species in the vapor phase, at the surface, be in vapor pressure equilibrium at the surface, the mean molecular weight may be determined (even without considering the chemical details of the species at the wall surface). After a study of American Petroleum Institute vapor pressure data (Ref. 2) on hydrocarbons, the following rule was evolved:

$$\mathcal{M} = \alpha P^{-\beta} \exp(\delta T_w) \qquad (1)$$

If P is in atmospheres, and T_w in K, the constants have the following values (to slide rule accuracy): $\alpha = 32.8$, $\beta = 0.2615$, and $\delta = 3.67 \times 10^{-3}$. The approximate nature of the extrapolations of this rule to AP/polymers from hydrocarbon data is recognized; but it is felt that for a simple physical quantity like the vapor pressure, the chemical nature of the molecules is not critically important. As a matter of fact, the experimental vapor pressures of heptane (Ref. 2) and methylmethacrylate monomer (Ref. 3), which have the same molecular weight of 100 g/g-mole, are very close over a range of temperature.

During the combustion of conventional AP/composite propellants, at a representative chamber pressure of 2×10^6 N/m^2, using the often-quoted value of 900 K for the wall temperature, we arrive (through Eq. 1) at a molecular weight of approximately 400 g/g-mole. This is much larger than the monomer molecular weights of most hydrocarbon fuel binders. If we consider AP deflagration alone, the value of 400 is not only much larger than the molecular weights of NH_3 and $HClO_4$ individually, it is much larger than the molecular weight of the (NH_4ClO_4) unit as well. Thus, it seems possible that microscopic fragments larger than a fuel monomer, or a (NH_4ClO_4) unit come off the surface. In polymer degradation studies, the presence of dimers, trimers, etc., has indeed been experimentally detected (Ref. 4). AP degradation studies have revealed the sublimation, as pure AP, under certain conditions. Even in experiments revealing the presence of NH_3 and $HClO_4$ species during the degradation of AP, it would seem logical to suppose that a crystal of AP (composed of many repeating units of NH_4ClO_4) would first degrade to smaller groups of NH_4ClO_4 before the final decomposition to NH_3 and $HClO_4$. In any attempt to experimentally determine the actual fragment size at the wall, it should be remembered that the entire process of propellant burning involves reacting species and that rapid quenching of all reactions is necessary, immediately after the species enter the vapor phase, to study the species leaving the surface. The mean fragment size of the species leaving the surface as a multiple of the fundamental repeating unit (in the condensed phase) will be designated the fragment size vaporizing, or simply *FSV*. The concept of *FSV* is a convenient (physically realistic) way of representing a more fundamental parameter in propellant combustion, namely the extent of degradation at the vaporization step. For a given backbone structure, the number of unbroken backbone bonds remaining in the fragments vaporizing is uniquely related to the *FSV*.

Now we consider the condensed phase reactions. In its unaffected state, AP (or the fuel) may be looked upon as a large "molecule" made up of the fundamental building blocks (NH_4ClO_4) (or the fuel monomer unit). Since the vapor pressure equilibrium criterion indicates that the *FSV* is approximately 2 to 10, under normally encountered chamber pressures, the question of the process by which the large "molecules" degrade into *FSV* arises naturally. As shown in Fig. 1, the propellant material in its travel from the deep solid region ($x \to \infty$) to the wall ($x = 0$) degrades from its unaffected (large molecular weight) state to vaporizable (small molecular weight) state. The reactions that bring about this degradation are therefore assumed to take place wholly within the condensed phase. Following the numerous studies on the degradation of AP (Ref. 5) and of polymeric fuels (Ref. 4), the degradation reactions are taken as first order Arrhenius reactions.

It is now necessary to consider the mechanistic details of the subsurface degradation of AP to relate the fundamental isothermal degradation rate of a homogeneous mass of AP to the degradation of macroscopic AP particles in

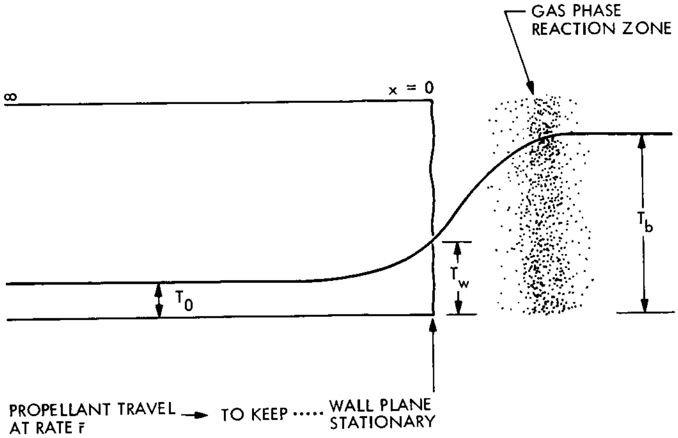

Fig. 1. General scheme of propellant combustion

the heterogeneous configuration in the propellant. The site of the active degradation of the AP particles in the solid is assumed to be a thin melt layer on the surface of AP particles. (It is to be clearly understood that such a model is put forward only as an "average" representation of the postulated physical phenomenon. The model is not to be interpreted too literally. If analogies help, it is suggested that the present model (shown in Fig. 2) be regarded in the same vein as the "plane" wall at the surface or the familiar flame "sheet", both of which are known to be inconsistent with physical reality, but nevertheless have proved extremely useful for analytical representation.) Assuming that the AP degradation is brought about by a reactive species that diffuses into the melt layer, the reaction rate is taken as directly proportional to the chamber pressure. Pressure-dependent degradation of AP has indeed been experimentally observed (Ref. 6), thus enhancing the credibility of the present model.

Next we consider the details of gas-phase processes in propellant burning. At atmospheric pressures the characteristic chemical kinetic time for air/hydrocarbon flames is of the order of 10^{-4} s. At much higher pressures, as in propellant burning, we expect the characteristic reaction times to be much smaller. The characteristic transport/mixing time (ratio of the combustion zone stand-off distance to the mean velocity of the vapors) in the burning of a composite propellant is of the order of 10^{-4} s. While these estimates are not conclusive, the general trend appears to be in favor of transport/mixing control and not of chemical kinetic control of the gas phase rate-limiting process. (It is to be remembered that the oxidizers used in propellant are much more powerful than air). In any case even the mixing time of 10^{-4} s is much too small in comparison with the typical time scale in the *condensed phase* (10^{-3} s). Thus the *overall* rate-limiting reactions in propellant burning are very likely to be in the condensed phase. Such a belief is consistent with the general feeling that among the three zones of interest to propellant

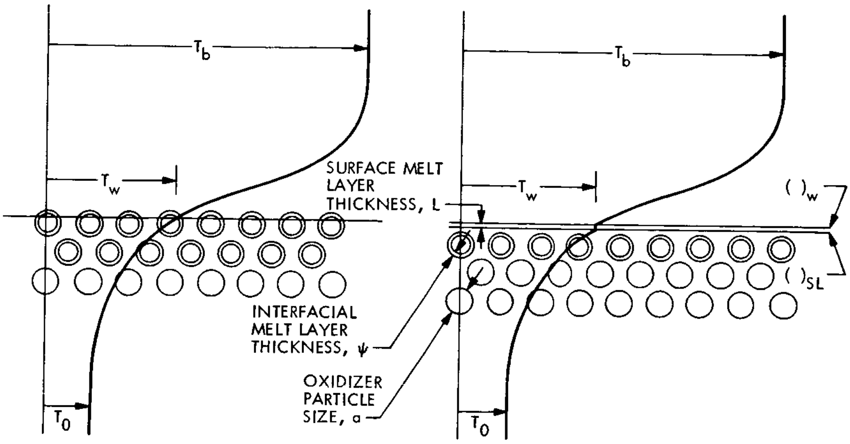

Fig. 2. Details of the postulated model for composite propellant combustion: (a) subsurface reactions only; (b) surface reactions in a melt layer augmenting subsurface reactions

combustion (high temperature vapor-phase, medium temperature gas/solid interface, and low temperature condensed phase) the processes in the condensed phase are probably the slowest.

The reactants burn in a nonpremixed combustion zone in the vapor phase except in the following two cases:

(1) Gas phase chemical-kinetic rates become very low because of very low pressures or special ingredients, so that molecular mixing processes take the gases to a premixed state before combustion.

(2) A thorough mixing of fuel and oxidizer takes place in a surface layer on the propellant before they enter a vapor phase.

It is seen in what follows that the simplest model of the gas phase combustion zone (treated like a "black box") is adequate for our purposes.

Numerical Values of Constants

The following values have been consistently used throughout this work (Ref. 7 has the explanation):

(1) Thermal diffusivity:

Pure polymer base	10^{-3} cm^2/s
Normal AP composites with heavy AP loading	1.1×10^{-3} cm^2/s
Pure AP	1.5×10^{-3} cm^2/s

(2) Fundamental rate data on pure AP (Ref. 5, p. 41):

$$B = 9.2 \times 10^7 \text{ s}^{-1}$$

$$E = 121.1 \times 10^3 \text{ J/mole}$$

(3) Heat of degradation D [Ref. 8]:

$$D = 2{,}450 \text{ J/g}$$

The remaining task is essentially mathematical analyses, along with the treatments of some details that arise naturally. The analyses are not presented in this article due to limitations of space. (They are available in Ref. 7.) Since a majority of AP composites are heavily loaded (≈80%) with ammonium perchlorate, the behavior of AP by itself is pursued in some detail in the following section. The time-independent combustion of composite propellants, and the oscillatory combustion of composite propellants are treated separately; the concluding remarks complete this article.

Degradation and Deflagration of Ammonium Perchlorate

The aim of this section is the theoretical prediction of the linear regression rate of AP as a function of chamber pressure (or other experimentally determined conditions). In the coordinate system used (Fig. 1), the wall surface is held stationary. We follow the changes in a plane (dx) as it moves up with time from deep solid ($x = \infty$) to the wall ($x = 0$). The temperature of the layer increases from the deep solid value (T_0) to the wall temperature (T_w); the mean fragment size of the AP changes from a very large value (approaching "infinity" for practical purposes) at T_0, to FSV at the wall, $(\ )_w$.

Following the numerous studies in the field, the degradation of AP is modeled as a first-order Arrhenius reaction. The pre-exponential factor is taken as directly proportional to the pressure in the molten state (discussed later), and independent of pressure in the solid. The cases of subsurface reactions only and surface reactions augmenting subsurface reactions are treated separately.

Although we are interested at present in the steady state only, the full (time-dependent) equations are written down since these are needed later in the analysis of oscillatory burning.

Energy:

$$k\frac{\partial^2 T}{\partial x^2} + c\rho r\frac{\partial T}{\partial x} - \rho c\frac{\partial T}{\partial t} = D\rho NB\exp(-E/\mathscr{R}T) \qquad (2)$$

Bond Conservation:

$$-\frac{dN}{dt} = NB\exp(-E/\mathscr{R}T) \qquad (3)$$

Boundary Conditions:

$$\left.\begin{array}{llll} x = 0: & T = T_w; & x = \infty: & T = T_0 \\ x = 0: & N = N_w = 1 - \dfrac{1}{FSV}; & x = \infty: & N = 1 \end{array}\right\} \qquad (4)$$

The regression rate eigenvalue (r) is thus determined by a solution of the above nonlinear system of equations. The activation energy E has a value like 125×10^3 J/mole, while the maximum temperature (which is at the wall) is like 900 to 1000 K. Hence, $E/\mathcal{R}T$ is at least 10 to 15. This implies that the right hand sides of Eqs. (2) and (3) assume exponentially small values even at short distances from the wall. Such a behavior is particularly suited for a matched asymptotic analysis (Ref. 7), the final result from which is

$$r = \left[\frac{(k/\rho c)\,B\exp\left(-E/\mathcal{R}T_w\right)}{(E/\mathcal{R}T_w)\left(\dfrac{T_w - T_0}{T_w}\right)\left[\left\{\dfrac{D}{c\,(T_w - T_0)} + 1\right\}\ln\left(\dfrac{FSV}{FSV - 1}\right) - \dfrac{D}{c\,(T_w - T_0)\,FSV}\right]}\right]^{1/2} \qquad (5)$$

Recalling that the above result does not include surface (heterogeneous) reactions, we should compare the results from experiments where there is little possibility of such surface reactions. The familiar hot-plate experiments come under this category. However there are indications that a criterion other than the vapor pressure equilibrium criterion is needed to specify the fragment size at the wall, because there exists no clearly-defined equilibrium interface between a condensed-phase and a vapor-phase. A mechanical strength criterion seems more appropriate. That is, as the material degrades from deep within the solid, a plane is reached where the increasing temperature and decreasing physical strength force the material out of the surface. It was seen (Ref. 9) that a constant molecular weight of 900 appears to match experimental data very well for the polymer PMMA in such hot-plate experiments. A molecular weight like 900 corresponds to an FSV value like 7 to 8 for AP (fundamental molecular weight of $NH_4\,ClO_4$ is 117.5 g/g-mole), and a value of 8 is used in the present study. At these high values of FSV, 7 or 8 will not make more than about 7% difference in the final regression rate (Eq. 5), an error that is much smaller than the general levels of uncertainty in such experiments.

Presented in Fig. 3 are the experimental data points collected by Powling (Ref. 10) from many different sources. The theoretical prediction (Eq. 5) is also plotted. Good agreement is evident. It is noted that because of the square root factor in Eq. (5), an overall activation energy of nearly 62.5×10^3 J/mole would be inferred by forcing an Arrhenius expression through the hot-plate data points. Actually, such curve fit procedures grossly average the fundamental processes. The valid procedure is to use the isothermal Arrhenius parameters (obtained from experiments on very small samples of AP) in Eq. (5), as has been done here.

While the hot-plate data support the model, several inconsistencies arise when an attempt is made to generalize the above model to self-deflagration

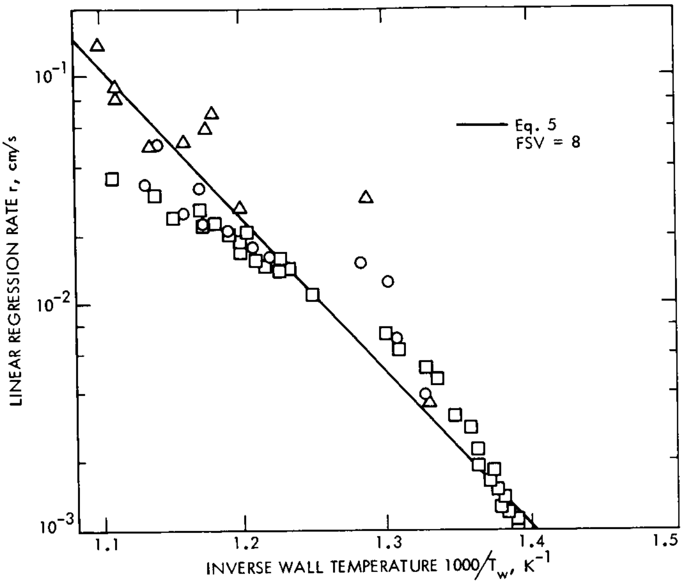

Fig. 3. Theoretical predictions for AP, and comparisons with the hot-plate data from Powling (Ref. 10)

flame-heated AP. The disagreements noted in Ref. 7 lead us to the following picture.

Since pressure dependence is an important aspect of self-deflagration, and since pressure-dependent reactions are difficult to visualize in the solid state, let us make the simple postulate that *surface degradation in a melt layer aids subsurface thermal degradation in producing vaporizable fragments and that at high pressures it completely overwhelms the subsurface contribution.* The experimental observation of a "liquid" layer on the surface of deflagrating AP (Ref. 11) lends credence to such a picture.

With the above physical picture, the value of the linear regression rate is given by the equation,

$$r = \frac{\text{Fundamental degradation rate in the melt layer of thickness } \ell}{\text{The number of bonds to be broken}} \qquad (6)$$

With the scheme of a first-order reaction, the degradation rate of the mass of AP in the melt layer depends on the extent of degradation in the melt layer, which is represented by the mean fragment size of AP in the melt layer. Consistent with the experimental evidence (Ref. 5) of considerable activity in the melt layer, a uniformly mixed layer is assumed. The arithmetic mean fragment size is used for the AP fragments in the melt layer. However, the fragment size *at the vaporization step* is specified by

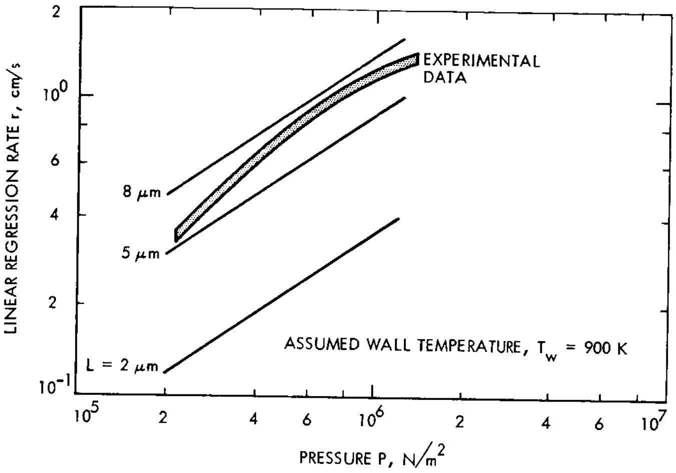

Fig. 4. Linear regression rate of self-deflagration flame heated AP and comparison with experimental data (Ref. 11)

the vapor pressure equilibrium rule. It is shown (Ref. 7) that the linear regression rate can be written,

$$r = \ell\,(FSV - 1/2)\,B_0\,(P/P_0)\exp(-E/\mathscr{R}T_w) \tag{7}$$

Predictions through Eq. (7) are compared with experimental data (Fig. 4) for three assumed values of the melt layer thickness ℓ. A constant value of the melt layer thickness (between 5 μm and 8 μm) is seen to match the experimental data quantitatively. However, since the melt layer thickness ℓ decreases with increasing regression rate (increasing pressure) as shown in Ref. 7, this agreement should be due to self-compensating effects of slight increase in wall temperature with pressure (Ref. 12) and the decrease in the melt layer thickness.

To explore the effects of initial temperature, it is noted that Eq. (5) is applicable for the solid phase below the melt layer; however, the fragment size at the solid-liquid interface (called *FSSL*) has to be used in place of *FSV*. Equation (5) predicts the dependence on initial temperature T_0 as

$$r \propto 1/[(T_w - T_0)/T_w]^{1/2}$$

The ℓ = 5 μm curve in Fig. 4 is plotted in Fig. 5 for three different values of T_0. The experimental data of Ref. 13 are also presented.

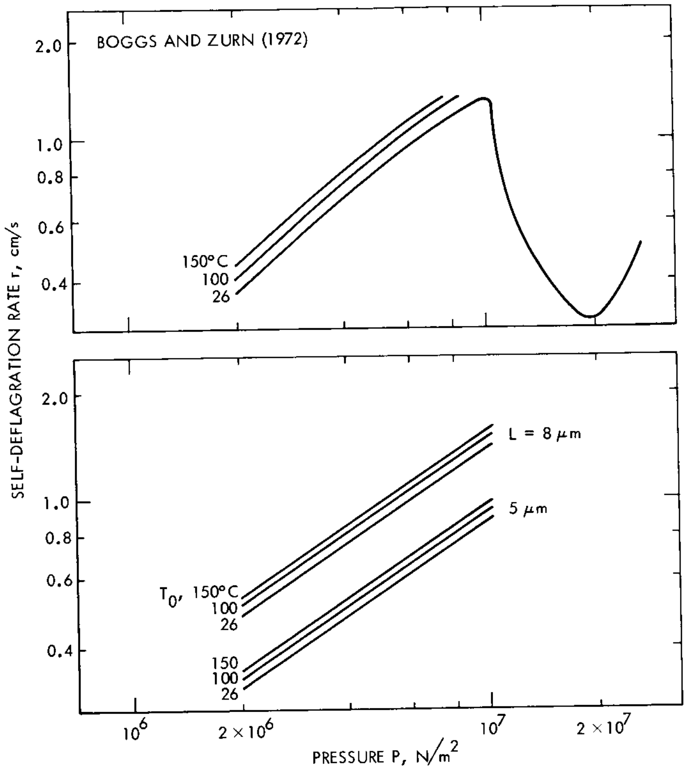

Fig. 5. Linear regression rate of self-deflagration flame heated AP and comparison with experimental data (Ref. 13) on initial temperature sensitivity

A striking feature of single crystal AP self-deflagration experiments is the abrupt dip in the regression rate that is observed around 1.38×10^7 N/m^2. The thickness of the melt layer used in this treatment is observed to (Ref. 5), and can be theoretically shown to (Ref. 7), decrease with increasing regression rates at a constant wall temperature. Finally, at a high enough regression rate, the melt layer may occupy only a very small portion of the surface. (In the ideal one dimensional picture, the melt layer disappears completely.) When this happens, the degradation by the reactive species becomes very slow because mobility through the solid is *much* slower than through a liquid. The process of degradation is now more likely to be controlled completely by subsurface thermal degradation. A marked drop in the regression rate may be expected after such a point is reached. An exploratory calculation has indicated that the sudden dip observed experimentally (around 1.38×10^7 N/m^2) may indeed be due to such a phenomenon.

Time-Independent Combustion of Composite Propellants

The hypotheses and principal conclusions from the previous sections are applied to the problem of composite propellant burning. We continue to consider only those cases in which chemical kinetic rates of combustion reactions in the gas phase are far greater than transport and mixing rates; the overall rate controlling reactions (viz., fundamental degradation of AP) occur in the condensed phase. The concept of *FSV* is generalized to include multicomponent vapor phase/condensed phase equilibrium. It is required to include the degradation kinetics of the binder as well. The influence of burning rate catalysts is examined in the light of the same model used for uncatalyzed propellants; the increased reaction rate in a surface layer accounts for the increased regression rate. The effect of the oxidizer particle size is studied in the simplest manner. In the condensed phase, its effect is introduced as variations in the surface area for the degradation of AP. The regression rate is predicted (by a slightly modified version of Eq. 5) as a function of the chamber pressure and the wall temperature. The case of the subsurface reactions only, and the case of surface reactions augmenting subsurface reactions are treated separately.

To render the system self-determined, it is required to specify the wall temperature through gas-phase energetics and fluid mechanics. For this purpose, the familiar one-dimensional gas phase model is invoked. In the absence of a satisfactory theory for the gas phase details, the two limiting cases considered here both lead to results sufficiently close to reality.

Rate-Controlling Reactions in the Subsurface Region

We start with the assumption that *the rate-controlling reactions (AP degradation) occur in a thin layer on the surface of AP crystals in the solid.* The propellant material is represented as homogeneous for the purposes of heat transfer calculations. The process of heat conduction is assumed to be adequately represented by Fourier's law with a properly averaged material property of thermal conductivity. It is necessary to have the above picture clearly understood to prevent the extrapolations of the results beyond their limits of validity. For example, the homogeneous solid assumption does not appear to be valid when the characteristic thermal depth in the solid (κ/r) becomes far less than the oxidizer particle size (a). That is, at high regression rates (and hence at high pressures) the results need careful interpretation.

When we consider the differential element dx in the analysis, and write the reaction rate in that element, we have to properly consider the actual volume in the differential element in which the degradation reactions are taking place. As a first approximation, a unimodal distribution of spherical AP particles is assumed. If the reactions take place in a layer of thickness ψ on the surface of AP particles, the volume of AP undergoing degradation reactions per particle is very nearly equal to $\pi a^2 \psi$, where a is the diameter of the AP particles. The physical volume of the AP particle is $\pi a^3/6$. If v is the volume fraction of AP loading in the propellant, the volume fraction undergoing degradation is $(6\psi v/a)$, so that the reaction rate in the layer of thickness dx is multiplied by this factor. The rest of the analysis is identical with that for a homogeneous solid. Hence, we substitute the above factor into Eq. 5 and obtain:

$$r = \left\{ \left(\frac{6\psi v}{a} \right) \frac{(k/\rho c)(B_0 P) \exp(-E/\mathcal{R}T_w)}{(E/\mathcal{R}T_w) \left(\frac{T_w - T_0}{T_w} \right) \left[\left\{ \frac{D}{c(T_w - T_0)} + 1 \right\} \ln \left(\frac{FSV}{FSV - 1} \right) - \frac{D}{c(T_w - T_0) FSV} \right]} \right\}^{1/2} \tag{8}$$

It is carefully noted that the value of $(k/\rho c)$ is that of the propellant and *not* of AP alone. The value of ψ is left as a parameter. For specifying the FSV through the vapor pressure equilibrium criterion, the statistical mean fragment size has to include averaging over the binder species also. The assumption of a plane regressing wall requires that the regression rate of the binder in the propellant has to equal the regression rate of the AP in the propellant. The regression rate of the binder is predicted by Eq. (5) if the thermochemical constants used in Eq. (5) are those of the binder material. For a typical binder (CTPB) and typical numerical values of the composite propellant characteristics, the predictions are presented in Fig. 6.

Joint Rate Control by Subsurface and Surface Reactions

The assumption of subsurface reactions alone is insufficient to account for all of the experimental observations. It is suggested that under certain circumstances surface reactions in a thin layer augment subsurface reactions. After the material reaches the plane SL (Fig. 2b) in its travel from the deep solid region (∞) to the surface, the binder and the oxidizer mix thoroughly in a melt layer of thickness L. This well stirred layer is assumed to be isothermal. In the case of catalyzed propellants, the catalyst is taken as inactive in the subsurface region (below the plane SL) and active in the surface layer. (The catalyst, for its action, has to mix well with the propellant on the microscopic level, a process that is difficult to visualize in the solid, but seems natural in the melt layer.) The regression rate eigenvalue determined by the subsurface reactions has to equal the regression rate determined by the surface reactions. The numerical solution for a typical case is presented in Fig. 7. The curves of regression rate versus pressure with L as a parameter may be considered the same as curves with the surface degradation rate as a parameter (possibly through catalysis), since the ultimate effect of either of the two is felt the same way in the regression rate. Since it is known that the melt layer thickness decreases with increasing regression rate, the regression rate versus pressure curve is likely to have the shape shown by the broken line in Fig. 7. Propellants with binders that *melt readily* have indeed been known (Ref. 14) to exhibit such a decreasing n behavior.

Gas Phase Details

In the combustion of propellants the wall temperature is determined by the interaction of the solid phase with general fluid dynamics and energetics

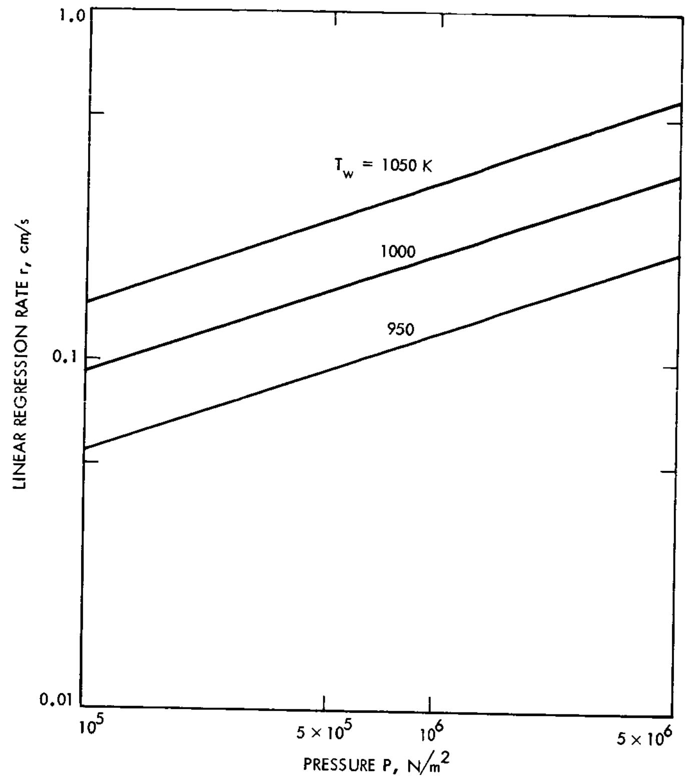

Fig. 6. Theoretical predictions for a typical composite propellant considering subsurface reactions only (mass fractions: 0.75 AP, 0.25 CTPB; AP particle size, a = 90 μm, interfacial reaction layer thickness, ψ = 5 μm)

of the gas phase. The detailed solution depends on the assumptions we make regarding mixing and combustion.

It is difficult to characterize the gas phase above the burning composite as either laminar or turbulent. For double base propellants (*and* for composites having extremely fine oxidizer particles) there appears to be little room for doubt regarding the existence of laminar flow, simply from Reynolds number considerations. For normal composite propellants, photographs of the combustion zone reveal that the gas phase is far from being laminar. There are present "spots" that give rise to transport and mixing on a scale far larger than molecular. However, the flow field may not merit the use of the word "turbulent" in that the origin of the large-scale spottiness has little to do with classical Tollmien-Schlichting instability. Moreover, and this is an important consideration, it is difficult to conceive of an exchange mechanism that would establish the standard turbulent energy spectrum that incorporates proven features such as, for example, Kolmogorov and Heisenberg limits. These thoughts render inapplicable a host of useful empirical rules that fluid dynamicists have evolved on flows that are truly turbulent. The

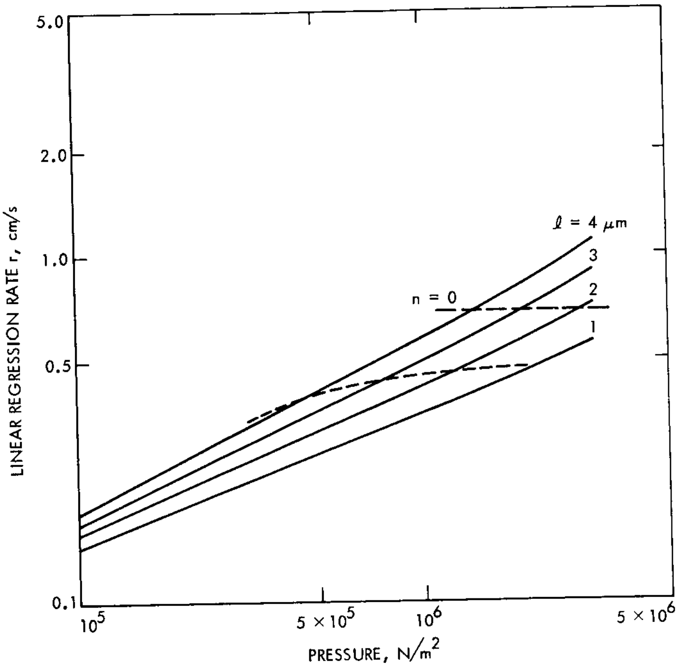

Fig. 7. Theoretical predictions for a typical AP composite propellant. Surface reactions in a melt layer (of thickness ℓ) augementing subsurface reactions

point to note is that we can not assume the flow to be *turbulent* simply because it is *not laminar.*

Two limiting cases are considered for the treatment of the gas phase here.

Case 1: The familiar flame-sheet approximation; no combustion until the gases have traversed a distance x^* from the surface, and complete combustion in a negligible distance after x^*.

Case 2: Uniform combustion at a constant rate $\dot{m}'''$ (g/cm^3-s) starting from the solid-gas interface plane $(\ )_w$.

Case 2, above, is recognized as the familiar concept of "well stirred reactor". Since the combustion rate is controlled by the molecular mixing processes, the gravimetric reaction rate may be taken as directly proportional to the density of the gases. Since, in the range of normal interest, the combustion temperature does not vary appreciably with mean pressure, it is seen through the state equation that the reaction rate $\dot{m}'''$ is directly proportional to the pressure (that is, $\dot{m}''' = A \cdot P$, where A is a constant).

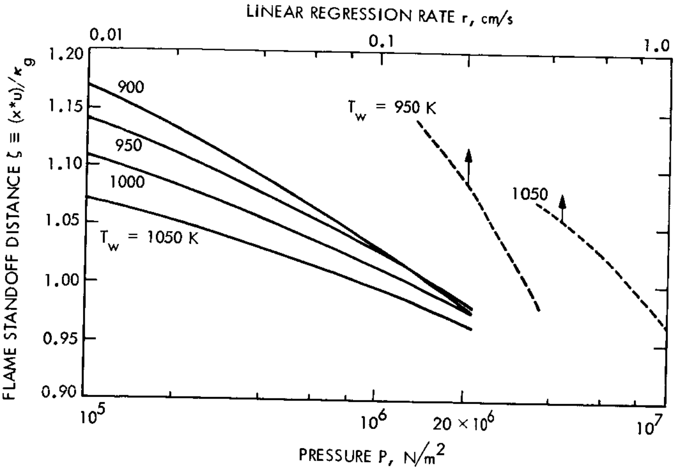

Fig. 8. Variations in flame standoff distance for a typical composite propellant within the flame sheet approximation (flame temperature T_b = 2750 K)

A solution to the energy equation applied between the wall plane $(\ )_w$ and the flame sheet $(\ )_b$, using the matching condition that the heat flux into the solid has to match the heat balance at the wall, yields the details of flame standoff distance (x^*) variations with pressure, with the wall temperature as a parameter. The results are presented in Fig. 8 for a typical case.

For the other case of uniform combustion, the solution requires the value of the reaction rate $\dot{m}'''$ which has been taken from Ref. 7. The solutions to the one-dimensional energy equation are presented in Figs. 9 and 10 and show the linear regression rate (r), wall temperature (T_w) and the distance of the plane of complete combustion (analogous to the earlier x^*) for a typical propellant for assumed values of the various parameters. In comparison with predictions based on the assumption of constant wall temperature/flame sheet, the general behavior is not appreciably different quantitatively or even qualitatively. It would appear that the actual model employed for the gas phase processes is not crucially important in determining the general trends so long as the overall rate controlling reactions occur in the condensed phase. Such a conclusion was anticipated earlier purely on physical grounds.

Oscillatory Burning of Composite Propellants

The role of the propellant in pressure-coupled instability is thought, at the present time, to be well represented by the response function, defined as

$$\mathscr{R} \equiv \frac{\tilde{\mu}}{\tilde{\epsilon}} = \frac{r'}{\bar{r}} \cdot \frac{\bar{P}}{P'}$$

with the familiar nomenclature. On the theoretical side, the numerous derivations of the response function have been shown to be essentially identical (Ref. 16), since the fundamental assumptions in the various analyses are identical. On the experimental side doubts exist regarding proper processing of the measured variables to yield the real part of the response function. Nevertheless, some of the general trends in the experimental response functions are thought to be well understood. (That is, comparisons of theory with experiments *are* meaningful.) The response function is usually found to be dependent upon the mean pressure, contrary to theoretical predictions. There exist experimental data that show very large values for the response function at low frequencies, while theoretical predictions suggest that the response function must tend to the limit of the steady-state pressure index (n), in the limit as frequency tends to zero.

In this section the response functions for model composite propellants are derived considering the two cases of subsurface reactions only, and surface reactions in a melt layer augmenting subsurface reactions; the gas phase fluctuations are modeled under the two cases of adiabatic processes and uniform combustion. These theoretical predictions are found to be consistent with several experimentally observed features including the mean-pressure dependence.

Subsurface Reactions with No Surface Reactions

The temperature change across the reaction zone is of the order of reciprocal activation energy parameter (i.e., $1/\theta_a$, with $\theta_a \equiv E/\mathscr{R}T_w$). This reaction zone has a physical thickness $\sim \kappa/\bar{r}\ \theta_a$. Thus, so long as we restrict our attention to small amplitude ($\sim 1/\theta_a$) fluctuations, the effect of the mean temperature variation across the reaction zone is a second order quantity that need not be included in a first order analysis. That is, if we visualize a (hypothetical) freezing layer below which chemical reaction rates are negligible compared to other processes, we can neglect the effects of the mean temperature variations between the wall and the freezing layer on fluctuations of temperature. Also, phase differences in variables may be neglected across the reaction zone except at very high frequencies. This fact can be exploited to write the exact expression for the wall boundary condition. We first use a coordinate frame of reference held fixed at the mean position of the fluctuating wall (or the freezing layer). We obtain the outer solution, neglecting the reaction term. This exact solution is then used to write the temperature-gradient boundary conditions both at the freezing layer (the interface between the "inner" and the "outer" regions) and on the

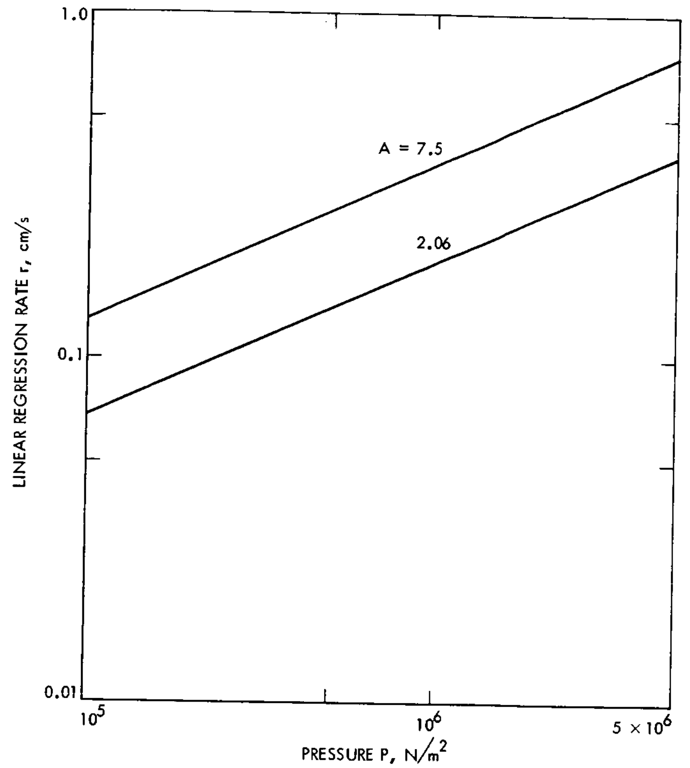

Fig. 9. Theoretical predictions for a typical composite propellant considering subsurface reactions only. The assumption of uniform combustion in the gas phase ($\dot{m}''' = AP$)

wall. Then we solve for the time-dependent regression rate in a manner analogous to the time-independent case. That is, we solve the full equation, including explicitly the Arrhenius reaction rate term in the "inner" region.

The analysis is then generalized to include the case of surface reactions augmenting the subsurface reactions.

After considerable algebra, detailed fully in Ref. 7, the response functions derived on the basis of condensed phase analyses are written.

$$\mathcal{R} \equiv \frac{\left(\frac{r'}{\bar{r}}\right)}{\left(\frac{P'}{\bar{P}}\right)} = \text{fn}\left[\Omega, \lambda, \bar{\theta}_a, \frac{\tau_w'}{\left(\frac{r'}{\bar{r}}\right)}, R_i\right]$$

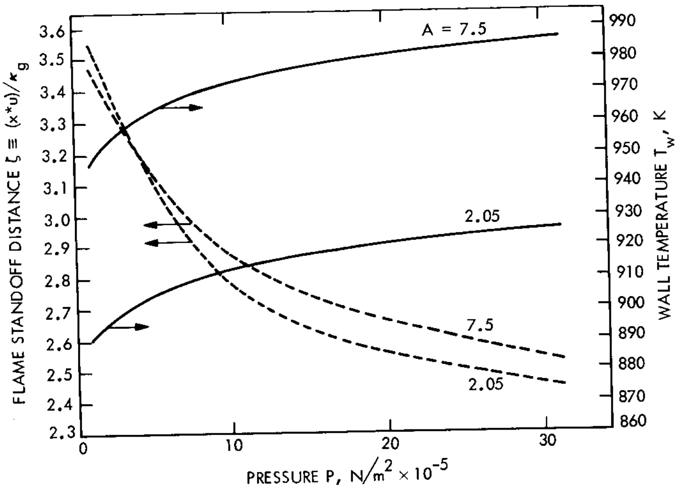

Fig. 10. Variations in flame standoff distance and wall temperature for a typical composite propellant within the uniform combustion approximation

where

Ω is the normalized frequency ($\equiv \omega\kappa/\bar{r}^2$)

λ is the normalized mean regression rate

$\bar{\theta}_a$ is the reduced activation energy parameter ($E/\mathcal{R}\bar{T}_w$)

$\tau_w{}'$ is the normalized amplitude of wall temperature fluctuations

R_i are constants dependent, for most part, on steady-state parameters in propellant burning.

The analysis of condensed phase details alone leaves the variable $\tau_w{}'$ to be specified from an analysis of the gas phase details. The same two models (flame sheet approximation and uniform combustion) used in time-independent combustion are used in the oscillatory case along with the assumption of adiabatic fluctuations at the flame sheet in the former model.

Surface Reactions Augmenting Subsurface Reactions

Considering the condensed phase details only, the case of surface reactions augmenting subsurface reactions is very similar to that of steady-state combustion (Fig. 2b). The only difference from the steady burning case is that the *fluctuating* part of the regression rates in the subsurface region and the surface melt layer need not be equal to each other, as the *steady* part of the regression rate has to be. The difference between the fluctuating parts of the regression rate in the surface and subsurface regions shows up as fluctuations in the thickness of the melt layer. In the time-independent combustion of composite propellants, the surface melt layer thickness (L) during time-independent combustion was supplied from considerations external to the condensed phase analysis. In the oscillatory case here we consider two limiting conditions: (1) the melt layer thickness is constant even during unsteady combustion, (2) the subsurface regression rate fluctuation vanishes and hence, all the fluctuation in the regression rate is entirely due to the fluctuating melt layer.

As shown in Fig. 11, six response functions are possible for the six models postulated here; all six of them are derived in Ref. 7. At the time of the present article, some of the details pertaining to the case of adiabatic fluctuations in the gas phase, with subsurface reactions only, are being carefully scrutinized and are not presented here. Three of the other five response functions are presented in Figs. 12, 13, and 14. The model propellants considered here are the same ones for which steady combustion rates were presented earlier.

A distinct feature of the present response functions is that they exhibit dependence on mean chamber pressure. As explained earlier, the pressure dependence during time-independent combustion arises from two independent processes: pressure-dependent degradation reactions, and the vapor pressure equilibrium effect. Due to phase differences among the various fluctuating quantities, it is possible for these two effects to be differently affected during oscillatory combustion as compared to time-independent combustion. The dependence on mean chamber pressure of the derived response functions is due to such an effect. For the special case of a zero-n propellant, strong oscillatory combustion is possible again for the same reason.

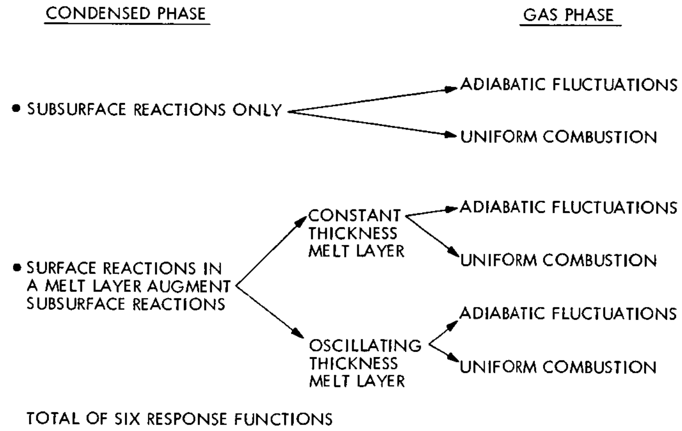

Fig. 11. General scheme of response function derivations in the present study

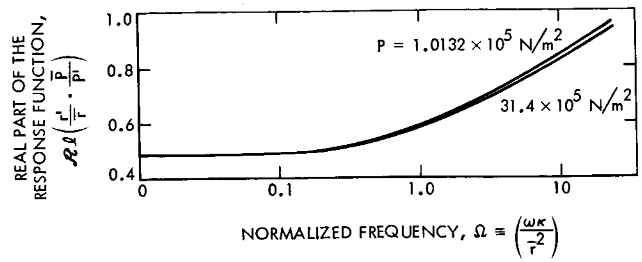

Fig. 12. Typical theoretical response functions of the present study, Example 1: subsurface reactions with no surface reactions, uniform combustion in the gas phase

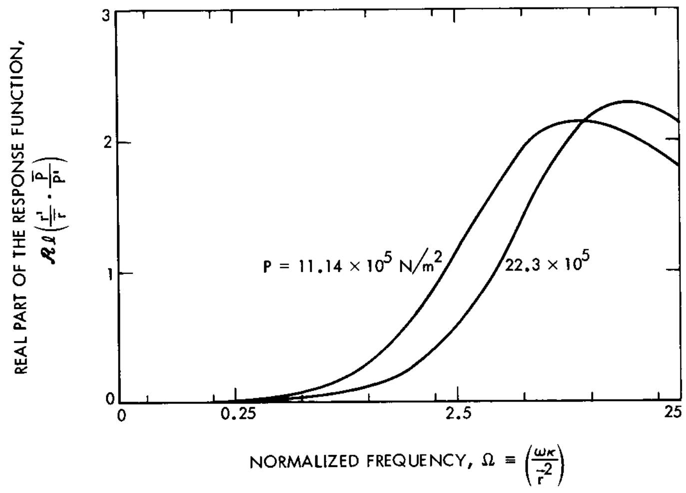

Fig. 13. Typical theoretical response functions of the present study, Example 2: surface reactions in a melt layer of fluctuating thickness, fluctuating part of regression rate due to subsurface reactions zero, adiabatic fluctuations in the gas phase

Two features of the present calculation are worth repetition. Simplifications were introduced by limiting our attention to moderate frequencies, so that the interpretation of the theoretical results above a nondimensional frequency (Ω) of 10 is questionable. Secondly, for the purposes of heat transfer calculations, the assumption of a homogeneous solid was made. That is, the assumption of the characteristic linear dimension (effective thermal

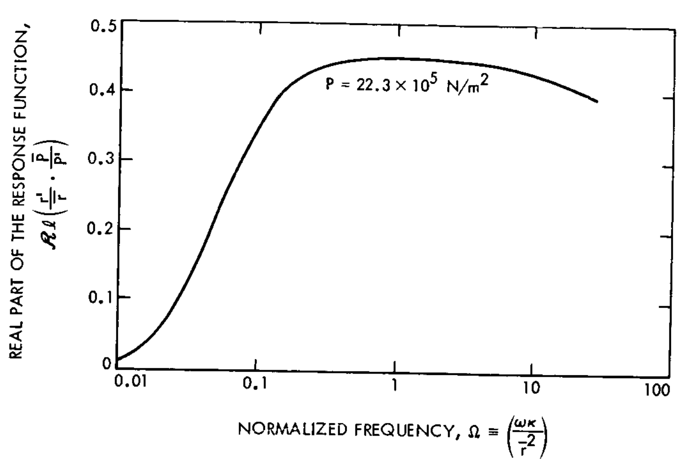

Fig. 14. Typical theoretical response functions of the present study, Example 3: a propellant having n = 0; uniform combustion in the gas phase

depth, $\sim\kappa/\bar{r}$) associated with the heat transfer process in the solid being far larger than the characteristic linear scale (oxidizer particle size, a) associated with solid heterogeneity is inherent in all of the present derivations. Since the thermal diffusivity (κ) may be taken as constant during the small variations, if any, in the wall temperature, the assumption of a homogeneous solid becomes questionable at high regression rates and hence at high pressures. This is an important consideration amply appreciated during the current experimental studies at JPL.

Examining reported experimental data on the response functions of composite propellants (Refs. 15 and 17), we note several similarities with the present theoretical predictions.

Conclusions

The present work on the combustion of AP/composite propellants leads to the following conclusions.

(1) The assumption of condensed-phase degradation of AP being the rate-limiting step in the overall pyrolysis of AP leads to theoretical results that match well with experimental hot-plate data.

(2) The hypothesis of pressure-dependent (condensed phase) degradation of AP in a surface layer controlling the overall regression rates of AP/composite propellants leads to predictions in agreement with experimental data covering both single-crystal AP self-deflagration and composite propellant combustion.

(3) The extent of degradation at the vaporization step can be specified through the vapor pressure equilibrium criterion.

(4) The hypothesis of gas-phase combustion rate completely determined by pressure-independent diffusive-mixing processes leads to analytical results in agreement with experimental trends.

(5) The response function of a composite propellant can be theoretically derived through the method of "inner" and "outer" expansions including explicitly the nonlinear (Arrhenius) degradation rate term in the condensed phase.

(6) The response functions so derived exhibit dependence on mean pressure, strongly so with the model of adiabatic fluctuations and weakly with the model of uniform combustion in the gas phase.

(7) A "zero-*n*" propellant *can* exhibit fairly strong instability behavior.

(8) A few unifying concepts enable us to coherently interpret a host of superficially diverse data.

The gas phase processes in composite propellant combustion form the darkest area in the field, and further research is badly needed to illuminate this important facet.

Nomenclature

A	constant in the uniform combustion law, g-cm^{-3}-s^{-1} (10^5 N/m^2)$^{-1}$
a	mean size of the oxidizer particles in the composite propellant, cm
B	pre-exponential factor in the Arrhenius law for thermal degradation, s^{-1}
c	specific heat, J-g^{-1}-°C^{-1}
D	heat of degradation of the solid, i.e., heat required to convert 1 g of the polymer (or crystal) into 1 g of the individual repeating units, J-g^{-1}
E	activation energy for thermal degradation, J-mole^{-1}
FSV	statistical mean fragment size vaporizing, dimensionless
$FSSL$	statistical mean fragment size at the solid-liquid interface, dimensionless
k	coefficient of thermal conductivity, J-cm^{-1}-s^{-1}-°C^{-1}
L	thickness of the surface melt layer in composite propellant combustion, cm
ℓ	thickness of the surface melt layer in the self-deflagration of AP single crystals, cm
$\mathcal{M}$	molecular weight, g • (g-mole)$^{-1}$

$\dot{m}'''$	gas phase combustion rate during uniform combustion, g-cm^{-3}-s^{-1}
N	fractional number of backbone bonds referred to the number in the undegraded state, dimensionless
n	empirical index of pressure in the steady burning rate law for propellants, dimensionless
P	pressure, N/m^2
R_i	constants (with $i = 1, 2, 3, \cdots$) used for shorthand notations, dimensionless
$\mathscr{R}$	universal gas constant, J-mole^{-1}-°C^{-1}
$\mathscr{R}$	complex (pressure) response function, dimensionless
r	linear regression rate, cm-s^{-1}
T	temperature, K
t	time coordinate, s
u	gas (mass flow) velocity above the burning propellant, cm-s^{-1}
v	volume fraction of oxidizer in a composite propellant, dimensionless
X, x	distance coordinate, cm
x^*	flame standoff distance, cm
α	empirical constant in the *FSV* rule, (N/m^2)$^\beta$
β	empirical index of pressure in the *FSV* rule, dimensionless
δ	empirical constant in the *FSV* equation, K^{-1}
ϵ	a small parameter used in the expansions; any first order quantity; $r'/\bar{r}$, dimensionless
ζ	normalized flame standoff distance, dimensionless
θ_a	activation energy parameter, $\equiv E/\mathscr{R}T_w$, dimensionless
κ	thermal diffusivity, cm^2-s^{-1}
λ	normalized time-independent regression rate eigenvalue, dimensionless
μ	normalized amplitude of pressure fluctuations, dimensionless
ρ	density, g-cm^{-3}
τ	normalized temperature, dimensionless
ψ	thickness of the surface melt layer on the oxidizer crystals in a composite propellant, cm

Ω normalized frequency of fluctuations, $\equiv \omega\kappa/\bar{r}^2$, dimensionless

ω frequency of fluctuations, s^{-1}

Subscripts and superscripts

$(\ )_b$ plane of burning, i.e., flame zone

$(\ )_0$ deep solid (ambient) conditions

$(\ )_{SL}$ solid-liquid interface plane

$(\ )_w$ wall plane

$\overline{(\ )}$ time-averaged part

$(\ )'$ fluctuating part

References

1. Kumar, R. N., and McNamara, R. P., *Some Experiments Related to L-Star Instability in Rocket Motors.* Daniel and Florence Guggenheim Jet Propulsion Center, California Institute of Technology, March 1973.

2. Fenske, M. R., Braun, W. G., and Thompson, W. H., *Technical Data Book - Petroleum Refining,* Chapter 5. American Petroleum Institute, New York, N.Y., 1966.

3. Ivin, K. J., "The Equilibrium Between Methyl Methacrylate and its Polymer," *Trans. Faraday Soc.*, Vol. 51, pp. 1273–1279, 1955.

4. Madorsky, S. L., *Thermal Degradation of Organic Polymers,* Interscience Publishers, New York, N.Y., 1964.

5. *Combustion of Solid Propellants and Low Frequency Combustion Instability,* NOTS TP4244. Naval Ordnance Test Station, China Lake, Calif., June 1967.

6. Shannon, L. J., *Composite Solid Propellant Ignition Mechanisms,* AFOSR Scientific Report, UTC 2138-ASR1. United Technology Center, Sunnyvale, Calif., Nov. 1966.

7. Kumar, R. N., *Some Considerations in the Combustion of AP/ Composite Propellants.* Daniel and Florence Guggenheim Jet Propulsion Center, California Institute of Technology, Pasadena, Calif., August 1972.

8. Guirao, C., and Williams, F. A., "A Model for Ammonium Perchlorate Deflagration between 20 and 100 Atm.," *AIAA J.*, Vol. 9, No. 7, pp. 1345–1356, July 1971.

9. Kumar, R. N., and Stickler, D. B., "Polymer Degradation Theory of Pressure Sensitive Hybrid Combustion," in *XIII Symposium (International) on Combustion*, pp. 1059–1072, The Combustion Institute, Pittsburgh, Pa., 1971.

10. Powling, J., "Experiments Relating to the Combustion of Ammonium Perchlorate-Based Propellants," in *XI Symposium (International) on Combustion* pp. 447–456, The Combustion Institute, Pittsburgh, Pa., 1967.

11. Boggs, T. L., et al., "The Deflagration of Pure and Isomorphously Doped Ammonium Perchlorate," in *XIII Symposium (International) on Combustion* pp. 995–1008, The Combustion Institute, Pittsburgh, Pa., 1971.

12. Maltzev, V., "Certain Problems Related to Mechanism of Combustion of Condensed Systems (Double-Base and Mixed Propellants)," Institute of Chemical Physics, USSR Academy of Sciences, Moscow, 1972.

13. Boggs, T. L., and Zurn, D. E., "The Temperature Sensitivity of the Deflagration Rates of Pure and Doped Ammonium Perchlorate," *Combustion Sci. Technol.*, Vol. 4, pp. 227–232, Jan. 1972.

14. Steinz, J. A., et. al., *The Burning Mechanism of Ammonium Perchlorate-Based Composite Solid Propellants.* AMS Report 830, Princeton University, Princeton N.J., Feb. 1969.

15. Muzzy, R. J., *Research on Combustion of Solid Propellants,* UTC 2136-TSR 2. United Technology Center, Sunnyvale, Calif., Oct. 11, 1967.

16. Culick, F. E. C., "A Review of Calculations for Unsteady Burning of a Solid Propellant," *AIAA J.*, Vol. 6, pp. 2241–2255, Dec. 1968.

7. Horton, M. D., and Rice, D. W., "Effect of Compositional Variables Upon Oscillatory Combustion of Solid Rocket Propellants," *Combust. and Flame,* Vol. 8, pp. 21–28, Mar. 1964.

JPL Quarterly Technical Review Volume 3, Number 2, July 1973

Index: particle physics, spacecraft environments and shielding, test facilities and equipment

Improved Spatial Uniformity of Beam-Plane Interaction by Means of Inverse Rastering

C. G. Miller

Applied Mechanics Division

An analysis is presented that shows the desirability and feasibility of conducting irradiations of large test objects by beams of penetrating radiation, by the method of moving the test object back and forth through the beam, rather than by sweeping the beam across the object. An extension of this method of inverse rastering allows the generation of composite beams with any desired intensity-vs-energy spectrum, obviating the need to determine equivalent damage factors for every energy in the spectrum.

Introduction

The study of the effects of penetrating nuclear radiation, particularly protons and electrons, on spacecraft-related parts, has been done in the past by allowing beams of these particles to emerge from an accelerator and fall upon the test objects. Test objects exposed to beams of radiation receive uniform exposure on all areas only when the beam is well collimated. If the beam is spread out with a large angular divergence, as needed for extended test objects, the uniformity of exposure suffers. If a collimated beam is rastered across a (large) extended object, the uniformity of exposure still suffers because of aberrations introduced into the beam when it is deviated farther and farther off axis in the rastering process.

Such off-axis aberrations are particularly important when using the high-energy beams from accelerators, such as beams of electrons over one MeV and beams of protons over 20 MeV, both of which are needed to simulate planetary radiation belt radiations.

Present practice consists of spreading the beam to a small angular divergence, typically 4- or 5-deg half-angle, which gives a 20- to 25-cm-diam field (8- to 10-in.) at a 1.5-m (60-in.) working distance from the end of the accelerator beam exit window. The field is then mapped, and the most uniform 10- × 15-cm (4- × 6-in.) section is used for test irradiations. The tests must then be conducted exposing one 10- × 15-cm board at a time. For a representative test involving 25 such boards, there are required 25 separate irradiations, leading to an expensive, in terms of man-hours, test.

Method of Approach

To avoid irradiating test boards one at a time, which requires shutting down and starting up before and after each change, we have developed a method of completing such tests in two, or at most three exposures, by irradiating groups of test boards comprising 9 or 12 individual boards. Furthermore, the method reduces the importance of uniform beam pattern so that a wider variety of accelerators becomes useful for tests.

This method is a variant of rastering, which is a widely used method of covering a large target with a small beam. Rastering involves relative motion between a small beam and a large target to give complete, although not simultaneous coverage of the target. There is thus time-sharing of the beam. Because the characteristics of the beam change due to aberrations introduced when the beam is magnetically deviated farther and farther off axis in a rastering process, simple sawtooth time-sharing drive of the beam does not give acceptable uniformity of exposure over the whole target area. An improved method consists of moving the individual boards through a matching, apertured-beam field, so as to superpose all parts of the beam on all parts of the test boards, and thus average out spatial variation in beam intensity. This is, of course, the equivalent of holding the test boards fixed in space, and moving the beam back and forth across all parts of the test board. The advantage of moving the test boards is that the beam profile and beam intensity distribution do not change, since the beam does not leave the fixed beam-optic axis along the centerline of the system.

An example of the application of such inverse rastering would consist of the exposure of 12 test boards ganged in a three-wide by four-high array on a 60 × 60 cm (24- × 24-in.) support; (Fig. 1). A moving beam, to raster the 12 boards, would have to cover a field of 45 × 45 cm (18 × 18 in.) with a half-angle of arctan 22.5/150 (9/60) = 8.5 deg assuming a practical quadrupole-to-exposure plane distance of 1.5 m. Such wide-angle uniformity cannot be achieved with simple quadrupole magnetic lenses. However, if the test boards are moved past a small, fixed beam spot, say of 12 × 15 cm (5 × 6 in.,) such difficulties disappear. In use, a simple X-Y scanner with 60 × 60 cm (24- × 24-in.) motion could be adapted with a minimum of effort to carry the array of test boards back and forth through an apertured beam field.

Calculations and Results

The most useful and stable beam distribution that has been achieved in past proton exposures at Crocker Radiation Laboratory is shown in Fig. 2. This meets the uniformity requirements needed for JPL tests, but the restricted size of the beam requires exposing the test boards one by one, as had been discussed. If the test boards are drawn across this field pattern repeatedly, from left to right, starting as shown in Fig. 3, and being raised an infinitesimal amount in the Y direction for each pass, the integrated

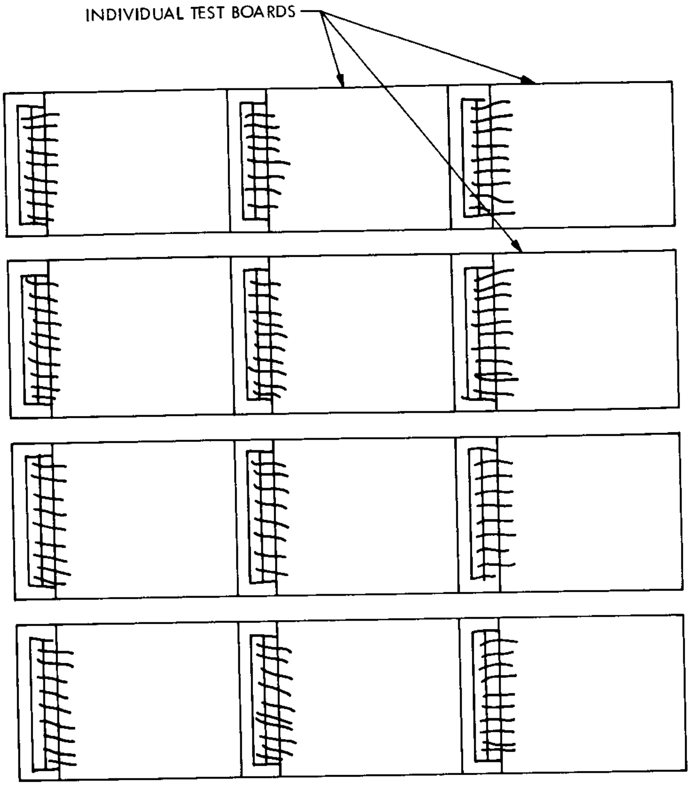

Fig. 1. Arrangement of assembly of test boards. Assembly to be moved as a group past fixed particle beam

exposure on every part of the test board would be precisely uniform no matter how greatly the distribution of intensity on the fixed particle field varied.

Since we cannot, in practice, conduct an irradiation using an infinite number of passes, it is necessary to see how satisfactory is a system using a small, finite number of passes per board. An examination of Fig. 2 shows that the horizontal sweeps of the beam by a segment of the test board delivers decreasing values of fluence as the sweeps take place at increasing *y* values of the proton field. Assuming, as is evident from Fig. 2, that successive, horizontal sweeps of short segments of the proton field give successively smaller proton fluences as the sweeps increase their *y* value, we can schematically plot the proton flux in relation to the *y* location, as in Fig. 4(a), where ϕ is the value of the proton flux rate, p^+/cm^2 s per unit of y distance, and ranges from a maximum of *a* when $y = 0$ to a minimum of *b* when $y = y_0$, y_0 being the height of the proton fixed field that is equal to the height of the test board. In general, the contour C that gives the value of ϕ for any chosen value of Y will be irregular. For the situation shown in Fig. 2, the

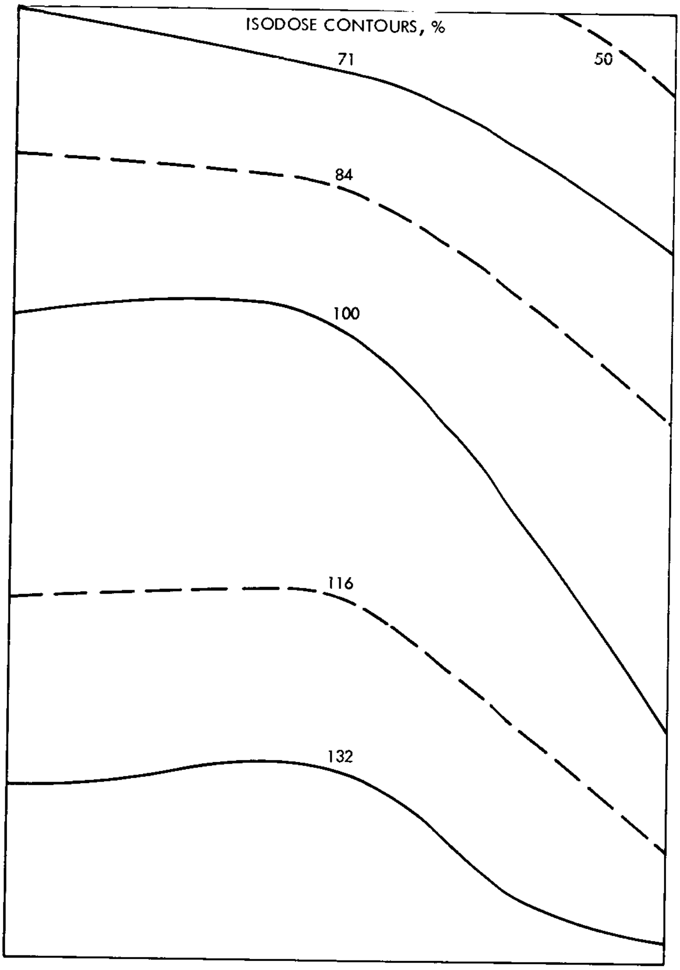

Fig. 2. Isodose contours, 10- x 15-cm beam, showing variation of intensity in proton beam at target plane

value of ϕ will decrease generally as shown in Fig. 4(a) from the value a to the value b.

To make the problem tractable, let us assume that a $y - \phi$ diagram can be represented as in Fig. 4(b) where the value of ϕ decreases uniformly from a to b. If a test board were simply exposed to the field, having a $y - \phi$ relation as shown, the bottom strip of the board would have a proton fluence of a, the top strip of the board would have a proton fluence of b, and the average exposure would be $((a + b)/2)$. The percentage variation from the average of the top strip is $100((a - b)/(a + b))$. If, as might be required by a test plan, the maximum variation in fluence across the test board must be less than ±30%, then $((a - b)/(a + b)) = < 0.30$, and $a < 1.86\ b$ for a stationary

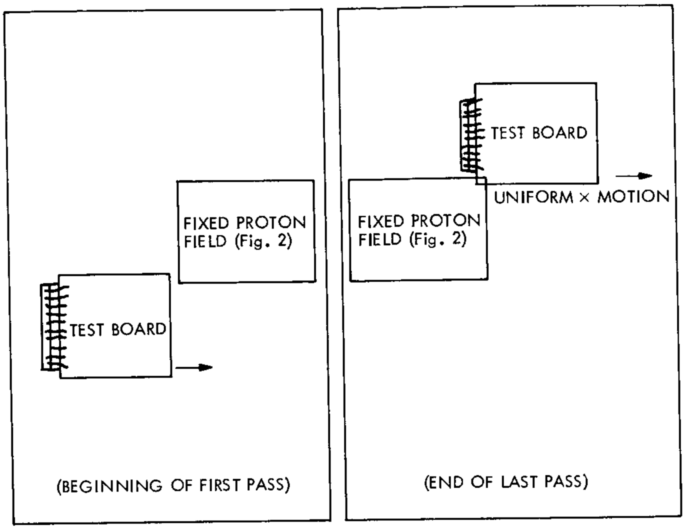

Fig. 3. Inverse rastering. Test board moves back and forth in X direction, advancing in fixed increments in Y direction between X sweeps

board exposure to be within ±30%. If the test boards are swept through the beam in the X direction, stepping Δy between steps, i.e., with an overlap $\Delta y/h_2$ or h_1/h_2 (Fig. 5) between steps, the uniformity increases markedly as shown in Table 1.

The analytical development is quite straightforward, but rather lengthy. If Table 1 be translated to resultant maximum deviation from the average fluence delivered to a test board, we find the values given in Table 2. It seems practical to allow the ratio a/b to be 3:1, and use three passes/board that will give a field flatness of ±16⅔%. A larger number of passes/board while possible, does not bring down the percentage variation very rapidly (Fig. 6).

The foregoing discussion leading to Table 2 represents a worst-case situation based on a uniform $y - \phi$ distribution, as shown in Fig. 4(b). If we were to select the beam so as to have more symmetry about a y traverse near the center of the apertured field, i.e., with a hot spot in the center of the apertured field, we should expect a $y - \phi$ diagram, as sketched in Fig. 4(c). In such a case, the percentage variation, similar to the values derived for Table 2 would depend on the relation between the number of passes (relative size of the Δy step in exposure sweep) and the ratio a/b, the values in Table 2 representing the worst-case percentages, so that uniformity would, in every case, be better than the values shown in Table 2.

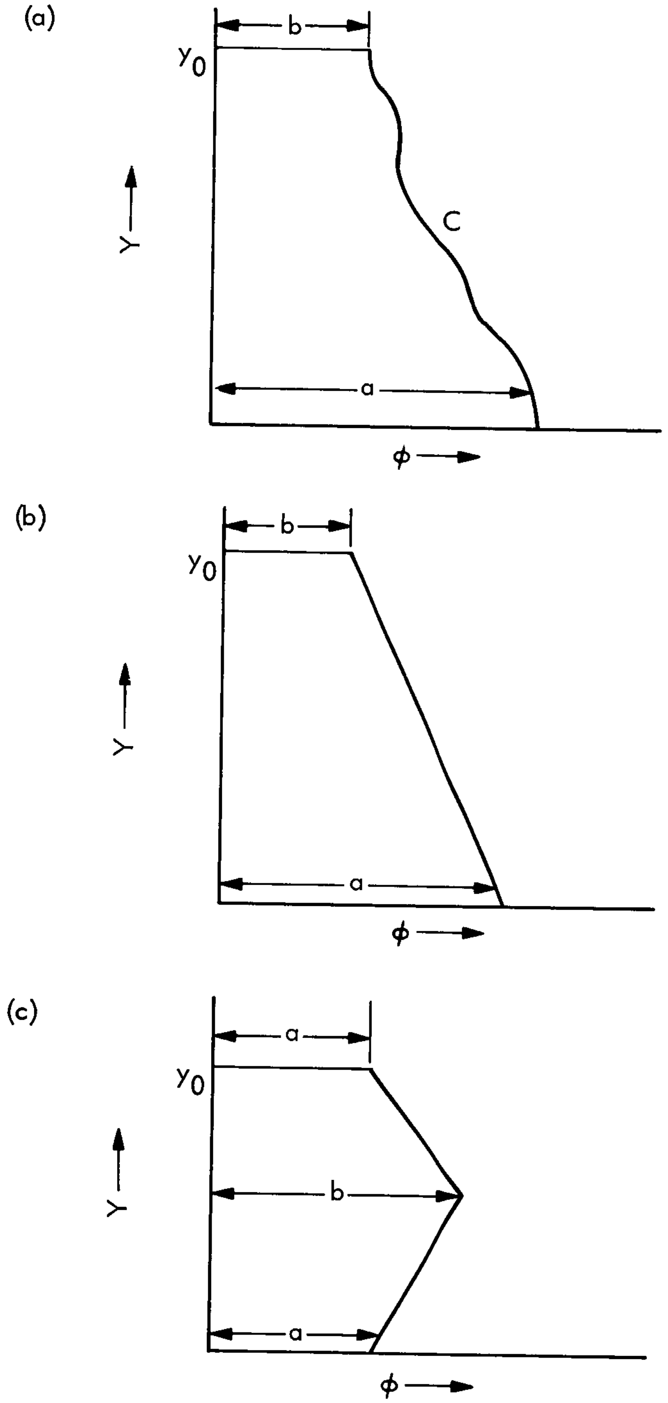

Fig. 4. Integrated fluence for traversal of nonuniform beam at varying values of y: (a) falling on differential element of area Δy · Δx, as element of area is drawn at uniform time rate across the fixed beam field shown in Fig. 2, for every value of y; (b) straight-line approximation to contour C shown in (a); (c) straight-line approximation to contour C when maximum φ is at an intermediate value of y rather than at extremum of y

Table 1. Ratio of maximum fluence to minimum fluence on any location on test board

No. of passes	Equivalent amount of overlap, %	Ratio a : b (see Fig. 4)			
		∞	3 : 1	2 : 1	1.5 : 1
1	100	∞	3.00	2.00	1.50
1.33	75	4.00	2.80	2.50	2.28
2	50	3.00	1.60	1.40	1.22
3	33	2.00	1.40	1.25	1.14
4	25	1.67	1.28	1.18	1.10
5	20	1.50	1.22	1.14	1.08
6	16.6	1.40	1.18	1.12	1.07

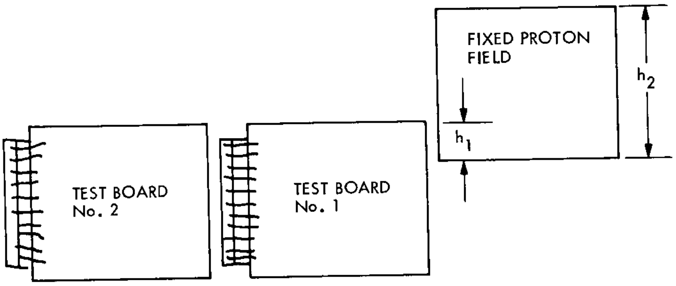

OVERLAP = h_1/h_2

NUMBER OF PASSES TO COVER ALL PARTS OF A TEST BOARD: (1/OVERLAP) = (h_2/h_1)

Fig. 5. Nomenclature for overlap (= h_1/h_2), and height (= h_2)

Special Features and Opportunities

Generating Spectral Intensity Matched Beam Instead of Monoenergetic Equivalent Beam

It has not, in the past, been practical to do any but monoenergetic electron or proton beam exposures, even though what we wish to simulate in the laboratory is the actual penetrating radiation flux that has a well known intensity-vs-energy spectrum (Fig. 7, adapted from Ref. 1). The use of a monoenergetic beam requires the test plan to have an equivalent damage function for each energy band in the spectrum. The equivalent damage function will vary for different types of test objects (e.g., npn and pnp transistor damage functions' response will require different equivalents). Since such damage equivalences are not known with sufficient precision, monoenergetic testing is less realistic, less satisfactory, and more costly than a matched energy spectrum-vs-intensity beam for testing.

It has always been possible to produce a variety of proton or electron energies in the form of abutting or overlapping parallel subbeams from an

Table 2. Percent variation of fluence, ± % from average

No. of passes	Equivalent amount of overlap, %	Ratio a:b (see Fig. 4)			
		∞	3:1	2:1	1.5:1
1	100	100	50	33	20
1.33	75	60	47.5	43.0	39.2
2	50	50	25	16.67	10
3	33	33.3	16.6	11.1	6.5
4	25	25	12.5	8.33	5
5	20	20	10	6.67	4
6	16.6	16.67	8.33	5.56	3.33

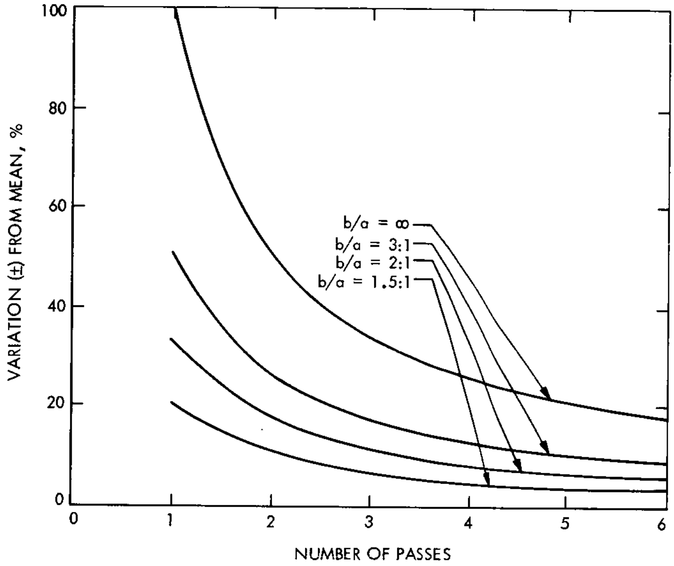

Fig. 6. Uniformity of exposure of test board as a result of inverse rastering. Percentage variation from mean exposure in relation to number of passes, for various ratios of maximum ϕ :minimum ϕ as in Fig. 4

original single high-energy beam by the method of placing a number of absorbers that act as energy degraders, side by side across the beam. Without relative motion of the beam and test area, however, each area of the test object would receive a different distribution of the several energy ranges produced by the absorbers. With the use of inverse rastering, it becomes practical and straightforward to superpose all parts of the various energy subbeams on every part of the test object, thus allowing any desired intensity-vs-energy spectrum distribution to be used for testing purposes.

The construction of a graduated absorber-set across the fixed beam aperture is shown in Fig. 8. Such an absorber-set, when placed in front of the high-energy proton beam, will give rise to subbeams of energy dependent on

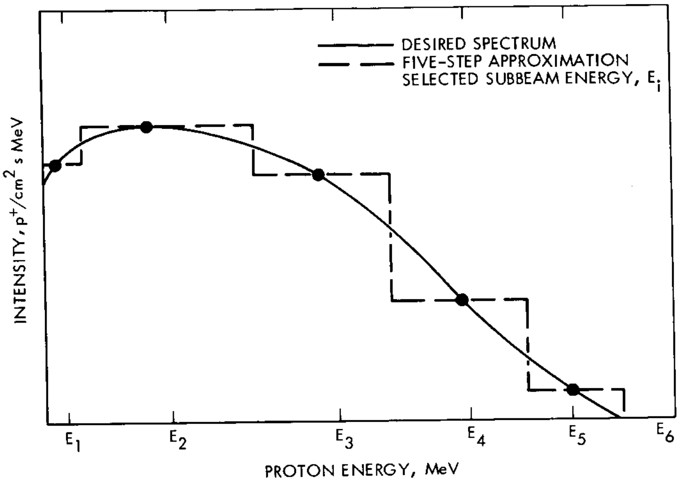

Fig. 7. Intensity-vs-energy distribution for planetary trapped radiation (schematic) and 5-step approximation to distribution

the depth, *d*, of the absorbing material. The relative contribution of each subbeam will be proportional to the width, *w*, of each absorber strip. The two factors, *w* and *d*, can be adjusted independently to allow any desired spectrum to be simulated in a finite, reasonable number of steps.

Some Possible Undesirable Consequences of Raster Exposure

The use of any rastering technique gives rise to high peak-to-average flux rates during the irradiation, since the beam is irradiating any given location only a small fraction of the total time of exposure. Under some circumstances, a high peak-to-average exposure may be undesirable.

A further point that must be taken into account is that every test exposure by means of high-energy radiation is accompanied by an induced flux of undesired, secondary radiation, e.g., neutrons and bremsstrahlung, caused by the interaction of the primary beam with the experimental environment. An irreducible minimum of contaminant radiation, even in nonrastered exposures, is that due to the interaction of primary beams with mounting hardware, and with the air in the vicinity of the test object. Figure 9 shows some neutron production efficiencies as a function of primary proton energy and atomic number. We note that for 12 boards ganged on an X-Y transport, as shown in Fig. 10, a complete exposure, with repeated passes through the beam, would keep each board in the vicinity of the "target area" and exposed to the contaminating radiation for a length of time equal to 30 times the stationary board exposure time. The 30× factor arises from the ratio of

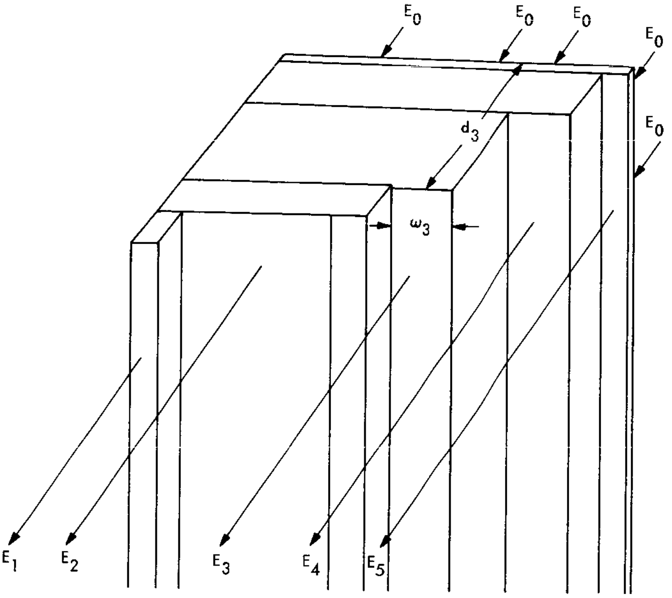

Fig. 8. Construction of stepped energy-degrader to generate 5 subbeams of energy E_1, $E_2 \cdots E_5$ from original beam of energy E_0

the total area shown in Fig. 10, including overtravel and the area of the beam at the test plane, here taken as 15 × 12 cm (6 × 5 in.) to agree with one test board. The factor of 30 could possibly be reduced to a factor of 18 by the use of a 2.5-cm-wide × 12-cm-high (1-in.-wide × 5-in.-high) fixed field, instead of the 15-cm-wide by 12-cm-high (6-in.-wide × 5-in.-high) fixed field, when exposing the test boards. This could eliminate almost all of the overtravel area on the right and left sides of the arrangements shown in Fig. 10. For tests of current interest, increases by a factor of 18 to 30 in contaminant secondary radiations would not compromise test results. Future tests that may require lower contamination levels can be accommodated if more attention is paid to the experimental arrangements. For example, less massive or lower atomic number materials in the mounting hardware, or replacement of the ambient air by helium gas or by vacuum environment will decrease the amount of secondary radiation markedly.

Summary and Conclusions

Uniform exposure of an extended test plane by a beam of penetrating nuclear radiation can be accomplished by a method of inverse rastering in which the workpiece moves, and the beam remains constant in direction. Methods to ensure that the beam remains stable in position and in time are described in the literature (Ref. 2).

The amount of exposure experienced by any area on the test plane as it is systematically moved back and forth across a fixed direction beam is found

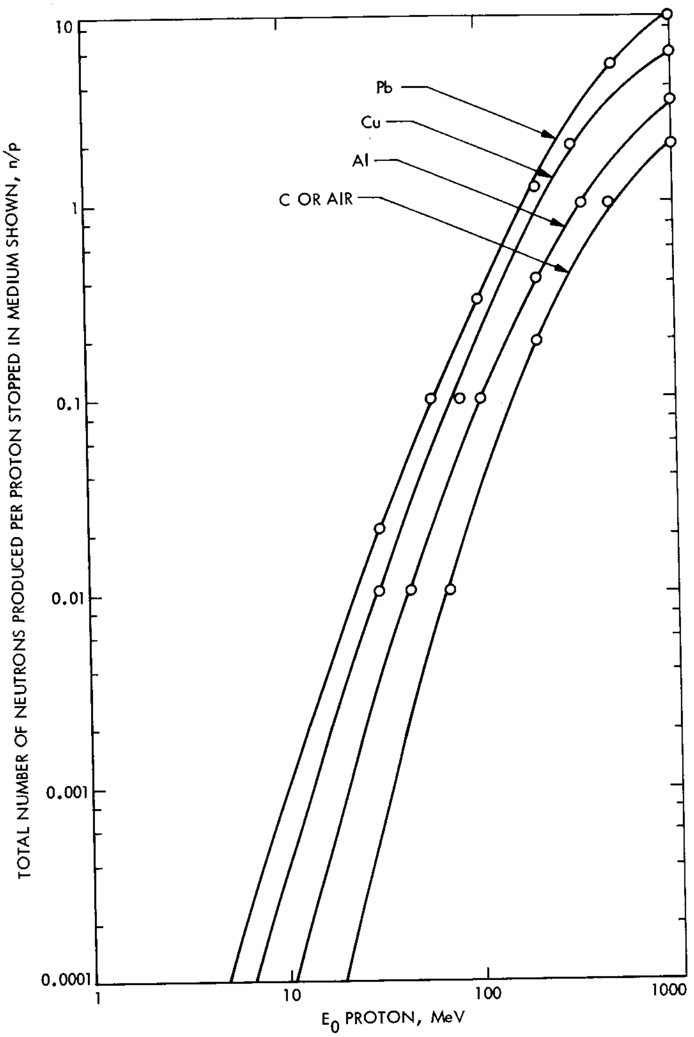

Fig. 9. Total neutron production efficiencies, n/p, for various energies of incident protons on varying atomic number targets

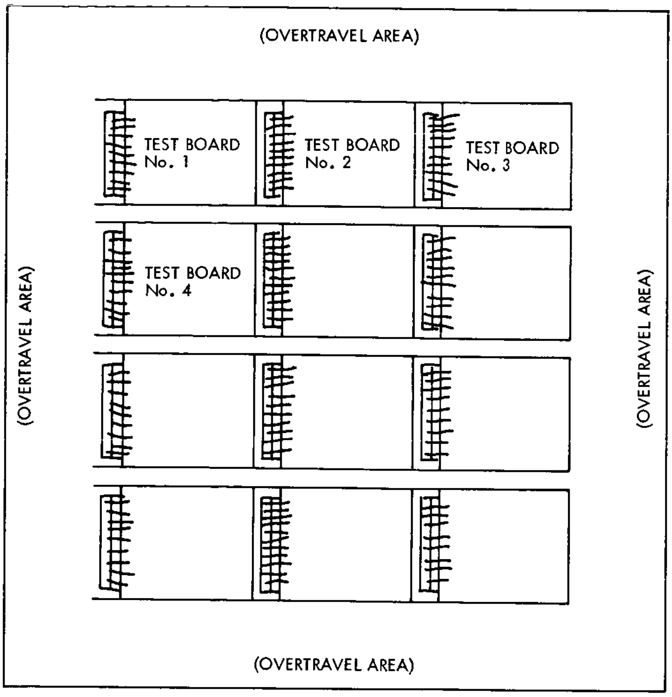

Fig. 10. Configuration, showing required overtravel area for inverse rastering of a 4 x 3 board array, when fixed beam is same size as any one test board

by numerical integration of the flux-time product for each point on the test plane field, as the test plane is rastered in the X direction and advanced in the Y direction with respect to the fixed beam. It is shown that for a nonuniform beam of intensity ratio 3:1, top to bottom, only two passes through the beam will reduce the test object variation to ±25% from the average. For a nonuniform beam of 100:1 intensity ratio, top to bottom, only four passes (through one beam height) will reduce the test object variation to ±25% from the average. Uniform exposure can result from the use of even exceedingly nonuniform beams as long as the beam does not vary with time.

The method of inverse rastering allows the generation of a composite, time-shared beam with any desired intensity-vs-energy spectrum. Such a beam can be used for testing purposes, avoiding the need to determine equivalent damage factors for each energy in the spectrum.

References

1. Parker, R.H., "Effects of Electrons and Protons on Science Instruments," in *Proceedings of the Jupiter Radiation Belt Workshop,*

Technical Memorandum 33-543, p. 173. Jet Propulsion Laboratory, Pasadena, Calif., July 1, 1972. (See also Divita, E., "Impact of Jovian Radiation Environmental Hazard on Spacecraft and Mission Development Design," Ibid., pp. 189, 190.)

2. Peterson, D.G., "Proton Beam Positioning System with Computer Control," *Nuclear Instruments and Methods*, Vol. 104, p. 451, 1972. (Note especially Refs. 1 to 12 in this citation.)

Bibliography of Current Reporting

Author Index With Abstracts

ABBOTT, E. A.

A01 **Mascons: Progress Toward a Unique Solution for Mass Distribution**

R. J. Phillips, J. E. Conel, E. A. Abbott,
W. L. Sjogren, and J. B. Morton

J. Geophys. Res., Vol. 77, No. 35, pp. 7106–7114,
December 10, 1972

For abstract, see Phillips, R. J.

AJELLO, J.

A02 **Ground Level Ultraviolet Solar Flux in Pasadena, California**

J. Ajello, J. King, Jr., A. L. Lane, and C. W. Odd

Bull. Am. Meteorol. Soc., Vol. 54, No. 2, pp. 114–115,
February 1973

Relative ultraviolet solar spectra were taken from Pasadena, California, as a function of solar zenith angle. The wavelength range extended from the cutoff wavelength at about 3000 Å to almost 3500 Å with a resolution of 15 Å. The cutoff wavelength was measured as a function of solar elevation angle and varies from 3160 Å at 4° solar elevation to 2955 Å at 41° solar elevation angle. This article displays calibrated spectra for four solar elevation angles as well as the cutoff wavelength as a function of solar elevation angle.

ALLEN, J. E.

A03 **DSN Progress Report for March–April 1973: Recent Modifications to the DSN Monitor and Control System**

J. E. Allen and W. Honer

Technical Report 32-1526, Vol. XV, pp. 185–189,
June 15, 1973

This article describes recent improvements to the monitor function of the DSN Monitor and Control System. The changes include the use of a new digital instrumentation subsystem computer program that will serve as a single monitor program for all deep space stations. The effects of the new or modified equipment on activities of operations personnel are also discussed.

ANDERSON, T. O.

A04 **DSN Progress Report for January–February 1973: Universal Parallel Analog-to-Digital Encoder Module**

T. O. Anderson

Technical Report 32-1526, Vol. XIV, pp. 94–100,
April 15, 1973

As more and higher frequency Deep Space Instrumentation Facility receiver operations become digitized, the DSN requires higher speed, simpler, and more cost-effective analog-to-digital converters. Besides meeting these requirements the converter described in this article is modular and lends itself to standardization.

The conversion method used is the all-parallel method that is optimum for high speed. One comparator-amplifier is used for each level of resolution and includes the digital-code converter that converts the output of the comparator–amplifier to binary code. The module contains four levels, so that an eight-level converter is made up of two externally connected modules, and a sixteen-level converter is made up of four externally connected modules.

A05 **DSN Progress Report for March–April 1973: Bit Synchronizer for Sample Data Antenna Pointing System**

T. O. Anderson, J. K. Holmes, and W. J. Hurd

Technical Report 32-1526, Vol. XV, pp. 128–132,
June 15, 1973

In the continuous effort to computerize antenna-pointing and control systems at the deep space stations, sample data systems are required. As a result of modular subsystems being readily available commercially, the sample data systems are designed in accordance with a decentralized-system design philosophy. A number of smaller subsystems are located close to the data sources. The subsystems feed data to collection centers which in turn feed data to the computer. The only connection between subsystems, collection centers, and computer is a single coaxial cable. Since there is no separate clock signal, bit synchronization must be extracted from the data signal in order to recover the serial binary data.

This article describes a particularly simple bit-synchronizer phase-locked loop especially designed for this noise-free environment. The performance of the loop has been analyzed and qualitatively verified on a laboratory breadboard model.

ARNOLD, J. R.

A06 Lunar Surface Radioactivity: Preliminary Results of the Apollo 15 and Apollo 16 Gamma-Ray Spectrometer Experiments

A. E. Metzger, J. I. Trombka (Goddard Spaceflight Center),
L. E. Peterson (University of California, San Diego),
R. C. Reedy (University of California, San Diego), and
J. R. Arnold (University of California, San Diego)

Science, Vol. 179, No. 4075, pp. 800–803,
February 23, 1973

For abstract, see Metzger, A. E.

BACK, L. H.

B01 Non-isothermal Laminar Flow of Gases Through Cooled Tubes

L. H. Back

Trans. ASME, Ser. C: J. Heat Transf., Vol. 95, No. 1,
pp. 85–92, February 1973

Numerical solutions of the laminar-flow equations in differential form are presented for gas flows through cooled tubes. For nearly isothermal flow there is good agreement with available experimental data, as is also found for the case of a large amount of wall cooling. This correspondence along with a check on the satisfaction of the global momentum and energy constraints allowed an appraisal of the effect of wall cooling on flow through tubes. In general, the effect of wall cooling was to decrease the wall friction and the change in pressure along tubes, but the average heat-transfer coefficient did not vary much.

BANTELL, M. H.

B02 Statistical Error Model for a Solar Electric Propulsion Thrust Subsystem

M. H. Bantell

Technical Memorandum 33-607, June 1, 1973

The statistical error model of the solar-electric-propulsion thrust subsystem was developed as a tool for investigating the effects of thrust-subsystem parameter uncertainties on navigation accuracy. The model is currently being used to evaluate the impact of electric-engine parameter uncertainties on navigation system performance for a baseline mission to Encke's Comet in the 1980s.

This memorandum presents data that represent the next generation in statistical error modeling for low-thrust applications. Principal improvements include the representation of thrust uncertainties and random-process modeling in terms of random parametric variations in the thrust-vector process for a multi-engine configuration.

BARENGOLTZ, J. B.

B03 The Electric Field in the Vicinity of a Photo-Emitting Plate in a Plasma

J. B. Barengoltz and C. Bauerle

JPL Quarterly Technical Review, Vol. 3, No. 1, pp. 26–32, April 1973

Knowledge of the electric field in the vicinity of a spacecraft provides necessary corrections to measurements of ambient fields and charged-particle fluxes and a required parameter to understand the motion of dust particles and grains around the spacecraft. Although the surface potential is sufficient to correct field and particle values, the more complex problem of the entire electric field, needed for grain-transport calculations, is treated here for the one-dimensional case.

By approximations to the analysis of a photo-emitting plate immersed in a dilute plasma, performed by Guernsey and Fu, explicit expressions for the potential and the electric field have been derived. The two classes of implicit solutions for the potential reported by them are shown to yield essentially identical results for the electric field within the Debye length for photoelectrons from the plate, under the conditions in our solar system. The values were obtained following assumptions of a later paper by Guernsey and Fu, in which the emitted photoelectron distribution is taken as Maxwellian. These results are compared with a simple model, due to Grard and Tunaley, wherein the effect of the dilute plasma is neglected entirely.

BARNUM, P. W.

B04 Tracking and Data System Support for the Mariner Mars 1971 Mission: Orbit Insertion Through End of Primary Mission

P. W. Barnum, N. A. Renzetti, G. P. Textor, and
L. B. Kelly

Technical Memorandum 33-523, Vol. III, May 15, 1973

This volume of the Tracking and Data System (TDS) support for the Mariner Mars 1971 Mission final report contains the deep-space-tracking and data-acquisition activities in support of orbital operations, which include the period from orbit insertion (November 14, 1971) to end of primary mission (April 1, 1972). Included are presentations of the TDS flight-support pass-chronology data for each of the deep space stations used, and performance evaluation for the DSN Telemetry, Tracking, Command, and Monitor Systems.

BATELAAN, P. D.

B05 DSN Progress Report for January–February 1973: S/X-Band Experiment: Zero Delay Device

T. Y. Otoshi and P. D. Batelaan

Technical Report 32-1526, Vol. XIV, pp. 73–80,
April 15, 1973

For abstract, see Otoshi, T. Y.

BATHKER, D. A.

B06 DSN Progress Report for January–February 1973: Dual Carrier Preparations for Viking

D. A. Bathker and D. W. Brown

Technical Report 32-1526, Vol. XIV, pp. 178–199, April 15, 1973

The problem of receive-band interference resulting from both single- and dual-carrier transmission from a deep space station has been synthesized and, to a large extent, resolved at the Venus Deep Space Station. Although there are remaining problems, this article discusses the application of this experience to 64-m-diameter-antenna stations, the Mars Deep Space Station in particular.

BAUERLE, C.

B07 **The Electric Field in the Vicinity of a Photo-Emitting Plate in a Plasma**

J. B. Barengoltz and C. Bauerle

JPL Quarterly Technical Review, Vol. 3, No. 1, pp. 26–32, April 1973

For abstract, see Barengoltz, J. B.

BAUMAN, A. J.

B08 **Spectrofluorometric Search for Porphyrins in Apollo 14 Surface Fines**

J. H. Rho, E. A. Cohen, and A. J. Bauman

"Proceedings of the Third Lunar Science Conference," *Supplement 3, Geochimica et Cosmochimica Acta*, Vol. 2, pp. 2149–2155, 1972

For abstract, see Rho, J. H.

B09 **Analyses of the Returned Lunar Surface Fines for Porphyrins**

J. H. Rho, A. J. Bauman, E. A. Cohen,
T. F. Yen (University of Southern California), and
J. Bonner (California Institute of Technology)

Space Life Sci., Vol. 3, No. 4, pp. 415–418, October 1972

For abstract, see Rho, J. H.

BAUMERT, L. D.

B10 **A Note on the Griesmer Bound**

L. D. Baumert and R. J. McEliece

IEEE Trans. Inform. Theory, Vol. IT-19, No. 1, pp. 134–135, January 1973

Griesmer's lower bound for the word length n of a linear code of dimension k and minimum distance d is shown to be sharp for fixed k, when d is sufficiently large. For $k \leqslant 6$ and all d the minimum word length is determined.

BEER, R.

B11 The Abundance of CH_3D and the D/H Ratio in Jupiter

R. Beer and F. W. Taylor

Astrophys. J., Vol. 179, No. 1, Pt. 1, pp. 309–327, January 1, 1973

From observations of the ν_2 parallel band of mono-deuterated methane (CH_3D) in the Jovian atmosphere, we have deduced a CH_3D abundance and mixing ratio and a value for the D/H ratio in this planet, with due regard to the problems of Jovian atmospheric structure and deuterium fractionation. We find the D/H ratio to be significantly less than the terrestrial value and discuss some of the implications to the early history of the solar system. This observation marks the first-ever detection of deuterium by any astronomical technique.

B12 Observation of the OH Radical in Betelgeuse

R. Beer, R. H. Norton, R. B. Hutchinson,
D. L. Lambert (University of Texas), and
J. V. Martonchik (University of Texas)

Mém. Soc. Roy. Sci. Liège, Vol. III, No. 6, p. 145, 1972

This article analyzes spectra of the M supergiant α Orionis and reports that more than 80 of the approximately 100 absorptions unique to the star are due to the fundamental vibration-rotation bands of the diatomic free radical OH. In addition, OH abundance is computed and turbulence in the stellar atmosphere estimated.

BEHAR, J. V.

B13 Hydrocarbons in Air Samples From Antarctic Dry Valley Drilling Sites

J. V. Behar (University of California, Riverside),
L. Zafonte (University of California, Riverside),
R. E. Cameron, and F. A. Morelli

Antarctic J. U.S., Vol. VII, No. 4, pp. 94–96, July–August 1972

One important aspect in the study of polluted atmospheres is the determination of the lowest levels attainable for several contaminants of interest. It is necessary to define the levels of the minor atmospheric constituents present in the cleanest air samples obtainable. Therefore, studies have been initiated utilizing the unique environment provided by the Antarctic Continent, primarily with respect to the lack of anthropogenic processes carried on as in the more populated regions of the earth. This article presents and analyzes the results of air samples collected during these studies.

BERGSTRALH, J. T.

B14 The Planet Venus: A New Periodic Spectrum Variable

L. D. G. Young, A. T. Young, J. W. Young, and J. T. Bergstralh

Astrophys. J., Vol. 181, No. 1, Pt. 2, pp. L5–L8, April 1, 1973

For abstract, see Young, L. D. G.

BERMAN, P. A.

B15 Study of Interaction Among Silicon, Lithium, Oxygen and Radiation-Induced Defects for Radiation-Hardened Solar Cells

P. A. Berman

JPL Quarterly Technical Review, Vol. 3, No. 1, pp. 33–44, April 1973

In order to improve reliability and the useful lifetime of solar-cell arrays for space use, a program was undertaken at JPL for development of radiation-hardened lithium-doped silicon solar cells. These cells have been shown to be significantly more resistant to degradation by ionized particles than the presently used *n–p* non-lithium-doped silicon solar cells. This article describes the results of various analyses performed to develop a more complete understanding of the physics of the interactions among lithium, silicon, oxygen, and radiation-induced defects. A discussion is given of those portions of the previous model of radiation-damage annealing which were found to be in error and those portions which were upheld by these extensive investigations.

BLANKENHORN, D. H.

B16 **Prediction of Lipid Uptake by Prosthetic Heart Valve Poppets From Solubility Parameters**

J. Moacanin, D. D. Lawson, H. P. Chin (University of Southern California), E. C. Harrison (University of Southern California), and D. H. Blankenhorn (University of Southern California)

Biomat., Med. Dev., Art. Org., Vol. 1, No. 1, pp. 183–190, 1973

For abstract, see Moacanin, J.

BÖER, K. W.

B17 **Photoconductor–Metal Contact at Higher Densities**

G. A. Dussel (University of Delaware),
K. W. Böer (University of Delaware), and R. J. Stirn

Phys. Rev., Pt. B: Solid State, Vol. 7, No. 4, pp. 1443–1454, February 15, 1973

For abstract, see Dussel, G. A.

B18 **CdS–Metal Contact at Higher Current Densities**

R. J. Stirn, K. W. Böer (University of Delaware), and
G. A. Dussel (University of Delaware)

Phys. Rev., Pt. B: Solid State, Vol. 7, No. 4, pp. 1433–1443, February 15, 1973

For abstract, see Stirn, R. J.

BONNER, J.

B19 **Analyses of the Returned Lunar Surface Fines for Porphyrins**

J. H. Rho, A. J. Bauman, E. A. Cohen,
T. F. Yen (University of Southern California), and
J. Bonner (California Institute of Technology)

Space Life Sci., Vol. 3, No. 4, pp. 415–418, October 1972

For abstract, see Rho, J. H.

BOOTH, R. W. D.

B20 **DSN Progress Report for March–April 1973: S-Band Microwave Weather Project Data for CY 1971**

M. S. Reid and R. W. D. Booth

Technical Report 32-1526, Vol. XV, pp. 88–91,
June 15, 1973

For abstract, see Reid, M. S.

BOWERS, M. T.

B21 **Thermal Energy Charge Transfer Reactions of Rare-Gas Ions to Methane, Ethane, Propane, and Silane: The Importance of Franck–Condon Factors**

M. T. Bowers (University of California, Santa Barbara) and
D. D. Elleman

Chem. Phys. Lett., Vol. 16, No. 3, pp. 486–491,
October 15, 1972

Thermal energy charge transfer rate constants from He^+, Ne^+, Ar^+, Kr^+, and Xe^+ to CH_4, CD_4, C_2H_6, C_3H_8, and SiH_4 have been measured using ion cyclotron resonance spectroscopy. The data are interpreted in terms of a model that presumes the magnitude of the rate constant is directly related to the magnitude of the Franck–Condon factor connecting the molecular neutral and ion. Additional measurements between N_2O^+, CO_2^+, CO^+, and N_2^+ charge transferring to SiH_4 indicate that the ion–neutral collision distorts the Franck–Condon manifold from that appropriate to sudden ionization processes (photon or electron impact).

BREJCHA, A. J.

B22 **Error Analysis for Mariner Venus/Mercury 1973 Conducted at the JPL Mesa West Antenna Range**

N. L. Vincent, C. A. Smith, A. J. Brejcha, and
H. A. Curtis

Technical Memorandum 33-625, June 1, 1973

For abstract, see Vincent, N. L.

BROWN, D. W.

B23 **DSN Progress Report for January–February 1973: Dual Carrier Preparations for Viking**

D. A. Bathker and D. W. Brown

Technical Report 32-1526, Vol. XIV, pp. 178–199,
April 15, 1973

For abstract, see Bathker, D. A.

BRYAN, A. I.

B24 **DSN Progress Report for March–April 1973: DSN System Testing: A Report on the DSN Pioneer G Compatibility Program**

A. I. Bryan

Technical Report 32-1526, Vol. XV, pp. 29–31,
June 15, 1973

The Pioneer G compatibility test program was nonstandard as no DSN/Pioneer G spacecraft testing was conducted prior to tests performed at Cape Kennedy on March 6, 1973. This article describes these compatibility tests and the test results for establishment of DSN/spacecraft compatibility.

BUTMAN, S.

B25 **DSN Progress Report for March–April 1973: Capacity for Noncoherent, Soft-Decision MFSK Signaling**

S. Butman and B. K. Levitt

Technical Report 32-1526, Vol. XV, pp. 146–155,
June 15, 1973

Planetary probes into the dense atmospheres of Venus, Jupiter, and Saturn may require noncoherent communication links to Earth. In this article, the capacity of noncoherent, multiple-frequency shift-keyed (MFSK) systems is determined as a function of the number of frequencies, receiver quantization, and signal-to-noise ratio. It is shown that the spacing of the quantizer levels is not critical, and that 8-level, uniform quantization is essentially as good as infinite quantization.

CAIN, D. L.

C01 **The Atmosphere of Mars From Mariner 9 Radio Occultation Measurements**

A. J. Kliore, D. L. Cain, G. Fjeldbo, B. L. Seidel, M. J. Sykes, and S. I. Rasool (National Aeronautics and Space Administration)

Icarus, Vol. 17, No. 2, pp. 484–516, October 1972

For abstract, see Kliore, A. J.

C02 **The Shape of Mars From the Mariner 9 Occultations**

D. L. Cain, A. J. Kliore, B. L. Seidel, and M. J. Sykes

Icarus, Vol. 17, No. 2, pp. 517–524, October 1972

The extinction time of the radio signal, as the Mariner 9 spacecraft was occultated by Mars, together with an accurate ephemeris of the spacecraft were used to determine radii from the mass center to the occulting feature. Similarly estimations were made of the radius to a point where the pressure reached a certain fixed value. Several simple models were proposed to fit both sets of radii data.

CAMERON, R. E.

C03 **Monitoring of Antarctic Dry Valley Drilling Sites**

F. A. Morelli, R. E. Cameron, D. R. Gensel, and L. P. Randall (Northern Illinois University)

Antarctic J. U.S., Vol. VII, No. 4, pp. 92–94, July–August 1972

For abstract, see Morelli, F. A.

C04 **Hydrocarbons in Air Samples From Antarctic Dry Valley Drilling Sites**

J. V. Behar (University of California, Riverside), L. Zafonte (University of California, Riverside), R. E. Cameron, and F. A. Morelli

Antarctic J. U.S., Vol. VII, No. 4, pp. 94–96, July–August 1972

For abstract, see Behar, J. V.

C05 **Bacterial Species in Soil and Air of the Antarctic Continent**

R. E. Cameron, F. A. Morelli, and R. M. Johnson (Arizona State University)

Antarctic J. U.S., Vol. VII, No. 5, pp. 187–189, September-October 1972

Increased emphasis has been given to monitoring aerial bacteria in the Antarctic, especially in regard to field party activities. As a Martian analogy, understanding of antarctic microbial ecology is of continuing interest as it applies to the Mars quarantine problem, selection of Martian landing sites for biological purposes, comparison with a possible Martian microbial ecology, and as a test model for the biological exploration of Mars. This article discusses the bacterial species identified to date, the common habitat of each, and the bacterial genera, while emphasizing the need to protect the Antarctic from contamination.

CARTWRIGHT, D. C.

C06 **Excitation of the $W^3\Delta_u$, $w^1\Delta_u$, $B'^3\Sigma_u^-$, and $a'^1\Sigma_u^-$ States of N_2 by Electron Impact**

A. Chutjian, D. C. Cartwright (The Aerospace Corporation), and S. Trajmar

Phys. Rev. Lett., Vol. 30, No. 6, pp. 195–198, February 5, 1973

For abstract, see Chutjian, A.

CHAO, C. C.

C07 **DSN Progress Report for January–February 1973: A New Method to Predict Wet Zenith Range Correction From Surface Measurements**

C. C. Chao

Technical Report 32-1526, Vol. XIV, pp. 33–41, April 15, 1973

A study of the radiosonde-balloon data measured in 1967 and 1968 indicates that during local noon the wet zenith-range correction of troposphere refraction is strongly correlated with surface vapor pressure. A simple analytical expression connecting the wet zenith-range correction with surface temperature and vapor pressure was found based on an adiabatic-atmosphere model. The agreement (1σ) between the surface prediction and balloon data is good to 2 cm.

CHAOTE, R.

C08 **Spacecraft Techniques for Lunar Research**

L. D. Jaffe, R. Chaote, and R. B. Coryell

The Moon, Vol. 5, Nos. 3-4, pp. 348-367, November-December 1972

For abstract, see Jaffe, L. D.

CHIN, H. P.

C09 **Prediction of Lipid Uptake by Prosthetic Heart Valve Poppets From Solubility Parameters**

J. Moacanin, D. D. Lawson, H. P. Chin (University of Southern California), E. C. Harrison (University of Southern California), and D. H. Blankenhorn (University of Southern California)

Biomat., Med. Dev., Art. Org., Vol. 1, No. 1, pp. 183–190, 1973

For abstract, see Moacanin, J.

CHIRIVELLA, J. E.

C10 **Operation of Small Rocket Engines in the JPL High-Vacuum Molecular Space Simulator (Molsink)**

J. E. Chirivella

JPL Quarterly Technical Review, Vol. 3, No. 1, pp. 1–13, April 1973

The feasibility of operating small rocket engines in the JPL Molsink facility has been demonstrated. A 0.44-N (0.1-lbf) hydrazine engine and a 0.18-N (0.04-lbf) thruster using cold gas from a hydrazine plenum system were operated for both flight duty cycles and off-nominal conditions. The exhaust gases from these thrusters contain NH_3, N_2 and H_2. The chamber was also calibrated for larger bipropellant engines using nitrogen tetroxide/monomethyl hydrazine. The exhaust products of these engines contain CO_2, CO, N_2, H_2O, and H_2. A mixture of cold gases simulating the engine exhaust was injected through a nozzle under conditions simulating thrust levels up to 26.7 N (6 lbf). Pulsing and continuous operations were investigated. The chamber background-pressure traces were compared with the traces obtained for the same thrusters operated with pure nitrogen at approximately equivalent thrust. Satisfactory recuperation times were encountered in all the pulsing modes. Test times greater than 20 s were obtained in steady-state operation before the vacuum chamber back pressure climbed to prohibitive values.

CHUTJIAN, A.

C11 Vibrational Excitation in CO by Electron Impact in the Energy Range 10–90 eV

A. Chutjian, D. G. Truhlar (University of Minnesota), W. Williams, and S. Trajmar

Phys. Rev. Lett., Vol. 29, No. 24, pp. 1580–1583, December 11, 1972

The ratio of the scattering intensity for the $v'' = 1$ excitation to the elastic scattering intensity at 40° and 80° scattering angles has been determined for 10- to 90-eV impact energies for electron scattering by CO. These ratio curves exhibit broad peaks near 20-eV impact energy which cannot be accounted for by plane-wave calculations based on potential scattering models. The peaks are indicative of a resonant excitation process (or processes) in the $v'' = 1$ channel in the range 15–25 eV.

C12 Excitation of the $W^3\Delta_u$, $w^1\Delta_u$, $B'^3\Sigma_u^-$, and $a'^1\Sigma_u^-$ States of N_2 by Electron Impact

A. Chutjian, D. C. Cartwright (The Aerospace Corporation), and S. Trajmar

Phys. Rev. Lett., Vol. 30, No. 6, pp. 195–198, February 5, 1973

Electron energy-loss spectra have been obtained for N_2 at 20.6 eV impact energy and scattering angles of 10–138°. These spectra have been analyzed to yield the first identification of excitation to the $W^3\Delta_u$, $w^1\Delta_u$, $B'^3\Sigma_u^-$, and $a'^1\Sigma_u^-$ states in electron impact spectroscopy, and the angular dependence of the excitations from 10 to 130°. The differential cross section for excitation of the $W^3\Delta_u$ state is the largest triplet-state cross section at all scattering angles, and is the largest inelastic cross section at angles greater than 70°

CLAUSS, R. C.

C13 DSN Progress Report for March–April 1973: Low Noise Receivers: Theory of "Noise Bursts" on Large Antennas

W. H. Higa, R. C. Clauss, and P. Dachel

Technical Report 32-1526, Vol. XV, pp. 80–83,
June 15, 1973

For abstract, see Higa, W. H.

COFFIN, R. C.

C14 DSN Progress Report for January–February 1973: Block IV Ranging Demodulator Assembly

R. C. Coffin

Technical Report 32-1526, Vol. XIV, pp. 161–166,
April 15, 1973

The Block IV Ranging Demodulator Assembly is a 10-MHz ranging receiver operating on the automatic-gain-controlled output of either a Block III or Block IV Deep Space Instrumentation Facility receiver. It demodulates the 10-MHz carrier that has been phase modulated with range code to provide two range-correlation voltages to the Planetary Ranging Assembly. The design of the Ranging Demodulator Assembly is compatible with either composite or sequential range-code schemes. Manual control of the Block IV Ranging Demodulator Assembly is straightforward and easy to comprehend, minimizing operator expense and operator errors. Computer-control capability is provided and may be implemented as soon as a suitable interface is developed.

C15 DSN Progress Report for March–April 1973: Reference Distribution Amplifier for the Block IV Subcarrier Demodulator Assembly

R. C. Coffin

Technical Report 32-1526, Vol. XV, pp. 177–180,
June 15, 1973

This article describes a reference distribution amplifier designed for the Block IV Subcarrier Demodulator Assembly. From one 10-MHz input, the unit generates three 10-MHz reference outputs. The references are variable in phase, and their level is fixed at 0 dBm. The control of phase and monitoring of output levels facilitate computer operation.

COHEN, E. A.

C16 Spectrofluorometric Search for Porphyrins in Apollo 14 Surface Fines

J. H. Rho, E. A. Cohen, and A. J. Bauman

"Proceedings of the Third Lunar Science Conference," *Supplement 3, Geochimica et Cosmochimica Acta*, Vol. 2, pp. 2149–2155, 1972

For abstract, see Rho, J. H.

C17 **Analyses of the Returned Lunar Surface Fines for Porphyrins**

J. H. Rho, A. J. Bauman, E. A. Cohen,
T. F. Yen (University of Southern California), and
J. Bonner (California Institute of Technology)

Space Life Sci., Vol. 3, No. 4, pp. 415–418, October 1972

For abstract, see Rho, J. H.

CONEL, J. E.

C18 **Mascons: Progress Toward a Unique Solution for Mass Distribution**

R. J. Phillips, J. E. Conel, E. A. Abbott,
W. L. Sjogren, and J. B. Morton

J. Geophys. Res., Vol. 77, No. 35, pp. 7106–7114, December 10, 1972

For abstract, see Phillips, R. J.

COOPER, M. A.

C19 **Evidence for a Steric Effect on Directly Bonded Carbon–Fluorine and Carbon–Proton Nuclear Magnetic Resonance Couplings**

S. L. Manatt, M. A. Cooper, C. W. Mallory (Bryn Mawr College), and F. B. Mallory (Bryn Mawr College)

J. Am. Chem. Soc., Vol. 95, No. 3, pp. 975–977, February 7, 1973

For abstract, see Manatt, S. L.

CORK, M. J.

C20 **From Earth to Mars Orbit—Mariner 9 Propulsion Flight Performance With Analytical Correlations**

M. J. Cork, R. L. French, C. J. Leising, and D. D. Schmit

AIAA Preprint 72-1185, AIAA/SAE Eighth Joint Propulsion Specialist Conference, New Orleans, Louisiana, November 29–December 1, 1972

The Mariner 9 spacecraft finished its primary mission as the first man-made satellite of another planet in March 1972. Propulsion performance during the 10-month mission and four maneuvers was perfect. Analytical models used to predict performance and analyze flight data are described. Flight data are presented, and analytical correlations are discussed for overall performance, zero-g heat transfer, and nitrogen permeation and diffusion within the propellant tanks. Orbit-insertion burn time, thrust, and specific impulse were within 1/2% of preburn predictions. Correlations between predictions and flight data demonstrated the validity of the analytical models used.

CORYELL, R. B.

C21 Spacecraft Techniques for Lunar Research

L. D. Jaffe, R. Chaote, and R. B. Coryell

The Moon, Vol. 5, Nos. 3–4, pp. 348–367, November–December 1972

For abstract, see Jaffe, L. D.

CROTTY, J. D.

C22 Ion Thruster Thermal Characteristics and Performance

L. C. Wen, J. D. Crotty, and E. V. Pawlik

J. Spacecraft Rockets, Vol. 10, No. 1, pp. 35–41, January 1973

For abstract, see Wen, L. C.

CURTIS, H. A.

C23 Error Analysis for Mariner Venus/Mercury 1973 Conducted at the JPL Mesa West Antenna Range

N. L. Vincent, C. A. Smith, A. J. Brejcha, and H. A. Curtis

Technical Memorandum 33-625, June 1, 1973

For abstract, see Vincent, N. L.

CUTTS, J. A.

C24 **Mariner 9—Image Processing and Products**

E. C. Levinthal (Stanford University), W. B. Green, J. A. Cutts, E. D. Jahelka, R. A. Johansen, M. J. Sander, J. B. Seidman, A. T. Young, and L. A. Soderblom (U.S. Geological Survey)

Icarus, Vol. 18, No. 1, pp. 75–101, January 1973

For abstract, see Levinthal, E. C.

DACHEL, P.

D01 **DSN Progress Report for March–April 1973: Low Noise Receivers: Theory of "Noise Bursts" on Large Antennas**

W. H. Higa, R. C. Clauss, and P. Dachel

Technical Report 32-1526, Vol. XV, pp. 80–83, June 15, 1973

For abstract, see Higa, W. H.

DAEGES, J. J.

D02 **DSN Progress Report for January–February 1973: Motor Run-Up and Control Unit**

J. J. Daeges

Technical Report 32-1526, Vol. XIV, pp. 167–169, April 15, 1973

A motor–generator set is used to convert 60-Hz line voltage to 400-Hz voltage for use in the high-power transmitter. The motors used in the motor–generator sets are either 1750- or 3500-hp synchronous motors. They must be brought up to speed before line voltage can be applied to avoid severe power-line transients. The present unit being used to bring the motor up to speed is an open-loop analog device and cannot compensate for drift, temperature changes, or line-frequency changes. The design of the new unit will compensate for all variations and is simple to set up and maintain.

DAVIS, E. K.

D03 **DSN Progress Report for January–February 1973: Mariner Venus/Mercury 1973 Mission Support**

E. K. Davis

Technical Report 32-1526, Vol. XIV, pp. 5–13,
April 15, 1973

During January and February 1973, DSN preparations for Mariner Venus/Mercury 1973 mission support included continuing implementation of new capabilities, initiation of training, test and operations planning, and revision of plans to match new budget guidelines. The DSN progress review was held on February 2, 1973 to evaluate the progress of these ongoing activities and much of the information in this article stems from progress-review material.

D04 DSN Progress Report for March–April 1973: Mariner Venus/Mercury 1973 Mission Support

E. K. Davis

Technical Report 32-1526, Vol. XV, pp. 5–9,
June 15, 1973

During March and April 1973, the DSN encountered problems in completing software development for deep-space-station telemetry and command data handling. This impacted follow-on test plans and schedules. A large part of this article is devoted to the software problem and the corrective action taken.

DeMORE, W. B.

D05 Activation Energies for Addition of O(^{3}P) to Simple Olefins

W. B. DeMore

Chem. Phys. Lett., Vol. 16, No. 3, pp. 608–610,
October 15, 1972

Relative rates have been measured for addition of O(^{3}P) to C_2H_4, C_2F_4, C_3H_6, and C_4H_8-1 in liquid Ar at 87.5°K. The results indicate that the activation energies for the C_3H_6 and C_4H_8-1 reactions are equal, to within 0.1 kcal/mole. A similar conclusion holds for C_2H_4 and C_2F_4. Further, the experiments suggest that the activation energy for addition of O(^{3}P) to the double bond of C_2H_4 may be as low as 0.6 kcal/mole, and is unlikely to be higher than about 1 kcal/mole.

D06 Intermediates in the Ozonation of Simple Alkynes

W. B. DeMore and C.-L. Lin

J. Org. Chem., Vol. 38, No. 5, pp. 985–989, March 9, 1973

The reactions of O_3 with $HC{\equiv}CH$, $CH_3C{\equiv}CH$, $CH_3C{\equiv}CCH_3$, and $C_2H_5C{\equiv}CH$ have been studied in liquid CO_2 at -45°. The initial products were observed by *in situ* infrared spectroscopy, and subsequent changes occurring upon warm-up or flash vaporization of the mixture were followed by ir or gc analysis. The principal new spectral feature for all alkynes except acetylene was a strong carbonyl absorption near 1740 cm^{-1}, and all alkynes gave relatively weak absorption bands in the carbonyl region which are attributed to the corresponding acid anhydrides. The 1740-cm^{-1} band was shown to be an unstable precursor of the acid anhydrides and other products. The overall mechanism, the identity of the precursor, and factors influencing the final product distribution are discussed.

D07 **Reactions of $O(^1D)$ With Methane and Ethane**

C.-L. Lin and W. B. DeMore

J. Phys. Chem., Vol. 77, No. 7, pp. 863–869, March 29, 1973

For abstract, see Lin, C.-L.

DIEMER, W. D.

D08 **DSN Progress Report for January–February 1973: Viewperiod Generator for Spacecraft and the Planets**

W. D. Diemer

Technical Report 32-1526, Vol. XIV, pp. 205–214, April 15, 1973

This article describes a method, and the supporting software, developed to provide an inexpensive means of generating spacecraft and planetary viewperiods for the deep space stations over a long period of time. In the past, the only method for obtaining this information was an expensive and complex computer program which provided these data as a secondary output to the actual station look angles.

DONNELLY, H.

D09 **DSN Progress Report for March–April 1973: S/X-Band Open-Loop Receivers**

H. Donnelly

Technical Report 32-1526, Vol. XV, pp. 51–53, June 15, 1973

The existing open-loop receivers at the Mars Deep Space Station (DSS 14) are being modified on an R&D basis to support the Mariner Venus/Mercury 1973 mission. These modifications will provide both S- and X-band phase-stable receivers to obtain occultation data. This article presents a description of the modifications.

D10 **DSN Progress Report for March–April 1973: Multiple-Mission Open-Loop Receiver**

H. Donnelly and S. E. Friedenberg

Technical Report 32-1526, Vol. XV, pp. 181–184, June 15, 1973

Existing Block III open-loop receivers are being modified to provide multiple-mission capability at S-band. These modifications provide greater flexibility in the selection of the receiver data bandwidth and the synchronizing signal frequency for analog recording and digital-data processing. This article describes the basic receiver design and the modifications required for multiple-mission capability.

DOWNS, G. S.

D11 **DSN Progress Report for March–April 1973: Simultaneous Detection of Pulsar Radiation at S- and X-Bands**

P. E. Reichley, G. S. Downs, and G. A. Morris

Technical Report 32-1526, Vol. XV, pp. 133–137, June 15, 1973

For abstract, see Reichley, P. E.

D12 **Martian Topography and Surface Properties as Seen by Radar: The 1971 Opposition**

G. S. Downs, R. M. Goldstein, R. R. Green, G. A. Morris, and P. E. Reichley

Icarus, Vol. 18, No. 1, pp. 8–21, January 1973

Taking advantage of the favorable opposition of 1971, the Goldstone radar system, operating at 2388 MHz, was used to scan the Martian surface. Measurements of altitude and reflected power were taken approximately every 3 days. Each measurement represents an area 8 km E–W × 80 km N–S, the highest resolution attained to date. Altitude measurements obtained on different observing days were combined to produce altitude profiles for three complete rotations, each at different latitudes. Large-scale variations in altitudes cover a range of 14 km. Altitude changes of 5 in 30 km of longitude were observed. The altitude profiles show the heavy cratering of the surface, and several large craters (50–100 km) 1–2 km deep are easily seen. Reflected power for different angles of incidence was measured, yielding the scattering properties of the surface as a function of longitude. Correlation was found between the peak intensity of the reflected signal and the width of the scattering function. The average relationship between the intensity and the width suggests a power reflection coefficient of at least 0.064 ± 0.012. Departures from the average are interpreted as deviations in the reflection coefficient from the mean value. These variations are presented as a function of longitude for each of the three rotations.

DUNN, G. L.

D13 DSN Progress Report For January–February 1973: Effects of Doppler Rate on Subcarrier Demodulator Assembly Performance

G. L. Dunn

Technical Report 32-1526, Vol. XIV, pp. 200–204,
April 15, 1973

A time-dependent, steady-state, static-phase-error equation that includes doppler-rate effects has been incorporated into the Subcarrier-Demodulator-Assembly efficiency program. With the program in its present form, the optimum possible bandwidths, bit rate, amount of nulling of static phase error, and expected degradation can be obtained for the tracking of a given two-way doppler-shift profile by various manipulations of the program.

DUSSEL, G. A.

D14 Photoconductor–Metal Contact at Higher Densities

G. A. Dussel (University of Delaware),
K. W. Böer (University of Delaware), and R. J. Stirn

Phys. Rev., Pt. B: Solid State, Vol. 7, No. 4,
pp. 1443–1454, February 15, 1973

The formation of space charge in the barrier region is discussed. This region extends to $x_0 \cong 200$ Å + 2λ (λ is the mean free path of majority carriers). The conventional transport equation can be used only for $x > x_0$, and the carrier density at x_0 represents a boundary condition for the bulk. Its change as a function of applied voltage, temperature, and light intensity in photoconducting CdS is discussed. The time dependence of the space-charge formation in the region $0 < x < x_0$ is analyzed. It is shown under which conditions the individuality of the metal contact is observable.

D15 CdS–Metal Contact at Higher Current Densities

R. J. Stirn, K. W. Böer (University of Delaware), and
G. A. Dussel (University of Delaware)

Phys. Rev., Pt. B: Solid State, Vol. 7, No. 4,
pp. 1433–1443, February 15, 1973

For abstract, see Stirn, R. J.

EDWARDS, J. N.

E01 DSN Progress Report for January–February 1973: Network Control System

J. N. Edwards

Technical Report 32-1526, Vol. XIV, pp. 141–145,
April 15, 1973

The Network Control System (NCS) is being implemented for the DSN. This article includes progress activities for final NCS hardware implementation, NCS data formats and Mission Operations Control interfaces, a software development summary, and an interim NCS hardware and software development summary.

EISENBERGER, I.

E02 DSN Progress Report for January–February 1973: A Comparison Between the Current and Proposed Inventory and Procurement Policies for the Deep Space Network

I. Eisenberger, F. R. Maiocco, and G. Lorden (California Institute of Technology)

Technical Report 32-1526, Vol. XIV, pp. 81–86,
April 15, 1973

This article presents a comparison between the performances of the current and a proposed inventory and procurement policy for the Network Supply Depot and the Complex Supply Facilities. Both policies were simulated on a computer using identical input demand data. The comparison is based on four criteria: average inventory level, frequency of procurement orders, frequency of shortages, and average inventory cost per year. The results of the study indicate that, with reference to maintenance and operating items, the inventory cost would be reduced by about 25% if the proposed policy were put into effect.

E03 **Detection of Failure Rate Increases**

G. Lorden (California Institute of Technology) and
I. Eisenberger

Technometrics, Vol. 15, No. 1, pp. 167–175, February 1973

For abstract, see Lorden, G.

ELLEMAN, D. D.

E04 **Thermal Energy Charge Transfer Reactions of Rare-Gas Ions to Methane, Ethane, Propane, and Silane: The Importance of Franck–Condon Factors**

M. T. Bowers (University of California, Santa Barbara) and
D. D. Elleman

Chem. Phys. Lett., Vol. 16, No. 3, pp. 486–491,
October 15, 1972

For abstract, see Bowers, M. T.

E05 **Temperature Dependence of the Accommodation Coefficient of Liquid-Helium Film**

T. G. Wang, D. D. Elleman, E. E. Olli, and M. M. Saffren

Phys. Rev. Lett., Vol. 30, No. 11, pp. 485–487,
March 12, 1973

For abstract, see Wang, T. G.

EMERSON, R. F.

E06 **DSN Progress Report for January–February 1973: A Minicomputer Vector Generator**

R. F. Emerson

Technical Report 32-1526, Vol. XIV, pp. 101–108,
April 15, 1973

A vector generator was designed and built as a peripheral for a minicomputer. The vector generator is a device which accepts two endpoints and draws a straight line between them on some display device. While this could be done point-by-point by a minicomputer, it would use valuable computing power in an inefficient way. This generator is part of the Precision Signal

Power Measurement System and is used to graph the power spectra of the measured signal to determine the performance of spacecraft and ground-telemetry transmitters and receivers. This hardware increases the graphing efficiency by an average of 4000 times over the point-by-point plotting method, requiring less than 15 μs of computer time per endpoint. The vectors are composed of points spaced 0.004 mm apart, providing excellent resolution and linearity.

E07 DSN Progress Report for March–April 1973: Precision Signal Power Measurement System Using Central Computing

R. F. Emerson

Technical Report 32-1526, Vol. XV, pp. 116–127,
June 15, 1973

A Precision Signal Power Measurement System was built for research, development, and demonstration of a digital technique for the measurement of spacecraft signal power. Demonstrations at the Mars Deep Space Station (DSS 14) have shown that the method is valid. Since the process relies heavily on digital computations and computers are in short supply at deep space stations, it was necessary to determine if centralized computation could be done. To test this feasibility, the system described in this article was developed from existing subsystems and additional or new programs. During design of this system, parameters and relationships were developed to predict the behavior of the completed system.

Tests of this system in January 1971 showed that it performed as predicted. The final demonstration was conducted using the Mark IIIA hardware/software system in the Mission Control and Computing Center. The results indicate that remote processing of precision signal-power measurement data is technically feasible. As implemented, the technique is limited to narrow-band spectra of signals with power levels between -140 and -170 dBm.

EPSTEIN, E. E.

E08 3C 120, BL Lacertae, and OJ 287: Coordinated Optical, Infrared, and Radio Observations of Intraday Variability

E. E. Epstein, et al.

Astrophys. J., Vol. 178, No. 2, Pt. 2, pp. L51–L59,
December 1, 1972

Simultaneous optical, infrared, and radio observations were made to search for intraday (time scale $< 24^h$) variability of the radiation from 3C 120, BL Lac, and OJ 287, sources known to be active at both radio and optical wavelengths on time scales of days or longer. Optical interday (time scale > 24^h) variability was found for all three sources. The finding of optical intraday variability for BL Lac verified earlier results. The 3.5-mm data strongly suggest intraday variations of OJ 287 with amplitudes as large as ~40%. The infrared data for OJ 287 show variability of ~25% on one night but show no correlation with the 3.5-mm data.

Contributors to this article include:

The Aerospace Corporation: E. E. Epstein and W. G. Fogarty

University of Florida: K. R. Hackney, R. L. Hackney, R. J. Leacock, R. B. Pomphrey, R. L. Scott, and A. G. Smith

University of Toronto: R. W. Hawkins and R. C. Roeder

Jet Propulsion Laboratory: B. L. Gary

Royal Greenwich Observatory: M. V. Penston and K. P. Tritton

Observatoire de Paris: C. Bertaud, M. P. Véron, and G. Wlérick

Observatoire de Lyon: A. Bernard, J. H. Bigay, and P. Merlin

Observatoire de Haute-Provence: A. Durand and G. Sause

Hale Observatories, California Institute of Technology, and Carnegie Institution of Washington: E. E. Becklin, G. Neugebauer, and C. G. Wynn-Williams

ERICKSON, D. E.

E09 DSN Progress Report for March–April 1973: An Experiment in Remote Monitoring of Mu-Ranging Operation at Mariner Mars 1971 Superior Conjunction

D. E. Erickson and J. W. Layland

Technical Report 32-1526, Vol. XV, pp. 156–166, June 15, 1973

This article describes the computer configurations and software used at JPL in an experimental remote monitoring and verification of the operation of the Sequential Component Ranging System during the superior conjunction of the Mariner Mars 1971 spacecraft. At the time of the spacecraft's closest approach to the Sun, the ranging operation was subjected to both an extremely low signal-to-noise ratio and perturbations from solar plasma.

The Sigma 5 computer at JPL was programmed to perform a maximum-likelihood range measurement, using the range-code correlation values supplied (in real time) from the ranging system at the Mars Deep Space Station (DSS 14). The maximum-likelihood decision process provided about a 1.5-dB improvement in ranging-error probability considering additive noise alone. The process was, however, relatively impractical to implement in the 920 computer which controlled the ranging operation at DSS 14 and performed range measurement via a sequential decision process.

ESCOBAL, P. R.

E10 DSN Progress Report for March–April 1973: A Global Model of the Earth's Ionosphere: The Nighttime Ionosphere

O. H. von Roos and P. R. Escobal

Technical Report 32-1526, Vol. XV, pp. 32–47,
June 15, 1973

For abstract, see von Roos, O. H.

FEDORS, R. F.

F01 A Method for Estimating Both the Solubility Parameters and Molar Volumes of Liquids

R. F. Fedors

JPL Quarterly Technical Review, Vol. 3, No. 1, pp. 45–53,
April 1973

The solubility parameters and molar volumes of substances can be used, in conjunction with suitable theory, to provide estimates of the thermodynamic properties of solutions. The solubility characteristics of polymer–solvent systems and the estimation of the equilibrium uptake of liquids by polymers are examples of the types of practical problems that are amenable to treatment. For low-molecular-weight liquids, the solubility parameter δ is conveniently calculated using expression $\delta = (\Delta E_v / V)^{1/2}$, where ΔE_v is the energy of vaporization at a given temperature and V is the corresponding molar volume which is calculated from the known values of molecular weight and density. For high-molecular-weight polymers, the volatility is much too low for ΔE_v to be obtained directly, and hence recourse must be made to indirect methods for estimating δ for these materials. One such widely used method is based on Small's additive group "molar-attraction constants," which when summed allow the estimation of δ from a knowledge of the structural formula of the material. However, the density must still be determined experimentally.

The proposed method of estimating δ, also based on group additive constants, is believed to be superior to Small's method for two reasons: (1) the contribution of a much larger number of functional groups has been evaluated, and (2) the method requires only a knowledge of the structural formula of the compound.

FERRERA, J. D.

F02 A Method for Calculating Transient Thrust and Flow-Rate Levels for Mariner Type Attitude Control Nitrogen Gas Jets

J. D. Ferrera

Technical Memorandum 33-604, January 1, 1972

The purpose of this memorandum is to define and program the transient pneumatic-flow equations necessary to determine, for a given set of conditions (geometry, pressures, temperatures, valve on time, etc.), the total nitrogen impulse and mass flow per pulse for the single pulsing of a Mariner-type reaction-control assembly valve. The rates of opening and closing of the valves are modeled, and electrical pulse durations of 20 to 100 ms are investigated.

The impulse results are compared to an equivalent square-wave impulse for both the Mariner Mars 1971 (MM'71) and Mariner Mars 1964 (MM'64) systems. It is demonstrated that, whereas in the MM'64 system, the actual impulse was as much as 56% higher than an assumed impulse (which is the product of the steady-state thrust and valve on time–i.e., the square wave), in the MM'71 system, the assumed impulse was in error in the same direction by only approximately 4% because of the larger nozzle areas and shorter valve stroke used.

FINNEGAN, E. J.

F03 DSN Progress Report for January–February 1973: New Arc Detector

E. J. Finnegan and R. A. Leech

Technical Report 32-1526, Vol. XIV, pp. 170–172, April 15, 1973

During this reporting period a new arc detector was constructed and tested both on the bench and at the Venus Deep Space Station. Test data show that the new arc detector meets or exceeds the performance of the existing arc detector and has the advantages of being simpler in construction and half the physical size.

FINNIE, C.

F04 **DSN Progress Report for January–February 1973: Tracking and Ground-Based Navigation: Hydrogen Maser Frequency Standard Automatic Cavity Tuning Servo**

C. Finnie

Technical Report 32-1526, Vol. XIV, pp. 56–59, April 15, 1973

This article describes the automatic cavity-tuning servomechanism to be incorporated in the DSN prototype hydrogen-maser frequency standard. It is a first-order sample-data control system, featuring stability-monitoring circuits for the detection of malfunctions in the maser and its receiver-frequency synthesizing system. The control system ignores error measurements exceeding an adjustable limit. The system's counter calibrates the Zeeman oscillator used to correct the maser output frequency for ambient magnetic fields.

FJELDBO, G.

F05 **The Atmosphere of Mars From Mariner 9 Radio Occultation Measurements**

A. J. Kliore, D. L. Cain, G. Fjeldbo, B. L. Seidel, M. J. Sykes, and S. I. Rasool (National Aeronautics and Space Administration)

Icarus, Vol. 17, No. 2, pp. 484–516, October 1972

For abstract, see Kliore, A. J.

FLETCHER, B. C.

F06 **Evaluation of Errors in Prior Mean and Variance in the Estimation of Integrated Circuit Failure Rates Using Bayesian Methods**

B. C. Fletcher

Technical Memorandum 33-614, June 1, 1972

Under the constraint of limited testing time, many attempts have been made to incorporate prior knowledge and experience into a quantitative assessment of reliability. This type of technique is known as Bayesian statistics. Since the length of time available for testing integrated circuits is frequently very limited, an analysis of Bayesian methods when applied to the integrated-circuit testing problem was conducted.

The critical point of any Bayesian analysis concerns the choice and quantification of the prior information. This memorandum is a study of the effects of prior data on a Bayesian analysis. Comparisons of the maximum-likelihood estimator, the Bayesian estimator, and the known failure rate are presented. The results of the many simulated trials are then analyzed to show the region of criticality for prior information being supplied to the Bayesian estimator. In particular, effects of prior mean and variance are determined as a function of the amount of test data available.

FOSTER, C. F.

F07 **DSN Progress Report for January–February 1973: S-Band Planetary Radar Receiver Development**

C. F. Foster and G. F. Lutes

Technical Report 32-1526, Vol. XIV, pp. 23–26,
April 15, 1973

This article describes the design of a wideband 2295/2388-MHz converter which is a part of the Mars Deep Space Station (DSS 14) bistatic radar receiver. The receiver is an open-loop superheterodyne receiver used for the development of communication techniques and this converter design eliminates the need for separate converters at each frequency. The 2295/2388-MHz converter has been installed at DSS 14 and is now being used in the Venus radar-mapping experiments.

FRAMAN, E. P.

F08 **Numerical Correlation and Evaluation in the Comparison of Evidentiary Materials**

D. D. Lawson and E. P. Framan

J. Forensic Sci., Vol. 18, No. 2, pp. 110–117, April 1973

For abstract, see Lawson, D. D.

FRANK, H. A.

F09 **Leak Rates in Sealed Cells**

H. A. Frank and A. A. Uchiyama

J. Electrochem. Soc., Vol. 120, No. 3, pp. 313–317,
March 1973

Water vapor loss rates were determined from simulated and imperfectly sealed alkaline cells in the vacuum environment. The observed rates were found to be in agreement with a semi-empirical equation employed in vacuum technology. Results thereby give support for using this equation for the prediction of loss rates of battery gases and vapors to the aerospace environment. On this basis it was shown how the equation can be applied to the solution of many heretofore unresolved questions regarding leaks in batteries. Among these are the maximum permissible leak size consistent with a given cell life and conversely the maximum life consistent with a given leak size. It was also shown that loss rates of these cells in the terrestrial environment are several orders of magnitude less than the corresponding loss rates in the aerospace environment.

FREILEY, A. J.

F10 DSN Progress Report for January–February 1973: Tracking and Ground-Based Navigation: Precision System Temperature Measurements at Goldstone

M. S. Reid, R. A. Gardner, and A. J. Freiley

Technical Report 32-1526, Vol. XIV, pp. 60–67,
April 15, 1973

For abstract, see Reid, M. S.

FRENCH, R. L.

F11 From Earth to Mars Orbit—Mariner 9 Propulsion Flight Performance With Analytical Correlations

M. J. Cork, R. L. French, C. J. Leising, and D. D. Schmit

AIAA Preprint 72-1185, AIAA/SAE Eighth Joint Propulsion Specialist Conference, New Orleans, Louisiana,
November 29–December 1, 1972

For abstract, see Cork, M. J.

FREY, W. C.

F12 DSN Progress Report for March–April 1973: Network Control System Development

W. C. Frey

Technical Report 32-1526, Vol. XV, pp. 167–176,
June 15, 1973

The development of the DSN Network Control System (NCS) has been authorized to provide centralized computer control and monitoring of deep space station equipment status and data flow. The NCS is being implemented with an interim capability for current spacecraft-support requirements. A final NCS, providing future spacecraft-support requirements, will be implemented by a complex of minicomputers with dedicated-subsystem functional capability.

FRIEDENBERG, S. E.

F13 DSN Progress Report for March–April 1973: Multiple-Mission Open-Loop Receiver

H. Donnelly and S. E. Friedenberg

Technical Report 32-1526, Vol. XV, pp. 181–184,
June 15, 1973

For abstract, see Donnelly, H.

FRIEDMAN, L. D.

F14 Estimating Trajectory Correction Requirements for Multiple Outer Planet Missions

L. D. Friedman, T. W. Hamilton, and R. H. Stanton

J. Spacecraft Rockets, Vol. 9, No. 12, pp. 909–914,
December 1972

The estimation of trajectory correction (ΔV) requirements for multiple outer planet flyby missions is a unique and challenging problem for the systems analyst. This article presents a general approach to solving this problem when the navigation system uses onboard optical measurements made during approach to each target planet to complement the ground-based radio measurements. The accuracy and reliability of the onboard measurement system plays a critical role in sizing the ΔV capability required. An illustration of the combined use of radio and optical measurements is provided for the particular case of a Jupiter–Uranus–Neptune mission. Use of the statistical technique developed for computing the ΔV margin required to account for uncertainties in subsystem performance permits ΔV savings of 100–120 m/s over "worst case" designs. This represents weight savings of about 50% of the science payload. For the example case ΔV requirements are estimated for two candidate optical systems and the radio alone case. The use of onboard measurements allows a ΔV savings of approximately 140 m/s.

F15 **Navigation Requirements for Advanced Deep Space Missions**

L. D. Friedman, J. W. Moore, and R. L. Sohn

Navigation: J. Institute Nav., Vol. 19, No. 3, pp. 266–280, Fall 1972

Throughout the history of space exploration, the navigation performance of spacecraft has been a prime driving factor in controlling mission value and mission design. In examining advanced interplanetary missions, it has been found that the navigation performance will be of even greater significance in future mission design. This article presents a survey of advanced deep space mission navigation requirements by an examination of the potential missions and their navigation system goals.

GARDNER, R. A.

G01 **DSN Progress Report for January–February 1973: Tracking and Ground-Based Navigation: Precision System Temperature Measurements at Goldstone**

M. S. Reid, R. A. Gardner, and A. J. Freiley

Technical Report 32-1526, Vol. XIV, pp. 60–67,
April 15, 1973

For abstract, see Reid, M. S.

GARY, B.

G02 **Observations of Jupiter at 13-cm Wavelength During 1969 and 1971**

S. Gulkis, B. Gary, M. Klein, and C. T. Stelzried

Icarus, Vol. 18, No. 2, pp. 181–191, February 1973

For abstract, see Gulkis, S.

G03 **Radio Observations of Cygnus X-3 and the Surrounding Region**

B. Gary, E. T. Olsen, and P. W. Rosenkranz

Nature Phys. Sci., Vol. 239, No. 95, pp. 128–130,
October 23, 1972

On September 7, 1972, Cygnus X-3 was observed with the Goldstone 64-m antenna at wavelengths of 13.1, 3.55, and 2.07 cm. At 13.1 cm a map of received flux density has been constructed for a region 0.5 × 0.6 arc deg with a resolution of 8.15 arc min. This map reveals the presence of several partially resolved features having integrated flux densities in excess of one flux unit. This article presents and discusses the map as well as a summary of the intensity measurements taken at the three wavelengths.

GENSEL, D. R.

G04 Monitoring of Antarctic Dry Valley Drilling Sites

F. A. Morelli, R. E. Cameron, D. R. Gensel, and L. P. Randall (Northern Illinois University)

Antarctic J. U.S., Vol. VII, No. 4, pp. 92–94, July–August 1972

For abstract, see Morelli, F. A.

GOLDSTEIN, R. M.

G05 Martian Topography and Surface Properties as Seen by Radar: The 1971 Opposition

G. S. Downs, R. M. Goldstein, R. R. Green, G. A. Morris, and P. E. Reichley

Icarus, Vol. 18, No. 1, pp. 8–21, January 1973

For abstract, see Downs, G. S.

GOSLINE, R. M.

G06 DSN Progress Report for January–February 1973: CONSCAN Implementation at DSS 13

R. M. Gosline

Technical Report 32-1526, Vol. XIV, pp. 87–90, April 15, 1973

The ability to do automatic boresighting of a large parabolic antenna without a monopulse feed or rotatable subreflector is desirable. A conical-scan technique based on the movement of the main reflector under computer control has been developed. This article describes the functional features of the hardware and software as implemented at the Venus Deep Space Station (DSS 13). Application to very precise antenna pointing is possible.

GOSS, W. C.

G07 Image Dissector Development

W. C. Goss

Technical Memorandum 33-608, April 15, 1973

A second-generation, electrostatically focused, image-dissector tube for use in spacecraft-attitude-control star trackers is being developed with the support of an industrial contractor. Significant improvements are being made in functional characteristics, as well as in package-dimension control, tolerance of a wide variety of environmental conditions, and expected reliability over long operational lifetimes.

GREEN, R. R.

G08 Martian Topography and Surface Properties as Seen by Radar: The 1971 Opposition

G. S. Downs, R. M. Goldstein, R. R. Green,
G. A. Morris, and P. E. Reichley

Icarus, Vol. 18, No. 1, pp. 8–21, January 1973

For abstract, see Downs, G. S.

GREEN, W. B.

G09 Mariner 9—Image Processing and Products

E. C. Levinthal (Stanford University), W. B. Green,
J. A. Cutts, E. D. Jahelka, R. A. Johansen, M. J. Sander,
J. B. Seidman, A. T. Young, and L. A. Soderblom (U.S.
Geological Survey)

Icarus, Vol. 18, No. 1, pp. 75–101, January 1973

For abstract, see Levinthal, E. C.

GROTCH, S. L.

G10 Computer Identification of Mass Spectra Using Highly Compressed Spectral Codes

S. L. Grotch

Anal. Chem., Vol. 45, No. 1, pp. 2–6, January 1973

In file search methods, storage is often a significant problem, particularly with mini-computers. Spectral abbreviation alleviates the problem by coding only 2 peaks/14 amu. This concept may be further exploited by noting that the mass position of any peak in a 14-amu window may be coded using only four bits. For nearly 7000 spectra in the Aldermaston collection, this code requires an average of 48 bits/spectrum. Tests indicate that this code is highly specific, and with appropriate matching algorithms will produce very effective identifications. Further improvements in identification accuracy are obtained when two bits of intensity information are added to the peak position. Using an IBM 360/44, a 7000-spectra library can be searched in less than 10 s. Since most computers now manufactured have word sizes which are multiples of four bits, this technique should lend itself well to most machines.

GULKIS, S.

G11 Observations of Jupiter at 13-cm Wavelength During 1969 and 1971

S. Gulkis, B. Gary, M. Klein, and C. T. Stelzried

Icarus, Vol. 18, No. 2, pp. 181–191, February 1973

Radio observations of Jupiter have been carried out at Goldstone, California at a wavelength of 13 cm during the oppositions of 1969 and 1971. In 1969, circular-polarization and total-flux measurements were made with a 64-m radio telescope. From May through October 1971, Jupiter's flux density was measured at weekly intervals with a 26-m antenna. Analysis of the 2 years of data has yielded the following results: (a) The upper limit to the degree of circular polarization over the longitude ranges 10–100° and 160–250° System III (1957.0) is 1%; (b) the flux data have been used to derive a magnetospheric rotation period which is approximately 0.37 s longer than the IAU System III (1957.0); (c) the flux-density data define beaming curves which are apparently different from 11-cm beaming curves measured in 1964; (d) Jupiter's peak flux density decreased by ~20% between 1964 and 1971, and 8% between 1969 and 1971.

G12 Thermal Radio Emission From Jupiter and Saturn

S. Gulkis and R. Poynter

Phys. Earth Planet. Interiors, Vol. 6, Nos. 1–3, pp. 36–43, December 1972

Microwave brightness temperature calculations have been carried out for a number of model atmospheres for Jupiter and Saturn. The models considered are characterized by helium to hydrogen number mixing ratios which range from 0 to 0.2. Gaseous ammonia is assumed to be a trace constituent in all the models. The ammonia abundance below the (NH_3) cloud level is a free parameter which is determined by comparing the observed thermal spectrum of Jupiter and the total spectrum of Saturn with the model calculations. The theoretical microwave spectra corresponding to those models in which the ammonia abundance is that expected from an atmosphere containing a solar abundance of elements are found to be in generally good agreement with the observations. This result is shown to be nearly independent of the helium to hydrogen ratio for the models considered. There is no evidence at this time that a nonthermal component contributes to Saturn's microwave spectrum.

G13 A Survey of the Outer Planets Jupiter, Saturn, Uranus, Neptune, Pluto, and Their Satellites

R. L. Newburn, Jr., and S. Gulkis

Space Sci. Rev., Vol. 14, No. 2, pp. 179–271, February 1973

For abstract, see Newburn, R. L., Jr.

GUPTA, K. K.

G14 Free Vibration Analysis of Spinning Structural Systems

K. K. Gupta

Int. J. Numer. Methods Eng., Vol. 5, No. 3, pp. 395–418, January 1973

This article presents an efficient digital computer procedure, along with the complete listing of the associated computer program, which may be conveniently utilized for the accurate solution of a wide range of practical eigenvalue problems. Important applications of the present work are envisaged in the natural frequency analysis of spinning structures discretized by the finite element technique, and in the determination of transfer functions associated with the dynamic blocks of control systems of spacecraft utilizing gas jets or reaction wheels for attitude control, as well as of spin-stabilized and dual-spin-stabilized satellites.

The validity of the Sturm sequence property is first established for the related matrix formulation involving Hermitian and real symmetric, positive-definite matrices, both being usually of highly banded configuration. A numerically stable algorithm based on the Sturm sequence method is then developed which fully exploits the banded form of the associated matrices. The related computer program written in FORTRAN V for the JPL UNIVAC 1108 computer proves to be extremely fast and economical in comparison to other existing methods of such analysis. Numerical results are presented for a spinning bent cantilever beam and the solar arrays of SKYLAB, the Earth-orbiting space station proposed by NASA.

G15 **Solution of Quadratic Matrix Equations for Free Vibration Analysis of Structures**

K. K. Gupta

Int. J. Numer. Methods Eng., Vol. 6, No. 1, pp. 129–135, 1973

An efficient digital computer procedure and the related numerical algorithm are presented herein for the solution of quadratic matrix equations associated with free vibration analysis of structures. Such a procedure enables accurate and economical analysis of natural frequencies and associated modes of discretized structures. The numerically stable algorithm is based on the Sturm sequence method, which fully exploits the banded form of associated stiffness and mass matrices. The related computer program written in FORTRAN V for the JPL UNIVAC 1108 computer proves to be substantially more accurate and economical than other existing procedures of such analysis. Numerical examples are presented for two structures: a cantilever beam and a semicircular arch.

HADEK, V.

H01 **Alkali Metal Intercalates of Molybdenum Disulfide**

R. B. Somoano, V. Hadek, and A. Rembaum

J. Chem. Phys., Vol. 58, No. 2, pp. 697–701, January 15, 1973

For abstract, see Somoano, R. B.

HAM, N. C.

H02 **DSN Progress Report for January–February 1973: Amplitude and Frequency Modulation Effects to Telemetry Link Reception**

N. C. Ham

Technical Report 32-1526, Vol. XIV, pp. 149–160, April 15, 1973

A spin-stabilized spacecraft can produce an amplitude and phase variation to the normally phase-modulated downlink carrier signal due to its antenna characteristics. The manifestation of these variations is equivalent to an amplitude and frequency modulation of the carrier signal, and the effects to the telemetry link must be considered. The Helios spacecraft and mission is a typical case, and means for simulating a certain portion of the flight profile, which will create such conditions, was utilized to test and evaluate the effect upon the Deep Space Instrumentation Facility Telemetry System. Initial test results indicated that the Telemetry System was more sensitive to phase variation than to amplitude variation in increasing the detected symbol error rate for a given telecommunication-link situation.

HAMILTON, T. W.

H03 **Estimating Trajectory Correction Requirements for Multiple Outer Planet Missions**

L. D. Friedman, T. W. Hamilton, and R. H. Stanton

J. Spacecraft Rockets, Vol. 9, No. 12, pp. 909–914, December 1972

For abstract, see Friedman, L. D.

HARRISON, E. C.

H04 **Prediction of Lipid Uptake by Prosthetic Heart Valve Poppets From Solubility Parameters**

J. Moacanin, D. D. Lawson, H. P. Chin (University of Southern California), E. C. Harrison (University of Southern California), and D. H. Blankenhorn (University of Southern California)

Biomat., Med. Dev., Art. Org., Vol. 1, No. 1, pp. 183–190, 1973

For abstract, see Moacanin, J.

HARSTAD, K. G.

H05 **One-Dimensional Line Radiative Transfer**

K. G. Harstad

J. Quant. Spectrosc. Radiat. Transfer, Vol. 13, No. 2, pp. 155–165, February 1973

Integrations over solid angle and frequency are performed in the expressions for the radiant heat flux and local energy loss of a line in a region of strong variations of the source function in one direction. Approximations are given for coefficients and kernels in the resulting forms which involve integrals over the physical coordinate.

HARTLEY, R. B.

H06 DSN Progress Report for January–February 1973: Apollo Mission Support

R. B. Hartley

Technical Report 32-1526, Vol. XIV, pp. 16–22, April 15, 1973

This article describes the support provided by the DSN to the Spaceflight Tracking and Data Network during the Apollo 17 mission. Support was provided by three 26-m-diameter-antenna deep space stations, the 64-m-diameter-antenna Mars Deep Space Station (DSS 14), the Ground Communications Facility, and the Mission Control and Computing Center. Premission and mission activities of the DSN are discussed, and the mission is described.

HARTOP, R. W.

H07 DSN Progress Report for March–April 1973: X-Band Waveguide Switches

R. W. Hartop

Technical Report 32-1526, Vol. XV, pp. 48–50, June 15, 1973

To accommodate the X-band requirements of the DSN, new microwave components, including high-performance waveguide switches, are being developed. Waveguide switches in the new WR-125 waveguide size are presently being evaluated. This article describes progress to date in prototype and preproduction model development.

HIGA, W. H.

H08 DSN Progress Report for March–April 1973: Low Noise Receivers: Theory of "Noise Bursts" on Large Antennas

W. H. Higa, R. C. Clauss, and P. Dachel

Technical Report 32-1526, Vol. XV, pp. 80–83, June 15, 1973

When a large, paraboloidal antenna is used simultaneously for high-power transmission and low-level reception of signals at different frequencies, frequent anomalous and random noise bursts appear at the receiver output. Also, if simultaneous transmission is made at two slightly separated frequencies, intermodulation products of high order number will often appear at the receiver output. Based on a plausible explanation for these phenomena, simple experiments have been performed in the laboratory to reproduce the observations.

HINNERS, N. W.

H09 **The Apollo 17 Surface Experiments**

N. W. Hinners (NASA Apollo Program Office) and
P. V. Mason

Astronaut. Aeronaut., Vol. 10, No. 12, pp. 40–54,
December 1972

During the Apollo 17 mission to be launched on December 6, 1972, Navy Captain Eugene Cernan, Dr. Harrison Schmitt, and Navy Commander Ronald Evans will carry out scientific activities of considerably greater sophistication than has been possible in previous missions. This article explains the scientific rationale behind the choice of the Apollo 17 Taurus-Littrow site, briefly notes the objectives of the mission in its entirety, and then describes in some detail the geophysical experiments as embodied in specific instruments.

HOLMES, J. K.

H10 **DSN Progress Report for March–April 1973: Bit Synchronizer for Sample Data Antenna Pointing System**

T. O. Anderson, J. K. Holmes, and W. J. Hurd

Technical Report 32-1526, Vol. XV, pp. 128–132,
June 15, 1973

For abstract, see Anderson, T. O.

HONER, W.

H11 **DSN Progress Report for March–April 1973: Recent Modifications to the DSN Monitor and Control System**

J. E. Allen and W. Honer

Technical Report 32-1526, Vol. XV, pp. 185–189,
June 15, 1973

For abstract, see Allen, J. E.

HURD, W. J.

H12 **DSN Progress Report for March–April 1973: Bit Synchronizer for Sample Data Antenna Pointing System**

T. O. Anderson, J. K. Holmes, and W. J. Hurd

Technical Report 32-1526, Vol. XV, pp. 128–132, June 15, 1973

For abstract, see Anderson, T. O.

HUTCHINSON, R. B.

H13 **Observation of the OH Radical in Betelgeuse**

R. Beer, R. H. Norton, R. B. Hutchinson,
D. L. Lambert (University of Texas), and
J. V. Martonchik (University of Texas)

Mém. Soc. Roy. Sci. Liège, Vol. III, No. 6, p. 145, 1972

For abstract, see Beer, R.

ISHIMARU, A.

I01 **Remote Sensing of the Turbulence Characteristics of a Planetary Atmosphere by Radio Occultation of a Space Probe**

R. Woo and A. Ishimaru (University of Washington)

Radio Sci., Vol. 8, No. 2, pp. 103–108, February 1973

For abstract, see Woo, R.

JACKSON, E. B.

J01 **DSN Progress Report for January–February 1973: DSN Research and Technology Support**

E. B. Jackson

Technical Report 32-1526, Vol. XIV, pp. 91–93, April 15, 1973

This article presents the activities of the Development Support Group in operating the Venus Deep Space Station (DSS 13) and the Microwave Test Facility for the period December 16, 1972 through February 15, 1973. Major activities include continuation of the intensive dual-carrier investigation, refurbishing of the S-band-megawatt-transmit cassegrain feedcone, implementation of the dedicated antenna-pointing computer for the 26-m-diameter antenna, and continuation of collection of Faraday-rotation data.

J02 **DSN Progress Report for March-April 1973: DSN Research and Technology Support**

E. B. Jackson, A. L. Price, and R. B. Kolbly

Technical Report 32-1526, Vol. XV, pp. 138–142, June 15, 1973

This article discusses the activities of the Development Support Group at the Venus Deep Space Station (DSS 13) and the Microwave Test Facility (MTF). Activities include interchange of the SDS-930 computers between DSS 13 and the Mars Deep Space Station (DSS 14) and subsequent installation and checkout; planetary radar support for the Mariner Venus/Mercury 1973 mission and modifications to DSS 14 and DSS 13 necessary to continue such support; installation of a new Faraday-rotation data-collection system; relocation of pulsar capability from DSS 13 to DSS 14; dual-carrier activity on the 26-m-diameter antenna; and dual-carrier activity for the Goddard Space Flight Center carried out at MTF on components of the Spaceflight Tracking and Data Network waveguide system. Also reported is a novel way to effect replacement of the 400-kW klystron without removing the assembly from the tricone support structure of the 64-m-diameter antenna.

JAFFE, L. D.

J03 **Spacecraft Techniques for Lunar Research**

L. D. Jaffe, R. Chaote, and R. B. Coryell

The Moon, Vol. 5, Nos. 3–4, pp. 348–367, November–December 1972

The most significant findings concerning the moon obtained by spacecraft so far, have resulted from measurements of gravity, electromagnetic properties, seismicity, mechanical properties, geologic features, composition, ages, and the lunar environment. A number of major lunar questions remain to be answered. Other properties, measurable with spacecraft, which may provide data critical to answering these questions include geometrical shape, motions, and heat flow. In this article specific measurements that should provide critical data for each of these questions are identified, with some candidate techniques. Among the suggested techniques that have not yet been used are very long baseline interferometry (Earth-moon baseline), gravity gradiometry, elemental analysis by neutron interactions, and remotely-controlled on-moon microscopy.

Different types of missions are suitable for the different measurements: lunar orbiters, soft-landers, long-range surface traverses, and sample return to Earth are all needed. The choice of manned vs remotely-controlled missions does not depend on scientific requirements but on other considerations. Both manned and remotely-controlled techniques have been used for orbiters, landers, and sample return, neither for a long-range traverse.

JAHELKA, E. D.

J04 Mariner 9—Image Processing and Products

E. C. Levinthal (Stanford University), W. B. Green, J. A. Cutts, E. D. Jahelka, R. A. Johansen, M. J. Sander, J. B. Seidman, A. T. Young, and L. A. Soderblom (U.S. Geological Survey)

Icarus, Vol. 18, No. 1, pp. 75–101, January 1973

For abstract, see Levinthal, E. C.

JAWORSKI, W.

J05 Effects of Overlaps, Stitches, and Patches on Multilayer Insulation

L. D. Stimpson and W. Jaworski

Progr. Astronaut. Aeronaut., Vol. 31, pp. 247–266, 1973

For abstract, see Stimpson, L. D.

JET PROPULSION LABORATORY

J06 Mariner Mars 1971 Project Final Report: Mission Operations System Implementation and Standard Mission Flight Operations

Jet Propulsion Laboratory

Technical Report 32-1550, Vol. III, July 1, 1973

The Mariner Mars 1971 mission was another step in the continuing program of planetary exploration in search of evidence of exobiological activity, information on the origin and evolution of the solar system, and basic science data related to the study of planetary physics, geology, planetology, and cosmology. The mission plan was designed for two spacecraft, each performing a separate but complementary mission. However, a single mission plan was actually used for Mariner 9 because of launch-vehicle failure for the first spacecraft.

This report describes the implementation of the Mission Operations System, including organization, training, and data processing development and operations, and discusses Mariner 9 spacecraft cruise and orbital operations from launch through completion of the standard mission in April 1972.

JOHANSEN, R. A.

J07 Mariner 9—Image Processing and Products

E. C. Levinthal (Stanford University), W. B. Green, J. A. Cutts, E. D. Jahelka, R. A. Johansen, M. J. Sander, J. B. Seidman, A. T. Young, and L. A. Soderblom (U.S. Geological Survey)

Icarus, Vol. 18, No. 1, pp. 75–101, January 1973

For abstract, see Levinthal, E. C.

JOHNSON, R. M.

J08 Bacterial Species in Soil and Air of the Antarctic Continent

R. E. Cameron, F. A. Morelli, and R. M. Johnson (Arizona State University)

Antarctic J. U.S., Vol. VII, No. 5, pp. 187–189, September–October 1972

For abstract, see Cameron, R. E.

JOHNSTON, A. R.

J09 Optical Proximity Sensors for Manipulators

A. R. Johnston

Technical Memorandum 33-612, May 1, 1973

A breadboard, optical proximity sensor intended for application to remotely operated manipulators has been constructed and evaluated. The sensing head was 20 × 15 × 10 mm in size, and could be made considerably smaller. Type I and Type II optical configurations are discussed, Type I having a sharply defined sensitive volume, Type II an extended one. The sensitive volume can be placed at any distance between 1 cm and approximately 1 m by choice of a replaceable prism. The Type I lateral resolution was 0.5 mm on one axis and 5 mm perpendicular to it for a unit focused at 7.5 cm. The corresponding resolution in the axial direction was 2.4 cm, but improvement to 0.5 cm is possible. The effect of surface reflectivity is discussed and possible modes of application are suggested.

JOSEPHS, R. H.

J10 The Mariner 9 Power Subsystem Design and Flight Performance

R. H. Josephs

Technical Memorandum 33-616, May 15, 1973

This memorandum documents the design and flight performance of the Mariner Mars 1971 power subsystem and discusses some of the power-management techniques employed to support an orbital mission far from Earth with marginal sunlight for its photovoltaic-battery power source. It also describes the performance of Mariner 9's nickel–cadmium battery during repetitive Sun-occultation phases of the mission and the results of unique in-flight tests to assess the performance capability of its solar array.

KATOW, M. S.

K01 DSN Progress Report for January–February 1973: 64-m-Diameter Antenna: Computation of RF Boresight Direction

M. S. Katow

Technical Report 32-1526, Vol. XIV, pp. 68–72,
April 15, 1973

With the addition of the new "kickers" on the 64-m-diameter antenna, foreknowledge of any change in the RF boresight-direction errors due to gravity loadings would be of operational value. Using ray-tracing techniques, the before and after boresight errors are computed, and the configurations are documented by line sketches of the RF surfaces and a table of linear and angular deflections. This method of analysis indicates that the RF boresight direction with respect to the intermediate reference surface will have lower deviations after the modifications.

K02 DSN Progress Report for March–April 1973: Wind Load Predictions for the 64-m-diameter Antenna

M. S. Katow and H. D. McGinness

Technical Report 32-1526, Vol. XV, pp. 96-101,
June 15, 1973

Analytically computed predictions of the performance of the 64-m-diameter antenna in the wind environment have been uncertain because (1) the final design change in the porosity of the paraboloid markedly altered the similarity between the prototype and the wind-tunnel models used at the preliminary design period and (2) the force values computed from static-pressure taps in porous plates were doubtful.

This article describes an effort to establish a correlation factor between the analytical model and the prototype using as a primary basis the field-measured azimuth torques of the 64-m-diameter antenna. A tentative conclusion is made that the maximum azimuth torque at 130-deg yaw angle computed from the static-pressure taps of wind-tunnel models using a full 50% reduction in forces to account for the 50% porosity must be increased by 40%.

KELLY, L. B.

K03 **Tracking and Data System Support for the Mariner Mars 1971 Mission: Orbit Insertion Through End of Primary Mission**

P. W. Barnum, N. A. Renzetti, G. P. Textor, and
L. B. Kelly

Technical Memorandum 33-523, Vol. III, May 15, 1973

For abstract, see Barnum, P. W.

KING, J., JR.

K04 **Ground Level Ultraviolet Solar Flux in Pasadena, California**

J. Ajello, J. King, Jr., A. L. Lane, and C. W. Odd

Bull. Am. Meteorol. Soc., Vol. 54, No. 2, pp. 114–115,
February 1973

For abstract, see Ajello, J.

KLEIN, M.

K05 **Observations of Jupiter at 13-cm Wavelength During 1969 and 1971**

S. Gulkis, B. Gary, M. Klein, and C. T. Stelzried

Icarus, Vol. 18, No. 2, pp. 181–191, February 1973

For abstract, see Gulkis, S.

KLIORE, A. J.

K06 The Atmosphere of Mars From Mariner 9 Radio Occultation Measurements

A. J. Kliore, D. L. Cain, G. Fjeldbo, B. L. Seidel, M. J. Sykes, and S. I. Rasool (National Aeronautics and Space Administration)

Icarus, Vol. 17, No. 2, pp. 484–516, October 1972

The Mariner 9 spacecraft was used to perform 160 radio occultation measurements in orbit about Mars during November and December of 1971. At that time, Mars was experiencing a severely obscuring global dust storm. The effect of dust in the atmosphere was reflected in the reduced temperature gradients measured, indicating heating of the atmosphere by solar radiation being absorbed by dust and a simultaneous cooling of the surface. A disparity in the pressures measured strongly suggests that the physical shape of Mars is more oblate than the shape of its gravitational equipotential surface, leading to higher atmospheric pressures near the poles than at the equator.

A daytime ionosphere was measured and showed some correlation between the variations in the peak density and the solar flux measured from the earth. The average topside plasma scale height showed little correlation with solar flux and solar zenith angle.

K07 The Shape of Mars From the Mariner 9 Occultations

D. L. Cain, A. J. Kliore, B. L. Seidel, and M. J. Sykes

Icarus, Vol. 17, No. 2, pp. 517–524, October 1972

For abstract, see Cain, D. L.

KOLBLY, R. B.

K08 DSN Progress Report for March–April 1973: DSN Research and Technology Support

E. B. Jackson, A. L. Price, and R. B. Kolbly

Technical Report 32-1526, Vol. XV, pp. 138–142, June 15, 1973

For abstract, see Jackson, E. B.

K09 **DSN Progress Report for March–April 1973: Intermodulation Product Generator**

R. B. Kolbly

Technical Report 32-1526, Vol. XV, pp. 143–145, June 15, 1973

This article describes a microwave circuit used to generate intermodulation products in a predictable manner. This circuit is used in connection with dual-carrier testing to provide a known signal to verify the correct tuning of exciters, receivers, and transmitters. An adjustable voltage probe for a waveguide system is also described.

KRON, M.

K10 **DSN Progress Report for March–April 1973: Minimum Inertia Design for Gear Trains**

M. Kron

Technical Report 32-1526, Vol. XV, pp. 102–108, June 15, 1973

In the design of gear trains, the load inertia is frequently small compared to the inertia of the gearing, and thus gear inertia becomes the major resistance to acceleration and also a large source of power consumption. The design program described in this article emphasizes minimum inertia for the gear train. Some high-acceleration and power-limited radar tracking systems can also benefit from minimum-inertia design even though the load inertia is significant. The optimization of gear-train ratios for minimum inertia provides smoother tracking and better system response.

The nonlinear differential equations used to determine minimum gear-train inertia are solved by the Newton–Raphson method. The final design, however, represents a solution to these equations constrained by allowable stresses, stiffness, and other standard American Gear Manufacturers Association specification requirements. Examples demonstrate the effectiveness of the procedure.

KROON, P. A.

K11 **Nuclear Magnetic Resonance of Phosphorus Compounds: VII. Evidence for Steric Effects on the ^{31}P–^{77}Se Coupling and ^{31}P Chemical Shifts**

R. P. Pinnell (Joint Science Department: Scripps, Pitzer, and Claremont Men's Colleges), C. A. Megerle (Joint

Science Department: Scripps, Pitzer, and Claremont Men's Colleges), S. L. Manatt, and P. A. Kroon

J. Am. Chem. Soc., Vol. 95, No. 3, pp. 977–978, January 7, 1973

For abstract, see Pinnell, R. P.

KUPPERMANN, A.

K12 Electron Impact Excitation of H_2O

S. Trajmar, W. Williams, and A. Kuppermann (California Institute of Technology)

J. Chem. Phys., Vol. 58, No. 6, pp. 2521–2531, March 15, 1973

For abstract, see Trajmar, S.

LAM, C.

L01 DSN Progress Report for January–February 1973: Data Storage and Data Compression II

C. Lam

Technical Report 32-1526, Vol. XIV, pp. 109–116, April 15, 1973

It has been shown that under certain idealized circumstances, a small increase in data-storage capability can lead to a dramatic increase in the rate at which data can be communicated reliably. This article presents a detailed investigation of the circumstances under which the maximum possible rate increase will occur.

LAMBERT, D. L.

L02 Observation of the OH Radical in Betelgeuse

R. Beer, R. H. Norton, R. B. Hutchinson,
D. L. Lambert (University of Texas), and
J. V. Martonchik (University of Texas)

Mém. Soc. Roy. Sci. Liège, Vol. III, No. 6, p. 145, 1972

For abstract, see Beer, R.

LANE, A. L.

L03 **Ground Level Ultraviolet Solar Flux in Pasadena, California**

J. Ajello, J. King, Jr., A. L. Lane, and C. W. Odd

Bull. Am. Meteorol. Soc., Vol. 54, No. 2, pp. 114–115, February 1973

For abstract, see Ajello, J.

LARSON, V.

L04 **Dynamical Models for a Spacecraft Idealized as a Set of Multi-Hinged Rigid Bodies**

V. Larson

Technical Memorandum 33-613, May 1, 1973

This memorandum provides a brief description of a canonical set of equations which governs the behavior of an n-body spacecraft. General results are given for the case in which the spacecraft is modeled in terms of n rigid bodies connected by dissipative elastic joints. The final equations are free from constraint torques and involve only r variables (r is the number of degrees of freedom of the system). An advantage which accompanies the elimination of the constraint torques is a decrease in the computer run time, especially when n is large.

LAWSON, C. L.

L05 **Sparse Matrix Methods Based on Orthogonality and Conjugacy**

C. L. Lawson

Technical Memorandum 33-627, June 15, 1973

A matrix having a high percentage of zero elements is called sparse. In the solution of systems of linear equations or linear least-squares problems involving large sparse matrices, significant savings in computer cost can be achieved by taking advantage of the sparsity. This memorandum derives and describes the well known conjugate-gradient algorithm and a set of related algorithms which are applicable to such problems. However, control of accuracy is a serious problem with this class of methods.

L06 **Prediction of Lipid Uptake by Prosthetic Heart Valve Poppets From Solubility Parameters**

J. Moacanin, D. D. Lawson, H. P. Chin (University of Southern California), E. C. Harrison (University of Southern California), and D. H. Blankenhorn (University of Southern California)

Biomat., Med. Dev., Art. Org., Vol. 1, No. 1, pp. 183–190, 1973

For abstract, see Moacanin, J.

L07 **Numerical Correlation and Evaluation in the Comparison of Evidentiary Materials**

D. D. Lawson and E. P. Framan

J. Forensic Sci., Vol. 18, No. 2, pp. 110–117, April 1973

One of the neglected areas in criminalistic laboratory techniques is the ability of the criminalist to compare and evaluate, quantitatively, sets of numerical data. At the present time, there does not exist in practice any uniformly accepted approach to determining a "figure-of-merit" (or rather a quantitative, reliable expression of the degree of match) for sets of data. The need for such a technique arose in a task designed to apply the phenomena of thermoluminescence to criminalistics. This task, funded and supported by NASA, was conducted through the Civil Systems Program Office at JPL. In this specific application, each piece of physical evidence provided, after processing, a continuous curve. In comparing the curve of an unknown with that of an exemplar, a need was established for a quantitative expression of the extent to which the two curves matched. A well-established statistical procedure was applied and was found to be fully satisfactory in resolving the problem.

The same technique, without modifications was also found to be applicable to the analysis of emission spectrography data, neutron activation analysis, gradient density measurements, and any other criminalistic technique where sets of numerical data are determined. The main attribute of this developed technique is that it allows the criminalist to make judgements on the quality of the evidentiary determinations.

LAYLAND, J. W.

L08 **DSN Progress Report for January–February 1973: Comment on Software Efficiency: Loops, Subroutines, and Interpretive Execution**

J. W. Layland

Technical Report 32-1526, Vol. XIV, pp. 124–130, April 15, 1973

This article discusses the relationship between the efficiency of software operation and the use within that software of conventional control structures such as loops and subroutines. These control structures "fold" a program to reduce its storage requirements at the expense of increased execution time. The typical intuitive response to this consideration is one of "the faster, the better." In some contexts, this is far from correct. The extent to which folding should be done depends upon many factors, especially the program's total size. The extent to which this folding can actually be done depends upon details of its operation. The analysis presented in this article is unrealistic in that it assumes the program in question can be folded arbitrarily.

L09 **DSN Progress Report for March–April 1973: An Experiment in Remote Monitoring of Mu-Ranging Operation at Mariner Mars 1971 Superior Conjunction**

D. E. Erickson and J. W. Layland

Technical Report 32-1526, Vol. XV, pp. 156–166, June 15, 1973

For abstract, see Erickson, D. E.

L10 **Scheduling Algorithms for Multiprogramming in a Hard-Real-Time Environment**

C. L. Liu (Massachusetts Institute of Technology) and J. W. Layland

J. Assoc. Comp. Mach., Vol. 20, No. 1, pp. 46–61, January 1973

For abstract, see Liu, C. L.

LEECH, R. A.

L11 **DSN Progress Report for January–February 1973: New Arc Detector**

E. J. Finnegan and R. A. Leech

Technical Report 32-1526, Vol. XIV, pp. 170–172,
April 15, 1973

For abstract, see Finnegan, E. J.

LEFLANG, J. G.

L12 DSN Progress Report for March–April 1973: Maser Development

J. G. Leflang

Technical Report 32-1526, Vol. XV, pp. 92–95,
June 15, 1973

Operational X-band masers are being developed for use in the Deep Space Instrumentation Facility. Mathematical models have been formulated that provide useful information about the amplitude and phase performance of the proposed X-band maser as well as the existing S-band masers. These models provide X–Y plots of frequency vs amplitude response, carrier phase shift, or time delay.

LEIBOWITZ, L. P.

L13 Measurements of the Structure of an Ionizing Shock Wave in a Hydrogen–Helium Mixture

L. P. Leibowitz

Phys. Fluids, Vol. 16, No. 1, pp. 59–68, January 1973

Shock structure during ionization of a hydrogen–helium mixture has been followed using hydrogen line and continuum emission measurements. A reaction scheme is proposed which includes hydrogen dissociation and a two-step excitation–ionization mechanism for hydrogen ionization by atom–atom and atom–electron collisions. Agreement has been achieved between numerical calculations and measurements of emission intensity as a function of time for shock velocities from 13 to 20 km/s in a 0.208 H_2–0.792 He mixture. The electron temperature was found to be significantly different from the heavy particle temperature during much of the ionization process. Similar time histories for H_β and continuum emission indicate upper level populations of hydrogen in equilibrium with the electron concentration during the relaxation process.

LEISING, C. J.

L14 **From Earth to Mars Orbit—Mariner 9 Propulsion Flight Performance With Analytical Correlations**

M. J. Cork, R. L. French, C. J. Leising, and D. D. Schmit

AIAA Preprint 72-1185, AIAA/SAE Eighth Joint Propulsion Specialist Conference, New Orleans, Louisiana, November 29–December 1, 1972

For abstract, see Cork, M. J.

LESH, J. R.

L15 **DSN Progress Report for March–April 1973: Theoretical Analysis of the Doppler System Test**

J. R. Lesh

Technical Report 32-1526, Vol. XV, pp. 190–202, June 15, 1973

This article formulates and analyzes models for the doppler-extraction and measurement processes used in the doppler-system test. The purpose of the article is to acquaint operations personnel with the doppler system as well as the corresponding system-test criteria.

LEU, R. L.

L16 **DSN Progress Report for January–February 1973: Computer Control of High-Power Transmitters**

R. L. Leu

Technical Report 32-1526, Vol. XIV, pp. 27–32, April 15, 1973

The objectives of computer control of high-power transmitters are development of techniques and equipment for complete control, monitoring, and fault isolation to ensure minimum recovery time from a fault and reduction of the skill level required for operation and maintenance. This article covers the computer program for the Venus Deep Space Station high-power transmitters.

LEVINTHAL, E. C.

L17 Mariner 9—Image Processing and Products

E. C. Levinthal (Stanford University), W. B. Green, J. A. Cutts, E. D. Jahelka, R. A. Johansen, M. J. Sander, J. B. Seidman, A. T. Young, and L. A. Soderblom (U.S. Geological Survey)

Icarus, Vol. 18, No. 1, pp. 75–101, January 1973

The purpose of this article is to describe the system for the display, processing, and production of image-data products created to support the Mariner 9 Television Experiment. Of necessity, the system was large in order to respond to the needs of a large team of scientists with a broad scope of experimental objectives. The desire to generate processed data products as rapidly as possible to take advantage of adaptive planning during the mission, coupled with the complexities introduced by the nature of the vidicon camera, greatly increased the scale of the ground-image processing effort.

This article describes the systems that carried out the processes and delivered the products necessary for real-time and near-real-time analyses. References are made to the computer algorithms used for the different levels of decalibration and analysis.

LEVITT, B. K.

L18 DSN Progress Report for March–April 1973: Intermodulation Products in Dual Carrier Transmission: Power Series Analysis

B. K. Levitt

Technical Report 32-1526, Vol. XV, pp. 70–79,
June 15, 1973

The proposed Viking Mars 1975 dual-carrier telemetry modes have generated an interest in determining the relative power levels of dual-carrier intermodulation products (IMPs) for a klystron amplifier. To this end, a finite-order power-series model for the time-domain input–output response of the klystron was investigated. The parameters needed to define the model for a particular klystron were derived from experimental measurements of the nonlinear power-transfer characteristic of the amplifier for single-carrier transmission. The power-series approach does not appear to be a useful analytic tool for predicting dual-carrier IMP levels. With the exception of the first-order IMP, the model is evidently too sensitive to small changes in the experimental single-carrier data to provide accurate IMP information.

L19 **DSN Progress Report for March–April 1973: Capacity for Noncoherent, Soft-Decision MFSK Signaling**

S. Butman and B. K. Levitt

Technical Report 32-1526, Vol. XV, pp. 146–155, June 15, 1973

For abstract, see Butman, S.

LEVY, R.

L20 **DSN Progress Report for January–February 1973: Structural Stiffness Matrix Wavefront Resequencing Program (WAVEFRONT)**

R. Levy

Technical Report 32-1526, Vol. XIV, pp. 42–45, April 15, 1973

The computer program WAVEFRONT is a preprocessor that resequences the stiffness matrix for wavefront reduction prior to processing by structural-analysis computer programs. This article describes the program operation, deck, input-data requirements, and suggested usage. Summary data extracted from example applications show that this program is an effective preprocessor for the NASTRAN structural-analysis program and is generally preferable to alternative bandwidth-reduction preprocessors.

LIN, C.-L.

L21 **Intermediates in the Ozonation of Simple Alkynes**

W. B. DeMore and C.-L. Lin

J. Org. Chem., Vol. 38, No. 5, pp. 985-989, March 9, 1973

For abstract, see DeMore, W. B.

L22 **Reactions of O(^{1}D) With Methane and Ethane**

C.-L. Lin and W. B. DeMore

J. Phys. Chem., Vol. 77, No. 7, pp. 863-869, March 29, 1973

Gas-phase reactions of O(^{1}D) with CH_4 and with C_2H_6 were studied by the photolyses of N_2O-CH_4 and N_2O-C_2H_6 mixtures using 1849-Å light. Pressure effects and radical scavenging techniques were used to identify the sources of the products. At low pressures, where stabilization of excited alcohol intermediates did

not occur, the main path of the O(^{1}D) + CH_4 reaction was to form CH_3 + OH radicals, which ultimately produce C_2H_6. Molecular elimination giving H_2 + CH_2O occurred to the extent of 9%, which is the same as when the reaction takes place in liquid Ar at 87°K. The main path of the O(^{1}D) + C_2H_6 reaction was to form C_2H_5 + OH and CH_3 + CH_2OH radicals, which ultimately produce *n*-C_4H_{10}, C_3H_8, and C_2H_6 as principal products. The total reaction does not proceed via ROH* intermediates. The OH radicals are produced both by fission of such intermediates and by direct abstraction of H atoms. Comparison with previous results in liquid argon indicates that the condensed medium suppresses the abstraction reaction in favor of the insertion reaction. The molecular process giving CH_2O + H_2 also does not involve the CH_3OH* intermediate, as shown by the fact that this path contributes equally both in the gas and liquid phases.

LINDSEY, W. C.

L23 A Bibliography of the Theory and Application of the Phase-Lock Principle

W. C. Lindsey (University of Southern California) and
R. C. Tausworthe

Technical Report 32-1581, April 1, 1973

Since much has been reported on the phase-locked loop, a literature search was conducted in an effort to collect and compile as many references on the subject as possible. Although not all inclusive, this report presents a comprehensive listing of phase-locked-loop references covering the past two decades throughout the world. The compilation is given in two parts: first by categories, and then alphabetically by authors.

LIU, C. L.

L24 Scheduling Algorithms for Multiprogramming in a Hard-Real-Time Environment

C. L. Liu (Massachusetts Institute of Technology) and
J. W. Layland

J. Assoc. Comp. Mach., Vol. 20, No. 1, pp. 46–61,
January 1973

The problem of multiprogram scheduling on a single processor is studied from the viewpoint of the characteristics peculiar to the program functions that need guaranteed service. It is shown that an optimum fixed priority scheduler possesses an upper bound to processor utilization which may be as low as 70% for large task sets. It is also shown that full processor utilization can be achieved by dynamically assigning priorities on the basis of their current deadlines. A combination of these two scheduling techniques is also discussed.

LORDEN, G.

L25 **DSN Progress Report for January-February 1973: A Comparison Between the Current and Proposed Inventory and Procurement Policies for the Deep Space Network**

I. Eisenberger, F. R. Maiocco, and G. Lorden (California Institute of Technology)

Technical Report 32-1526, Vol. XIV, pp. 81-86, April 15, 1973

For abstract, see Eisenberger, I.

L26 **Detection of Failure Rate Increases**

G. Lorden (California Institute of Technology) and I. Eisenberger

Technometrics, Vol. 15, No. 1, pp. 167-175, February 1973

The problem of devising systematic policies for replacement of equipment subject to wear-out involves the detection of increases in failure rates. In this article detection procedures are defined as stopping times N with respect to the observed sequence of random failures. The concepts of "quickness of detection" and "frequency of false reactions" are made precise and a class of procedures is studied which optimizes the former asymptotically as the latter is reduced to zero. Results of Monte Carlo experiments are given which show that efficient quickness of detection is attainable simultaneously for various levels of increase in failure rates.

LORELL, J.

L27 **Gravity Field of Mars From Mariner 9 Tracking Data**

J. Lorell, et al.

Icarus, Vol. 18, No. 2, pp. 304-316, February 1973

Further reduction of Doppler tracking data from Mariner 9 confirms an earlier conclusion that the gravity field of Mars is considerably rougher than the fields of either the Earth or the moon. The largest positive gravity anomaly uncovered is in the Tharsis region which is also topographically high and geologically unusual. The best determined coefficients of the harmonic expansion of the gravitational potential are presented in this article.

The value obtained for the inverse mass of Mars is in good agreement with prior determinations from Mariner flyby trajectories. The direction found for the rotational pole of Mars is in excellent agreement with recent values determined from Earth-based observations of Mars satellites. Other important physical constants that have either been refined or confirmed by the Mariner 9 data include the dynamical flattening, maximum principal moment of inertia, and the period of precession of Mars' pole.

Contributors to this article include:

Jet Propulsion Laboratory: J. Lorell, G. H. Born, E. J. Christensen, P. B. Esposito, J. F. Jordan, P. A. Laing, W. L. Sjogren, and S. K. Wong

Massachusetts Institute of Technology: R. D. Reasenberg, I. I. Shapiro, and G. L. Slater

L28 Estimation of Gravity Field Harmonics in the Presence of Spin-Axis Direction Error Using Radio Tracking Data

J. Lorell

J. Astronaut. Sci., Vol. XX, No. 1, pp. 44–54, August 1972

The problem of estimating a planet's gravity harmonic coefficients using tracking data from an orbiting spacecraft is complicated by many factors, one of which is the uncertainty of spin-axis direction. In this article, formulas relating the spin-axis direction error to the second-degree gravity coefficients are derived. The error induced in the harmonic coefficients is then evaluated, and methods are suggested for correction. Finally, the effect of rotation is accounted for.

LUDWIG, A. C.

L29 Determination of the Maximum Scan-Gain Contours of a Beam-Scanning Paraboloid and Their Relation to the Petzval Surface

W. V. T. Rusch and A. C. Ludwig

IEEE Trans. Anten. Prop., Vol. AP-21, No. 2, pp. 141–147, March 1973

For abstract, see Rusch, W. V. T.

LUSHBAUGH, W. A.

L30 DSN Progress Report for March–April 1973: A Driver/Receiver Unit for an Intercomputer Communications Link

W. A. Lushbaugh

Technical Report 32-1526, Vol. XV, pp. 109–115,
June 15, 1973

One of the most likely configurations for the computational complement of future tracking stations is a number of small computers, each performing a dedicated function and interfacing with some specific subset of the tracking-station equipment and with the other computers. This article describes in some detail the line-interface or driver/receiver (D/R) unit for intercomputer communications.

This unit is capable of receiving and transmitting digital information a distance of up to 600 m via coaxial cable. The trilevel signaling format used to code the information is discussed, as well as the various interactions that are involved between computer and D/R unit and between transmitting and receiving D/R units. Status information is supplied to the associated computer via the status register, and a bit-by-bit description of this status register is given.

LUTES, G. F.

L31 DSN Progress Report for January–February 1973: S-Band Planetary Radar Receiver Development

C. F. Foster and G. F. Lutes

Technical Report 32-1526, Vol. XIV, pp. 23–26,
April 15, 1973

For abstract, see Foster, C. F.

LYTTLETON, R. A.

L32 On the Formation of Planets From a Solar Nebula

R. A. Lyttleton

Mon. Not. R. Astr. Soc., Vol. 158, No. 4, pp. 463–483,
1972

The development of planets within a solar nebula of both gas and dust is shown to occur in two main stages. First, in a time comparable with the orbital period at any distance the dust comes to move with Keplerian motion in a thin plane disc. This is an essential prerequisite since the volume-density in such a disc is amply sufficient for the self-gravitation of condensations to overcome the differential action of the Sun. By such means small solid planets can form independently of the gaseous component of the nebula. Second, the range-of-influence of a planet (of mass m moving at distance R) out to which its gravitation dominates over that of the Sun is $(m/3M)^{1/3}R$. At any stage material within this distance can be captured, and the growth of bodies to mass of lunar order requires about 10^4 yr. It seems probable that many small bodies would begin to form separately, and then themselves combine by collisions to yield larger bodies fewer in number.

L33 A New Solution to the Accretion Problem

R. A. Lyttleton

Mon. Not. R. Astr. Soc., Vol. 160, No. 3, pp. 255–270, 1972

In this article a previously-reported theory of line-accretion is briefly reviewed, and it is shown that there are an infinity of steady-state solutions satisfying the requirements originally imposed as boundary conditions. Questions are raised as to the applicability of these solutions to physical reality. The existence is demonstrated of an entirely different type of steady-state solution that implies slow velocity in the accretion stream beyond the neutral point. Accurate numerical values are obtained of this solution for a number of cases. The braking action given by this solution, for any selected cutoff distance, is far stronger than that of the earlier theory. Consideration of the physical state in the accretion stream shows that for this slow solution the appropriate cutoff range would be only of the order 10^2 AU rather than of interstellar-distance order. With stronger braking action, the velocity of stars relative to interstellar material will be reduced in correspondingly shorter times, and more rapid accretion will thereby come about. This result, combined with recent measures of gas densities at various regions of the galaxy, suggests that the problem posed by the brightest stars may well be resolvable on the basis of the accretion process.

MACIE, T. W.

M01 Electromagnetic Interference of Power Conditioners for Solar Electric Propulsion

A. C. Whittlesey and T. W. Macie

Technical Memorandum 33-623, July 1, 1973

For abstract, see Whittlesey, A. C.

MAIOCCO, F. R.

M02 **DSN Progress Report for January-February 1973: A Comparison Between the Current and Proposed Inventory and Procurement Policies for the Deep Space Network**

I. Eisenberger, F. R. Maiocco, and G. Lorden (California Institute of Technology)

Technical Report 32-1526, Vol. XIV, pp. 81-86, April 15, 1973

For abstract, see Eisenberger, I.

MALLORY, C. W.

M03 **Evidence for a Steric Effect on Directly Bonded Carbon-Fluorine and Carbon-Proton Nuclear Magnetic Resonance Couplings**

S. L. Manatt, M. A. Cooper, C. W. Mallory (Bryn Mawr College), and F. B. Mallory (Bryn Mawr College)

J. Am. Chem. Soc., Vol. 95, No. 3, pp. 975-977, February 7, 1973

For abstract, see Manatt, S. L.

MALLORY, F. B.

M04 **Evidence for a Steric Effect on Directly Bonded Carbon-Fluorine and Carbon-Proton Nuclear Magnetic Resonance Couplings**

S. L. Manatt, M. A. Cooper, C. W. Mallory (Bryn Mawr College), and F. B. Mallory (Bryn Mawr College)

J. Am. Chem. Soc., Vol. 95, No. 3, pp. 975-977, February 7, 1973

For abstract, see Manatt, S. L.

MANATT, S. L.

M05 **Evidence for a Steric Effect on Directly Bonded Carbon-Fluorine and Carbon-Proton Nuclear Magnetic Resonance Couplings**

S. L. Manatt, M. A. Cooper, C. W. Mallory (Bryn Mawr College), and F. B. Mallory (Bryn Mawr College)

J. Am. Chem. Soc., Vol. 95, No. 3, pp. 975–977, February 7, 1973

This article presents data indicating $^1J_{^{13}C-F}$ sensitivity to steric effects. Previously reported steric effects on $^1J_{^{13}C-H}$ and values of $^1J_{^{13}C-F}$ for a number of fluorobenzenes and other fluoroaromatic molecules are summarized for comparison purposes.

M06 **Nuclear Magnetic Resonance of Phosphorus Compounds: VII. Evidence for Steric Effects on the ^{31}P–^{77}Se Coupling and ^{31}P Chemical Shifts**

R. P. Pinnell (Joint Science Department: Scripps, Pitzer, and Claremont Men's Colleges), C. A. Megerle (Joint Science Department: Scripps, Pitzer, and Claremont Men's Colleges), S. L. Manatt, and P. A. Kroon

J. Am. Chem. Soc., Vol. 95, No. 3, pp. 977–978, January 7, 1973

For abstract, see Pinnell, R. P.

MARTONCHIK, J. V.

M07 **Observation of the OH Radical in Betelgeuse**

R. Beer, R. H. Norton, R. B. Hutchinson, D. L. Lambert (University of Texas), and J. V. Martonchik (University of Texas)

Mém. Soc. Roy. Sci. Liège, Vol. III, No. 6, p. 145, 1972

For abstract, see Beer, R.

MASON, P. V.

M08 **The Apollo 17 Surface Experiments**

N. W. Hinners (NASA Apollo Program Office) and P. V. Mason

Astronaut. Aeronaut., Vol. 10, No. 12, pp. 40–54, December 1972

For abstract, see Hinners, N. W.

MAXWORTHY, T.

M09 **A Review of Jovian Atmospheric Dynamics**

T. Maxworthy

Planet. Space Sci., Vol. 21, No. 4, pp. 623–641, April 1973

A brief review is presented of available knowledge of the fluid motions within Jupiter's atmosphere. Evidence is presented to support the contention that the observed cloud masses are probably not simply convected by the main zonal flows. It is likely that an understanding of wave motions within the atmosphere will be of great importance in interpreting data gathered both from the ground and from spacecraft.

McDANELL, J. P.

M10 Orbit Determination for Low-Thrust Spacecraft: Concepts and Analysis

J. P. McDanell

Technical Memorandum 33-609, April 15, 1973

This memorandum re-evaluates the Earth-based orbit-determination capability for solar–electric-propulsion spacecraft in the light of recent developments both in multi-station tracking concepts and in thrust-subsystem error modeling. Five different tracking strategies are applied to a 15-day segment of an Encke rendezvous mission. Both optimal and suboptimal orbit-determination performance are determined for a wide range of process-noise parameter values. The multi-station tracking techniques are found to be extremely effective, reducing orbit-determination errors by orders of magnitude over that obtained with conventional single-station tracking. Explicitly differenced multi-station data is found to be least sensitive to gross modeling errors, but if a reasonably good process-noise model is available, explicit differencing is not required.

McELIECE, R. J.

M11 Weight Congruences for p-ary Cyclic Codes

R. J. McEliece

Discrete Math., Vol. 3, Nos. 1–3, pp. 177–192, September 1972

The largest integer λ is identified such that all weights in a p-ary cyclic code C are divisible by p^λ, and give a congruence for the weights mod $p^{\lambda+1}$. λ turns out to be $\omega/(p-1)-1$, where ω is the smallest multiple of $p-1$ such that there is an equation of the form $1=\theta_1\theta_2\cdots\theta_\omega$, each θ_i being a root of the check polynomial of C. Several related results are presented.

M12 **A Note on the Griesmer Bound**

L. D. Baumert and R. J. McEliece

IEEE Trans. Inform. Theory, Vol. IT-19, No. 1,
pp. 134–135, January 1973

For abstract, see Baumert, L. D.

M13 **Comment on "A Class of Codes for Asymmetric Channels and a Problem From the Additive Theory of Numbers"**

R. J. McEliece

IEEE Trans. Inform. Theor., Vol. IT-19, No. 1, p. 137,
January 1973

This article comments on error-correcting codes for asymmetric channels previously reported. Evidence is constructed to attest to the superiority of these codes over other error-correcting codes currently in use.

McGINNESS, H. D.

M14 **DSN Progress Report for January–February 1973: Design of Shipping Containers for Master Equatorials**

H. D. McGinness

Technical Report 32-1526, Vol. XIV, pp. 226–234,
April 15, 1973

The delicate nature of the master equatorials makes them highly susceptible to damage, especially during transit. A special container has been designed and built for the purpose of shipping assembled master equatorials to overseas antenna sites in Australia and Spain. This article outlines the design features of the shipping containers and describes the advantageous use of motor-vehicle shock absorbers.

M15 **DSN Progress Report for March–April 1973: Wind Load Predictions for the 64-m-diameter Antenna**

M. S. Katow and H. D. McGinness

Technical Report 32-1526, Vol. XV, pp. 96-101,
June 15, 1973

For abstract, see Katow, M. S.

McPEAK, W. L.

M16 DSN Progress Report for March–April 1973: Arithmetic Processing Unit

W. L. McPeak

Technical Report 32-1526, Vol. XV, pp. 66–69, June 15, 1973

This article describes an arithmetic processing unit being developed to provide more meaningful numerical data from meters mounted in the antenna portion of high-power transmitters. This unit will compute directly changes in temperature, power dissipation, and water-flow levels. The design constraints, requirements, and concepts are discussed.

MEGERLE, C. A.

M17 Nuclear Magnetic Resonance of Phosphorus Compounds: VII. Evidence for Steric Effects on the ^{31}P–^{77}Se Coupling and ^{31}P Chemical Shifts

R. P. Pinnell (Joint Science Department: Scripps, Pitzer, and Claremont Men's Colleges), C. A. Megerle (Joint Science Department: Scripps, Pitzer, and Claremont Men's Colleges), S. L. Manatt, and P. A. Kroon

J. Am. Chem. Soc., Vol. 95, No. 3, pp. 977–978, January 7, 1973

For abstract, see Pinnell, R. P.

MENICHELLI, V. J.

M18 Nondestructive and Impulsive Testing of Electroexplosive Devices

V. J. Menichelli

J. Spacecraft Rockets, Vol. 9, No. 12, pp. 936–937, December 1972

Since failure of an electroexplosive device (EED) during a space mission can result in partial or complete failure of the mission, a detailed knowledge of the quality of each EED used is required. JPL has developed nondestructive test techniques and instrumentation that demonstrate the quality and normal behavior of 1-W/1-A no-fire EEDs without firing or degrading the units. This article describes nondestructive tests and impulsive firings performed on three groups of aerospace-type EEDs.

METZGER, A. E.

M19 Lunar Surface Radioactivity: Preliminary Results of the Apollo 15 and Apollo 16 Gamma-Ray Spectrometer Experiments

A. E. Metzger, J. I. Trombka (Goddard Spaceflight Center),
L. E. Peterson (University of California, San Diego),
R. C. Reedy (University of California, San Diego), and
J. R. Arnold (University of California, San Diego)

Science, Vol. 179, No. 4075, pp. 800–803,
February 23, 1973

Gamma-ray spectrometers on the Apollo 15 and Apollo 16 missions have been used to map the moon's radioactivity over 20% of its surface. The highest levels of natural radioactivity are found in Mare Imbrium and Oceanus Procellarum with contrastingly lower enhancements in the eastern maria. The ratio of potassium to uranium is higher on the far side than on the near side, although it is everywhere lower than commonly found on the earth.

MILLER, R. B.

M20 DSN Progress Report for March–April 1973: Pioneer 10 and 11 Mission Support

R. B. Miller

Technical Report 32-1526, Vol. XV, pp. 22–28,
June 15, 1973

The DSN has completed more than a full year of continuous telemetry-data acquisition, command, and radio metric tracking support for Pioneer 10. Pioneer 11 was successfully launched on April 5, 1973. Detailed encounter-support planning activity was initiated. This article describes recent organizational changes in JPL support of the Pioneer Project.

MOACANIN, J.

M21 Prediction of Lipid Uptake by Prosthetic Heart Valve Poppets From Solubility Parameters

J. Moacanin, D. D. Lawson, H. P. Chin (University of Southern California), E. C. Harrison (University of Southern California), and D. H. Blankenhorn (University of Southern California)

Biomat., Med. Dev., Art. Org., Vol. 1, No. 1, pp. 183–190, 1973

Most prosthetic heart valves currently implanted consist of a silicone rubber poppet situated within a metallic cage. Recent reports indicate that gradual deterioration of the poppet can occur and lead to serious valve malfunction. Physical changes (variance) observed in recovered prosthesis include discoloration, swelling, and cracking.

MOORE, J. W.

M22 Navigation Requirements for Advanced Deep Space Missions

L. D. Friedman, J. W. Moore, and R. L. Sohn

Navigation: J. Institute Nav., Vol. 19, No. 3, pp. 266–280, Fall 1972

For abstract, see Friedman, L. D.

MORELLI, F. A.

M23 Monitoring of Antarctic Dry Valley Drilling Sites

F. A. Morelli, R. E. Cameron, D. R. Gensel, and
L. P. Randall (Northern Illinois University)

Antarctic J. U.S., Vol. VII, No. 4, pp. 92–94, July–August 1972

Man's relatively recent permanent occupancy of the Antarctic, his past, present, and anticipated activities and practices, and a deeper appreciation for the environment have given rise to a microbiological monitoring program during the past field season in the dry valleys. The monitoring effort was centered around the activities of the Dry Valley Drilling Project, which investigated various sites for drilling operations. This article describes the microbiological monitoring activities and results.

M24 Hydrocarbons in Air Samples From Antarctic Dry Valley Drilling Sites

J. V. Behar (University of California, Riverside),
L. Zafonte (University of California, Riverside),
R. E. Cameron, and F. A. Morelli

Antarctic J. U.S., Vol. VII, No. 4, pp. 94–96, July–August 1972

For abstract, see Behar, J. V.

M25 **Bacterial Species in Soil and Air of the Antarctic Continent**

R. E. Cameron, F. A. Morelli, and R. M. Johnson (Arizona State University)

Antarctic J. U.S., Vol. VII, No. 5, pp. 187–189, September–October 1972

For abstract, see Cameron, R. E.

MORRIS, G. A.

M26 **DSN Progress Report for March–April 1973: Simultaneous Detection of Pulsar Radiation at S- and X-Bands**

P. E. Reichley, G. S. Downs, and G. A. Morris

Technical Report 32-1526, Vol. XV, pp. 133–137, June 15, 1973

For abstract, see Reichley, P. E.

M27 **Martian Topography and Surface Properties as Seen by Radar: The 1971 Opposition**

G. S. Downs, R. M. Goldstein, R. R. Green, G. A. Morris, and P. E. Reichley

Icarus, Vol. 18, No. 1, pp. 8–21, January 1973

For abstract, see Downs, G. S.

MORTON, J. B.

M28 **Mascons: Progress Toward a Unique Solution for Mass Distribution**

R. J. Phillips, J. E. Conel, E. A. Abbott, W. L. Sjogren, and J. B. Morton

J. Geophys. Res., Vol. 77, No. 35, pp. 7106–7114, December 10, 1972

For abstract, see Phillips, R. J.

MUDGWAY, D. J.

M29 **DSN Progress Report for January–February 1973: Viking Mission Support**

D. J. Mudgway

Technical Report 32-1526, Vol. XIV, pp. 14–15,
April 15, 1973

DSN support for Viking Mars 1975 has been reexamined in the light of new budget constraints. Some impact on existing plans and schedules is expected to result. An earlier decision to use the single-station configuration for providing dual-carrier capability was abandoned in favor of the more predictable dual-station approach. The first Viking/DSN progress review has been postponed to permit the impact of the changes necessitated by the budget constraints to be evaluated.

M30 **DSN Progress Report for March–April 1973: Viking Mission Support**

D. J. Mudgway

Technical Report 32-1526, Vol. XV, pp. 10–21,
June 15, 1973

Because of budget constraints, previous plans and schedules for Viking Mars 1975 have been reworked to minimize the impact on readiness dates committed to the Viking Project. An improved implementation schedule has been developed to manage hardware and software progress toward Viking configurations in the DSN. Several significant reviews have been held and some new problem areas identified. In the particular case of deep-space-station longitude accuracy, a task team has been formed to try to resolve the problem. Operations activity in support of Viking is introduced.

NEWBURN, R. L., JR.

N01 **A Survey of the Outer Planets Jupiter, Saturn, Uranus, Neptune, Pluto, and Their Satellites**

R. L. Newburn, Jr., and S. Gulkis

Space Sci. Rev., Vol. 14, No. 2, pp. 179–271,
February 1973

A survey of current knowledge of Jupiter, Saturn, Uranus, Neptune, Pluto, and their satellites is presented. The best available numerical values are given for physical parameters, including orbital and body properties, atmospheric composition and structure, and photometric parameters. The more acceptable current theories of these bodies are outlined with thorough referencing offering access to the details.

NORTON, R. H.

N02 Observation of the OH Radical in Betelgeuse

R. Beer, R. H. Norton, R. B. Hutchinson,
D. L. Lambert (University of Texas), and
J. V. Martonchik (University of Texas)

Mém. Soc. Roy. Sci. Liège, Vol. III, No. 6, p. 145, 1972

For abstract, see Beer, R.

ODD, C. W.

O01 Ground Level Ultraviolet Solar Flux in Pasadena, California

J. Ajello, J. King, Jr., A. L. Lane, and C. W. Odd

Bull. Am. Meteorol. Soc., Vol. 54, No. 2, pp. 114–115, February 1973

For abstract, see Ajello, J.

OLIVER, R. E.

O02 Furlable Spacecraft Antenna Development: Second Interim Report

R. E. Oliver and A. H. Wilson

Technical Memorandum 33-606, May 15, 1973

This memorandum describes recent activities at JPL directed toward the development of large, furlable spacecraft antennas using conical main reflectors. Development of two basic antenna configurations conceived at JPL and utilizing conical main reflectors has been pursued. A 4.3-m(14-ft)-diameter model based on the two-reflection conical–Gregorian concept and a 1.8-m(6-ft)-diameter model based on the four-reflection Quadreflex concept have been made and RF tested.

RF gain measurements for the 4.3-m(14-ft)-diameter conical–Gregorian model were 48.83 dB at X-band (8.448 GHz) and 37.82 dB at S-band (2.297 GHz). These gains correspond to efficiencies of 53.6 and 57.5%, respectively. RF gain measurements for the 1.8-m(6-ft)-diameter Quadreflex model were 47.59 dB at Ku-band (16.33 GHz) and 41.30 dB at X-band (8.448 GHz), corresponding to efficiencies of 58.6 and 51.5%, respectively.

OLLI, E. E.

003 Temperature Dependence of the Accommodation Coefficient of Liquid-Helium Film

T. G. Wang, D. D. Elleman, E. E. Olli, and M. M. Saffren

Phys. Rev. Lett., Vol. 30, No. 11, pp. 485–487,
March 12, 1973

For abstract, see Wang, T. G.

OLSEN, E. T.

004 Radio Observations of Cygnus X-3 and the Surrounding Region

B. Gary, E. T. Olsen, and P. W. Rosenkranz

Nature Phys. Sci., Vol. 239, No. 95, pp. 128–130,
October 23, 1972

For abstract, see Gary, B.

OTOSHI, T. Y.

005 DSN Progress Report for January–February 1973: S/X-Band Experiment: Zero Delay Device

T. Y. Otoshi and P. D. Batelaan

Technical Report 32-1526, Vol. XIV, pp. 73–80,
April 15, 1973

This article describes a zero-delay device currently being developed for the S/X-band experiment. Preliminary group-delay and transmission-coefficient phase data are presented for some of the components in the zero-delay device.

006 DSN Progress Report for March–April 1973:S/X-Band Experiment: Zero-Delay-Device Step Attenuator Evaluation

T. Y. Otoshi

Technical Report 32-1526, Vol. XV, pp. 84–87,
June 15, 1973

This article presents test results for a coaxial step attenuator to be used in the zero-delay device for the S/X-band experiment. The test results at 182, 2113, 2295, 6302, and 8415 MHz indicate that the attenuator group-delay changes about 0.07 ns over a 69-dB range. Tests made over a temperature range from 4.4°C (40°F) to

37.8°C (100°F) indicate that group delay and phase changes, as functions of temperature, are small.

O07 An Analytical Expression for the Limits of Error in the Measurement of Reflection-Coefficient Phase

T. Y. Otoshi

IEEE Trans. Microwave Theor. Techniq., Vol. MTT-21, No. 3, pp. 151–153, March 1973

An exact analytical expression for calculating the limits of phase error that can occur when the reflection coefficient of a load is measured through a lossless two-port network is presented. An empirical expression previously reported agrees well with the exact expression, except when the reflection coefficients of the lossless two-port and the load are nearly the same in magnitude.

PARKER, R. H.

P01 Effects of Proton Irradiation on Several Spacecraft Science Components

R. H. Parker

IEEE Trans. Nucl. Sci., Vol. NS-19, No. 6, pp. 156–159, December 1972

During the course of the Thermoelectric Outer Planets Spacecraft Outer Planets Grand Tour programs and Mariner Jupiter/Saturn 1977, several models have been developed and used to analyze the radiation hazard to the spacecraft. During this time typical components found in space flight science instruments have been selected and, using very small sample sizes, tested to determine their capability to function properly before, after, and, in some cases, during exposures to energy equivalenced levels predicted by the models. This article describes the proton irradiation tests performed and analyzes the test results.

PATTERSON, R. E.

P02 Parametric Performance Characteristics and Treatment of Temperature Coefficients of Silicon Solar Cells for Space Application

R. E. Patterson and R. K. Yasui

Technical Report 32-1582, May 15, 1973

This report presents the electrical performance characteristics of 2- and 10-Ω-cm *n*/*p*-type silicon solar cells at simulated solar intensities of 5, 50, 100, 140, 250, 400, 550, 700, and 850 mW/cm^2. At each intensity, the temperature was varied in increments of 20° between extremes of +160 and -160°C. Short-circuit current, open-circuit voltage, and maximum power are presented in graphical format. This report also describes three methods for predicting solar-cell electrical performance as a function of temperature and intensity. Two of the methods are suitable for use at extreme temperature–intensity conditions. These methods were used successfully to predict the performance of the short-circuit current, open-circuit voltage transducer on board the Mariner Mars 1971 spacecraft.

P03 Design and Flight Performance Evaluation of the Mariners 6, 7, and 9 Short-Circuit Current, Open-Circuit Voltage Transducers

R. E. Patterson

Technical Memorandum 33-603, April 15, 1973

The purpose of the short-circuit current, open-circuit voltage transducer is to provide engineering data to aid the evaluation of array performance during flight. This memorandum describes the design, fabrication, and calibration of these tranducers and discusses their in-flight performance on board the Mariner 6, 7, and 9 spacecraft. No significant differences were observed in the in-flight electrical performance of the three transducers. There was no evidence of solar flares causing abrupt degradation, and no significant particulate–radiation cell degradation was observed. The transducers did experience significant "non-cell degradation" which refers to losses due to coverslides or adhesive darkening, increased surface reflection, or spectral shifts within coverslide assembly.

PAWLIK, E. V.

P04 Ion Thruster Thermal Characteristics and Performance

L. C. Wen, J. D. Crotty, and E. V. Pawlik

J. Spacecraft Rockets, Vol. 10, No. 1, pp. 35–41, January 1973

For abstract, see Wen, L. C.

PEELGREN, M. L.

P05 **Thermionic Reactor Ion Propulsion System (TRIPS)—Its Multi-mission Capability**

M. L. Peelgren

AIAA Preprint 72-1060, AIAA/SAE Eighth Joint Propulsion Specialist Conference, New Orleans, Louisiana, November 29–December 1, 1972

The unmanned planetary exploration to be conducted the last two decades of this century includes many higher energy missions which tax all presently available propulsion systems beyond their limit. One candidate with the versatility and performance to meet these mission objectives is Nuclear Electric Propulsion (NEP). Additionally, the NEP System is feasible in orbit raising operations with the Shuttle or Shuttle/Tug combination. In this article a representative planetary mission is described (Uranus–Neptune flyby with probe) and geocentric performance and tradeoffs are discussed. The NEP system is described in more detail with particular emphasis on the power subsystem comprised of the thermionic reactor, heat rejection subsystem, and the neutron shield.

PEREZ, R.

P06 **DSN Progress Report for January–February 1973: DC Current Sensor**

R. Perez

Technical Report 32-1526, Vol. XIV, pp. 173–177, April 15, 1973

A current sensor has been developed which is capable of measuring a differential dc current and also, within a few microseconds, detecting the burst of current caused by a high-voltage arc. This sensor was designed to measure the klystron body current and, in conjunction with a crowbar, protect the tube against internal high-voltage arcs. This article describes the operational characteristics of the current sensor and test results for the characteristics that were investigated.

PETERSON, L. E.

P07 **Lunar Surface Radioactivity: Preliminary Results of the Apollo 15 and Apollo 16 Gamma-Ray Spectrometer Experiments**

A. E. Metzger, J. I. Trombka (Goddard Spaceflight Center), L. E. Peterson (University of California, San Diego),

R. C. Reedy (University of California, San Diego), and
J. R. Arnold (University of California, San Diego)

Science, Vol. 179, No. 4075, pp. 800-803,
February 23, 1973

For abstract, see Metzger, A. E.

PHILLIPS, R. J.

P08 Mascons: Progress Toward a Unique Solution for Mass Distribution

R. J. Phillips, J. E. Conel, E. A. Abbott,
W. L. Sjogren, and J. B. Morton

J. Geophys. Res., Vol. 77, No. 35, pp. 7106–7114,
December 10, 1972

Through a series of analyses with high-altitude Lunar Orbiter and low-altitude Apollo 15 doppler gravity data, it is shown that the Serenity mascon is a thin body whose horizontal dimensions are well-determined and show a strong correlation with circular wrinkle ridge structure. Analysis to date has not uniquely determined the depth of the anomalous mass. However, geologic evidence strongly suggests that the mass excess is near the surface, because (1) the surface solution has a geometry highly suggestive of the partial filling of a ringed circular basin, and (2) the boundaries of the anomalous mass separate regions of shallow and deep mare flooding.

PHILLIPS, W. M.

P09 Experimental Evaluation of Thermal Ratcheting Behavior in UO_2 Fuel Elements

W. M. Phillips

Technical Memorandum 33-622, July 1, 1973

The effects of thermal cycling of UO_2 at high temperatures has been experimentally evaluated to determine the rates of distortion of UO_2-clad fuel elements. Two capsules were tested in the 1500°C range, one with a 50°C thermal cycle, the other with a 100°C thermal cycle. It was observed that eight hours at the lower cycle temperature produced sufficient UO_2 redistribution to cause clad distortion. The amount of distortion produced by the 100°C cycle was less than double that produced by the 50°C, indicating smaller thermal cycles would result in clad distortion. An incubation period was observed to occur before the onset of distortion with cycling similar to fuel swelling observed in-pile at these temperatures.

PINNELL, R. P.

P10 Nuclear Magnetic Resonance of Phosphorus Compounds: VII. Evidence for Steric Effects on the ^{31}P–^{77}Se Coupling and ^{31}P Chemical Shifts

R. P. Pinnell (Joint Science Department: Scripps, Pitzer, and Claremont Men's Colleges), C. A. Megerle (Joint Science Department: Scripps, Pitzer, and Claremont Men's Colleges), S. L. Manatt, and P. A. Kroon

J. Am. Chem. Soc., Vol. 95, No. 3, pp. 977–978, January 7, 1973

In connection with an investigation of the question of p_π–d_π bonding involving phosphorus, there has been occasion to synthesize and study the phosphorus nmr spectra of a number of triarylphosphines and triarylphosphine selenides. This article presents evidence that indicates how the nmr parameters for phosphorus whose local electronic environment is sterically perturbed can deviate from those expected on the basis of observed substituent effect correlations in less crowded molecules.

PIVIROTTO, T. J.

P11 Pressure and Current Effects on the Thermal Efficiency of an MPD Arc Used as a Plasma Source

T. J. Pivirotto

AIAA J., Vol. 11, No. 1, pp. 12–13, January 1973

In several types of laboratory experiments, such as magnetoplasmadynamic power generation, gas dynamic lasers, and basic gaseous plasma studies, a reliable and efficient continuous source of plasma is useful. This article describes one such source, the magnetoplasmadynamic arc operated without an applied magnetic field and presents data on its thermal efficiency, principal heat loss, and arc voltage over a range of argon mass flow rates not previously reported and at several arc currents. A comparison between this data and an existing empirical theory is also made with good agreement.

POTTER, P. D.

P12 **DSN Progress Report for March–April 1973: S- and X-Band Feed System**

P. D. Potter

Technical Report 32-1526, Vol. XV, pp. 54–62, June 15, 1973

In support of the Mariner Venus/Mercury 1973 X-band experiment, it is necessary to provide the Mars Deep Space Station (DSS 14) 64-m-diameter antenna with a dual-frequency microwave feed system. To fulfill this requirement, a particularly attractive approach, the reflex feed system, has been implemented. Completion of the reflex-feed-system installation into the DSS 14 antenna was accomplished on January 24, 1973 and the performance of this system was evaluated from January 25 to January 30, 1973.

This evaluation established the reflex-feed-system performance as completely acceptable to the Mariner Venus/Mercury 1973 X-band experiment. In two cases, S-band antenna gain and S-band system noise temperature, the reflex-feed-system performance is actually superior to that of the standard S-band feed system. This article briefly reviews the feed-system design, including a new dichroic reflector developed at JPL, and presents performance data.

POYNTER, R.

P13 **Thermal Radio Emission From Jupiter and Saturn**

S. Gulkis and R. Poynter

Phys. Earth Planet. Interiors, Vol. 6, Nos. 1–3, pp. 36–43, December 1972

For abstract, see Gulkis, S.

PRICE, A. L.

P14 **DSN Progress Report for March–April 1973: DSN Research and Technology Support**

E. B. Jackson, A. L. Price, and R. B. Kolbly

Technical Report 32-1526, Vol. XV, pp. 138–142, June 15, 1973

For abstract, see Jackson, E. B.

QUINN, R. B.

Q01 DSN Progress Report for January–February 1973: Low-Noise Receivers: Solid-State Pump Source for S-Band Traveling-Wave Masers

R. B. Quinn

Technical Report 32-1526, Vol. XIV, pp. 50–55,
April 15, 1973

Low-noise traveling-wave masers have been used by the DSN for ten years. The requirements for the maser pump source are presently met by reflex klystron oscillators, although other microwave energy sources have been tested and evaluated on the basis of cost, reliability, output power, tunability, frequency stability, and power stability. Gunn-effect diode oscillators have recently reached a stage of development that makes them superior to the reflex klystron oscillator. This article describes a Gunn-effect oscillator that has been tested, packaged, and evaluated in the laboratory and is now ready for installation in the DSN.

RANDALL, L. P.

R01 Monitoring of Antarctic Dry Valley Drilling Sites

F. A. Morelli, R. E. Cameron, D. R. Gensel, and
L. P. Randall (Northern Illinois University)

Antarctic J. U.S., Vol. VII, No. 4, pp. 92–94, July–August 1972

For abstract, see Morelli, F. A.

RASOOL, S. I.

R02 The Atmosphere of Mars From Mariner 9 Radio Occultation Measurements

A. J. Kliore, D. L. Cain, G. Fjeldbo, B. L. Seidel,
M. J. Sykes, and S. I. Rasool (National Aeronautics and Space Administration)

Icarus, Vol. 17, No. 2, pp. 484–516, October 1972

For abstract, see Kliore, A. J.

REEDY, R. C.

R03 **Lunar Surface Radioactivity: Preliminary Results of the Apollo 15 and Apollo 16 Gamma-Ray Spectrometer Experiments**

A. E. Metzger, J. I. Trombka (Goddard Spaceflight Center),
L. E. Peterson (University of California, San Diego),
R. C. Reedy (University of California, San Diego), and
J. R. Arnold (University of California, San Diego)

Science, Vol. 179, No. 4075, pp. 800–803,
February 23, 1973

For abstract, see Metzger, A. E.

REICHLEY, P. E.

R04 **DSN Progress Report for March–April 1973: Simultaneous Detection of Pulsar Radiation at S- and X-Bands**

P. E. Reichley, G. S. Downs, and G. A. Morris

Technical Report 32-1526, Vol. XV, pp. 133–137,
June 15, 1973

The reflex feed system installed in January 1973 on the 64-m-diameter antenna at the Goldstone Deep Space Communications Complex was used to receive weak wide-band signals from pulsars. This article illustrates the use of wide-band sources of radiation to test multifrequency antenna and receiver systems.

R05 **Martian Topography and Surface Properties as Seen by Radar: The 1971 Opposition**

G. S. Downs, R. M. Goldstein, R. R. Green,
G. A. Morris, and P. E. Reichley

Icarus, Vol. 18, No. 1, pp. 8–21, January 1973

For abstract, see Downs, G. S.

REID, M. S.

R06 **DSN Progress Report for January–February 1973: An Analysis of Noise Bursts on the 64-m-Diameter Antenna at Goldstone**

M. S. Reid and C. T. Stelzried

Technical Report 32-1526, Vol. XIV, pp. 46–49,
April 15, 1973

To provide more information for the noise-burst study, a comparison of noise bursts with the polarization-diversity S-band (PDS) and S-band megawatt-transmit (SMT) cones was made. For a period of approximately one month, the Mars Deep Space Station conducted its regular tracking missions alternately with the PDS and SMT cones. The S-band total-power-system temperature strip-chart recordings were analyzed for noise bursts. The conclusion is that, with respect to noise-burst performance, the PDS and SMT cones are similar.

R07 **DSN Progress Report for January–February 1973: Tracking and Ground-Based Navigation: Precision System Temperature Measurements at Goldstone**

M. S. Reid, R. A. Gardner, and A. J. Freiley

Technical Report 32-1526, Vol. XIV, pp. 60–67,
April 15, 1973

This article reports the system operating noise-temperature performance of the low-noise research cones at the Goldstone Deep Space Communications Complex for the period October 1, 1972 through January 31, 1973. System temperatures are reported for the S-band radar operational cone at the Venus Deep Space Station (DSS 13), the S-band megawatt-transmit cone, and the polarization-diversity S-band cone at the Mars Deep Space Station (DSS 14). In addition to these measurements, system-temperature calibrations and antenna-elevation profiles are reported for the 26-m-diameter antenna at DSS 13 with and without the quadripod, and for the 64-m-diameter antenna at DSS 14 at S- and X-bands with and without the reflex feed system.

R08 **DSN Progress Report for March–April 1973: S-Band Microwave Weather Project Data for CY 1971**

M. S. Reid and R. W. D. Booth

Technical Report 32-1526, Vol. XV, pp. 88–91,
June 15, 1973

The Weather Project forms part of an overall Radio Systems Development Project which seeks to optimize the spacecraft-to-ground communications link. The objective of the Weather Project is the statistical prediction of the performance of the DSN at X-band, and in the future at K-band. This article reports on the analysis of the S-band data for calendar year 1971, with results presented in tabular form. Cumulative frequency distribution of percentages of excess system temperature is tabulated as a function of time (whole year and quarterly periods) and of antenna elevation angle (four elevation ranges and for all elevation angles); averages, standard deviations, and confidence limits are also tabulated.

REMBAUM, A.

R09 Alkali Metal Intercalates of Molybdenum Disulfide

R. B. Somoano, V. Hadek, and A. Rembaum

J. Chem. Phys., Vol. 58, No. 2, pp. 697-701,
January 15, 1973

For abstract, see Somoano, R. B.

RENZETTI, N. A.

R10 DSN Progress Report for January–February 1973: DSN Functions and Facilities

N. A. Renzetti

Technical Report 32-1526, Vol. XIV, pp. 1–4,
April 15, 1973

The Deep Space Network (DSN), established by the NASA Office of Tracking and Data Acquisition and under the system management and technical direction of JPL, is designed for two-way communications with unmanned spacecraft traveling approximately 16,000 km (10,000 mi) from Earth to planetary distances. The objectives, functions, and organization of the DSN are summarized, and the Deep Space Instrumentation Facility, the Ground Communications Facility, and the Network Control System are described.

R11 DSN Progress Report for March–April 1973: DSN Functions and Facilities

N. A. Renzetti

Technical Report 32-1526, Vol. XV, pp. 1–4,
June 15, 1973

The Deep Space Network (DSN), established by the NASA Office of Tracking and Data Acquisition and under the system management and technical direction of JPL, is designed for two-way communications with unmanned spacecraft traveling approximately 16,000 km (10,000 mi) from Earth to planetary distances. The objectives, functions, and organization of the DSN are summarized, and the Deep Space Instrumentation Facility, the

Ground Communications Facility, and the Network Control System are described.

R12 **Tracking and Data System Support for the Pioneer Project: Pioneers 6–9. Extended Missions: July 1, 1971–July 1, 1972**

N. A. Renzetti and A. J. Siegmeth

Technical Memorandum 33-426, Vol. XI, May 1, 1973

The Tracking and Data System supported the deep space phases of the Pioneer 6, 7, 8, and 9 missions, with two spacecraft in an inward trajectory and two spacecraft in an outward trajectory from the Earth in heliocentric orbits. During the period covered in this memorandum, scientific instruments aboard each of the spacecraft continued to register information relative to interplanetary particles and fields, and radio metric data generated by the network continued to improve our knowledge of the celestial mechanics of the solar system. In addition to network support activity detail, network performance and special support activities are covered.

R13 **Tracking and Data System Support for the Mariner Mars 1971 Mission: Orbit Insertion Through End of Primary Mission**

P. W. Barnum, N. A. Renzetti, G. P. Textor, and
L. B. Kelly

Technical Memorandum 33-523, Vol. III, May 15, 1973

For abstract, see Barnum, P. W.

RHEIN, R. A.

R14 **The Formation of Hydrochloric Acid Aerosol From the Interaction of the Space Shuttle Rocket Exhaust With the Atmosphere**

R. A. Rhein

Technical Memorandum 33-619, June 1, 1973

This memorandum describes the conditions of atmospheric temperature and relative humidity under which hydrochloric-acid aerosol is expected upon interaction of the proposed Space-Shuttle-rocket exhaust products with the atmosphere. It was found that aerosol is expected under conditions of cool weather and high humidity. Including the effect of after burning results in a predicted small increase in the amount of aerosol.

RHO, J. H.

R15 **Spectrofluorometric Search for Porphyrins in Apollo 14 Surface Fines**

J. H. Rho, E. A. Cohen, and A. J. Bauman

"Proceedings of the Third Lunar Science Conference," *Supplement 3, Geochimica et Cosmochimica Acta,* Vol. 2, pp. 2149–2155, 1972

Benzene-methanol extracts of surface fines 14163,179,181 from Fra Mauro have been analyzed for porphyrins by means of fluorescence spectroscopy augmented by computer data treatment. Signal averaging and background removal revealed no porphyrin fluorescence features under conditions expected to produce a signal-to-noise ratio of 2:1 for 1.6×10^{-14} moles of extractable metalloporphyrin per gram of fines. These results are based upon the assumption that if metalloporphyrins were present they would be demetallated with the same efficiency as is Ni-mesoporphyrin IX.

R16 **Fluorescence Spectroscopy**

J. H. Rho

Space Life Sci., Vol. 3, No. 4, pp. 360–373, October 1972

This article discusses some practical aspects of the use of spectrophotofluorometers as applied to the organic analyses of returned lunar samples and other geological materials. Because of the single beam nature of spectrophotofluorometers many instrumental artifacts such as grating anomalies, irregular spectral output of light sources and response characteristics of photodetectors are apparent in sample spectra. In order to avoid some of these instrumental artifacts from influencing sample spectra, the performance characteristics of each optical component have been described and the necessity of instrumental calibration has been emphasized.

R17 **Analyses of the Returned Lunar Surface Fines for Porphyrins**

J. H. Rho, A. J. Bauman, E. A. Cohen,
T. F. Yen (University of Southern California), and
J. Bonner (California Institute of Technology)

Space Life Sci., Vol. 3, No. 4, pp. 415–418, October 1972

In the present studies, no porphyrins were found in the lunar surface fines collected from the Sea of Tranquillity by the Apollo 11 mission, from the Ocean of Storms by the Apollo 12 mission, and from the nonmare Fra Mauro Formation by the Apollo 14 expedition under the conditions in which porphyrins would have been detected had they been present in amounts as small as 10^{-14} mole.

ROSENKRANZ, P. W.

R18 Radio Observations of Cygnus X-3 and the Surrounding Region

B. Gary, E. T. Olsen, and P. W. Rosenkranz

Nature Phys. Sci., Vol. 239, No. 95, pp. 128–130, October 23, 1972

For abstract, see Gary, B.

ROSS, R. G., JR.

R19 Optimum Shell Design

A. M. Salama and R. G. Ross, Jr.

AIAA J., Vol. 11, No. 3, pp. 366–368, March 1973

For abstract, see Salama, A. M.

RUSCH, W. V. T.

R20 Determination of the Maximum Scan-Gain Contours of a Beam-Scanning Paraboloid and Their Relation to the Petzval Surface

W. V. T. Rusch and A. C. Ludwig

IEEE Trans. Anten. Prop., Vol. AP-21, No. 2, pp. 141–147, March 1973

The scan-plane fields in the focal region of a beam-scanning paraboloid are determined from physical optics. Amplitude and phase contours are presented, and comparisons are made with the geometrical-optics results. Contours for maximum scan-gain are determined as a function of F/D and illumination taper and compared with the Petzval surface. Unless the F/D is very large or spillover is excessive, a higher scan gain is achieved when the axis of a directional feed is parallel to the axis of the reflector than when the feed is directed toward the vertex. The contour of maximum scan-gain is a function of both illumination taper and F/D. In general, larger F/D values tend to have a maximum-gain contour close to the focal plane, while the smaller F/D values tend to have a maximum-gain contour closer to the Petzval surface. Increasing the illumination taper moves the maximum-gain contour closer to the Petzval surface. Normalized maximum-gain contours are presented as a function of beamwidths of scan. The frequency dependence of these results is discussed.

RYDGIG, R. C.

R21 **DSN Progress Report for January–February 1973: Overseas 64-m Station Implementation Status**

R. C. Rydgig

Technical Report 32-1526, Vol. XIV, pp. 146–148, April 15, 1973

This article presents the activities associated with implementing the overseas 64-m-diameter antenna stations in Australia (DSS 43) and Spain (DSS 63). It gives the current status of the project, describes the system configuration as implemented, and discusses the activities involved in reaching the desired configuration.

SAFFREN, M. M.

S01 **Temperature Dependence of the Accommodation Coefficient of Liquid-Helium Film**

T. G. Wang, D. D. Elleman, E. E. Olli, and M. M. Saffren

Phys. Rev. Lett., Vol. 30, No. 11, pp. 485–487, March 12, 1973

For abstract, see Wang, T. G.

SALAMA, A. M.

S02 **Optimum Shell Design**

A. M. Salama and R. G. Ross, Jr.

AIAA J., Vol. 11, No. 3, pp. 366–368, March 1973

Two methods for obtaining the minimum weight of rotational shells under certain constraints are compared. The constraints may be one or any combination of (1) manufacturing limits on the shell thickness (2) constraints on the jth buckling load or the mth natural frequency (3) a maximum allowable deflection may be required or (4) using a suitable yield criterion, the shell may be required to withstand the applied loads without yielding.

The two minimization techniques employed here are the simplex method and the variable metric method. While the simplex method requires only function evaluation during the search, the variable metric method requires both function and partial derivative evaluation. The objective function to be minimized is the shell total weight (or material volume) subjected to one or more of the above mentioned constraints.

SANDER, M. J.

S03 Mariner 9—Image Processing and Products

E. C. Levinthal (Stanford University), W. B. Green, J. A. Cutts, E. D. Jahelka, R. A. Johansen, M. J. Sander, J. B. Seidman, A. T. Young, and L. A. Soderblom (U.S. Geological Survey)

Icarus, Vol. 18, No. 1, pp. 75–101, January 1973

For abstract, see Levinthal, E. C.

SCHMIT, D. D.

S04 From Earth to Mars Orbit—Mariner 9 Propulsion Flight Performance With Analytical Correlations

M. J. Cork, R. L. French, C. J. Leising, and D. D. Schmit

AIAA Preprint 72-1185, AIAA/SAE Eighth Joint Propulsion Specialist Conference, New Orleans, Louisiana, November 29–December 1, 1972

For abstract, see Cork, M. J.

SCHUMACHER, L.

S05 Mariner Mars 1971 Sun Sensor Model Development and Simulation

L. Schumacher

Technical Memorandum 33-610, May 1, 1973

The Mariner Mars 1971 spacecraft was launched with an incorrectly sized resistor at the Sun-sensor circuit interface with its power supply. The design error caused 72 days of anomalous spacecraft operation. This memorandum analyzes the Sun-sensor flight-performance data and the results of a newly developed cruise-sensor life test.

A set of mathematical models was constructed which closely approximated the observed Sun-sensor flight and laboratory test results. These models revealed that (1) the aging phenomena in the sintered-cadmium-sulfide light detector varies across the detector width in proportion to the illumination history, (2) the current cruise Sun-sensor design is extremely sensitive to changes in the reflected illumination within the sensor housing, (3) the reflected illumination within the detector housing is proportional to the area and intensity of the solar disk observed at the spacecraft, and (4) the acquisition Sun sensor becomes a low-impedance path across the sensor bridge when in the vicinity of a large-angular-diameter, low-intensity light source. It is concluded that a computer model can be developed which will accurately predict Sun-sensor performance in a variety of flight conditions.

SEIDEL, B. L.

S06 The Atmosphere of Mars From Mariner 9 Radio Occultation Measurements

A. J. Kliore, D. L. Cain, G. Fjeldbo, B. L. Seidel, M. J. Sykes, and S. I. Rasool (National Aeronautics and Space Administration)

Icarus, Vol. 17, No. 2, pp. 484–516, October 1972

For abstract, see Kliore, A. J.

S07 The Shape of Mars From the Mariner 9 Occultations

D. L. Cain, A. J. Kliore, B. L. Seidel, and M. J. Sykes

Icarus, Vol. 17, No. 2, pp. 517–524, October 1972

For abstract, see Cain, D. L.

SEIDMAN, J. B.

S08 Mariner 9—Image Processing and Products

E. C. Levinthal (Stanford University), W. B. Green, J. A. Cutts, E. D. Jahelka, R. A. Johansen, M. J. Sander, J. B. Seidman, A. T. Young, and L. A. Soderblom (U.S. Geological Survey)

Icarus, Vol. 18, No. 1, pp. 75–101, January 1973

For abstract, see Levinthal, E. C.

SEQUEIRA, E. A.

S09 Mariner 9 Solar Array Design, Manufacture, and Performance

E. A. Sequeira

Technical Memorandum 33-615, May 15, 1973

Throughout the Mars orbital mission, the Mariner 9 solar array successfully supported the power requirements of the spacecraft without experiencing anomalies. Basically, the design of the solar array was similar to those of Mariners 6 and 7; however, Mariner 9 had the additional flight-operational requirement to perform in a Mars-orbit-environment mode. The special array tests provided information on the current–voltage characteristics and array degradation. Tests indicated that total solar-array current degradation was 3.5%. Flight data also verified that the solar panels had successfully survived the Sun occultation periods without additional degradation or failures. Final array tests indicated very close correlation between predicted and actual flight-array performance with no significant additional current degradation.

SIEGMETH, A. J.

S10 Tracking and Data System Support for the Pioneer Project: Pioneers 6–9. Extended Missions: July 1, 1971–July 1, 1972

N. A. Renzetti and A. J. Siegmeth

Technical Memorandum 33-426, Vol. XI, May 1, 1973

For abstract, see Renzetti, N. A.

SJOGREN, W. L.

S11 Mascons: Progress Toward a Unique Solution for Mass Distribution

R. J. Phillips, J. E. Conel, E. A. Abbott,
W. L. Sjogren, and J. B. Morton

J. Geophys. Res., Vol. 77, No. 35, pp. 7106–7114,
December 10, 1972

For abstract, see Phillips, R. J.

S12 Lunar Shape via the Apollo Laser Altimeter

W. L. Sjogren and W. R. Wollenhaupt

Science, Vol. 179, No. 4070, pp. 275–278,
January 19, 1973

Data from the Apollo 15 and Apollo 16 laser altimeters reveal the first accurate elevation differences between distant features on both sides of the moon. The large far-side depression observed in the Apollo 15 data is not present in the Apollo 16 data. When the laser results are compared with elevations on maps from the

Aeronautical Chart and Information Center, differences of 2 km over a few hundred km are detected in the Mare Nubium and Mare Tranquillitatis regions. The Apollo 16 data alone would put a 2-km bulge toward the Earth; however, the combined data are best fit by a sphere of radius 1737.7 km. The offset of the center of gravity from the optical center is about 2 km toward the Earth and 1 km eastward. The polar direction parameters are not well determined.

SMITH, C. A.

S13 Error Analysis for Mariner Venus/Mercury 1973 Conducted at the JPL Mesa West Antenna Range

N. L. Vincent, C. A. Smith, A. J. Brejcha, and H. A. Curtis

Technical Memorandum 33-625, June 1, 1973

For abstract, see Vincent, N. L.

SMITH, R. H.

S14 DSN Progress Report for March–April 1973: Data Collection System for the Dual-Carrier Exciter

R. H. Smith

Technical Report 32-1526, Vol. XV, pp. 63–65, June 15, 1973

A method was needed to monitor the dual-carrier exciter to be used at the 64-m-diameter-antenna deep space stations for the Viking Mars 1975 mission. This article describes the data-collection system to be used for diagnostic purposes to determine the status of the dual-carrier exciter. This system was developed to sample sequentially each analog test point in the dual-carrier exciter (mounted in the tricone of the antenna), digitally serialize each sample, send it over a single set of wires to the control room on the ground, convert the data from serial to parallel, and display the sampled data with digital displays or supply the sampled-data information to a computer for automatic monitoring of the dual-carrier exciter.

SMITH, R. M.

S15 DSN Progress Report for January–February 1973: The DSN Hydromechanical Equipment Service Program

I. D. Wells and R. M. Smith

Technical Report 32-1526, Vol. XIV, pp. 215–221,
April 15, 1973

For abstract, see Wells, I. D.

SODERBLOM, L. A.

S16 Mariner 9—Image Processing and Products

E. C. Levinthal (Stanford University), W. B. Green, J. A. Cutts, E. D. Jahelka, R. A. Johansen, M. J. Sander, J. B. Seidman, A. T. Young, and L. A. Soderblom (U.S. Geological Survey)

Icarus, Vol. 18, No. 1, pp. 75–101, January 1973

For abstract, see Levinthal, E. C.

SOHN, R. L.

S17 Navigation Requirements for Advanced Deep Space Missions

L. D. Friedman, J. W. Moore, and R. L. Sohn

Navigation: J. Institute Nav., Vol. 19, No. 3, pp. 266–280, Fall 1972

For abstract, see Friedman, L. D.

SOMOANO, R. B.

S18 Alkali Metal Intercalates of Molybdenum Disulfide

R. B. Somoano, V. Hadek, and A. Rembaum

J. Chem. Phys., Vol. 58, No. 2, pp. 697–701, January 15, 1973

Natural molybdenite and single crystals of MoS_2 grown by chemical vapor transport were intercalated with the alkali group of metals (Li, Na, K, Rb, and Cs) by means of the liquid ammonia technique. Stoichiometries and X-ray data of all intercalates were determined and a complete indexing of the X-ray patterns of $K_{0.4}MoS_2$ and $Rb_{0.3}MoS_2$ was achieved. The X-ray results show insignificant changes in the a_0 axis and considerable expansion of the c_0 axis after intercalation. All intercalated crystals were superconducting. The superconductivity is believed to be due to an electron transfer from the alkali metal to an empty band of MoS_2, resulting in an increase in electron density as well as in the density of states at the Fermi surface.

STANLEY, R. P.

S19 **DSN Progress Report for January–February 1973: A Study of Varshamov Codes for Asymmetric Channels**

R. P. Stanley and M. F. Yoder

Technical Report 32-1526, Vol. XIV, pp. 117–123,
April 15, 1973

This article presents a study of an important class of single-error-correcting codes for binary and nonbinary discrete asymmetric channels recently discovered by Varshamov. A wide generalization of Varshamov's construction is given, and the complete weight distribution of Varshamov's codes is calculated.

STANTON, R. H.

S20 **Estimating Trajectory Correction Requirements for Multiple Outer Planet Missions**

L. D. Friedman, T. W. Hamilton, and R. H. Stanton

J. Spacecraft Rockets, Vol. 9, No. 12, pp. 909–914,
December 1972

For abstract, see Friedman, L. D.

STELZRIED, C. T.

S21 **DSN Progress Report for January–February 1973: An Analysis of Noise Bursts on the 64-m-Diameter Antenna at Goldstone**

M. S. Reid and C. T. Stelzried

Technical Report 32-1526, Vol. XIV, pp. 46–49,
April 15, 1973

For abstract, see Reid, M. S.

S22 **Observations of Jupiter at 13-cm Wavelength During 1969 and 1971**

S. Gulkis, B. Gary, M. Klein, and C. T. Stelzried

Icarus, Vol. 18, No. 2, pp. 181–191, February 1973

For abstract, see Gulkis, S.

STIMPSON, L. D.

S23 Effects of Overlaps, Stitches, and Patches on Multilayer Insulation

L. D. Stimpson and W. Jaworski

Progr. Astronaut. Aeronaut., Vol. 31, pp. 247–266, 1973

The effects of spacecraft installation-type discontinuities on aluminized Mylar multilayer insulation have been measured, using an electrically heated cylindrical calorimeter. The experimental results have been reproducible within ±10% or better for identical blankets and less than ±5% for the same blanket. Good blanket performance can be obtained using short interleaving for joints, eliminating stitched seams, or using small patches, particularly over the hot side of stitches. The heat loss through stitching is excessive but highly localized. Analytical models were matched to thermocouple test results. High lateral heat transfer is established as an important phenomenon in the vicinity of a discontinuity.

STIRN, R. J.

S24 Photoconductor–Metal Contact at Higher Densities

G. A. Dussel (University of Delaware),
K. W. Böer (University of Delaware), and R. J. Stirn

Phys. Rev., Pt. B: Solid State, Vol. 7, No. 4,
pp. 1443–1454, February 15, 1973

For abstract, see Dussel, G. A.

S25 CdS–Metal Contact at Higher Current Densities

R. J. Stirn, K. W. Böer (University of Delaware), and
G. A. Dussel (University of Delaware)

Phys. Rev., Pt. B: Solid State, Vol. 7, No. 4,
pp. 1433–1443, February 15, 1973

The current density as a function of applied voltage, optical excitation, and temperature in photoconducting CdS crystals with different non-Ohmic contacts (Au, Ag, Cu, Pt, Ni, and Sn) and the transient behavior of this current after switching-on of the applied voltage is investigated. High-field domains adjacent to these contacts are used as tools to measure the fields near the contacts. These domains are analyzed for different light intensities and temperatures. It is concluded from the experimental results that the observed high current density is caused by tunneling through the barrier and that in a slab of about 600-Å thickness at the cathode, the field must increase by about one order of magnitude from the field in the high-field domain. The space charge necessary for this must be stored in levels inaccessible for detection with conventional methods. It is proposed that in CdS about 10^{18}-cm^{-3} levels caused by native defects at about 0.8 eV below the conduction band are responsible for this space charge. These levels are probably also responsible for the fact that CdS is never observed to be *p* type under equilibrium doping conditions.

SYKES, M. J.

S26 **The Atmosphere of Mars From Mariner 9 Radio Occultation Measurements**

A. J. Kliore, D. L. Cain, G. Fjeldbo, B. L. Seidel,
M. J. Sykes, and S. I. Rasool (National Aeronautics and Space Administration)

Icarus, Vol. 17, No. 2, pp. 484–516, October 1972

For abstract, see Kliore, A. J.

S27 **The Shape of Mars From the Mariner 9 Occultations**

D. L. Cain, A. J. Kliore, B. L. Seidel, and M. J. Sykes

Icarus, Vol. 17, No. 2, pp. 517–524, October 1972

For abstract, see Cain, D. L.

TAUSWORTHE, R. C.

T01 **A Bibliography of the Theory and Application of the Phase-Lock Principle**

W. C. Lindsey (University of Southern California) and
R. C. Tausworthe

Technical Report 32-1581, April 1, 1973

For abstract, see Lindsey, W. C.

TAYLOR, F. W.

T02 **The Abundance of CH_3D and the D/H Ratio in Jupiter**

R. Beer and F. W. Taylor

Astrophys. J., Vol. 179, No. 1, Pt. 1, pp. 309–327,
January 1, 1973

For abstract, see Beer, R.

TEXTOR, G. P.

T03 **Tracking and Data System Support for the Mariner Mars 1971 Mission: Orbit Insertion Through End of Primary Mission**

P. W. Barnum, N. A. Renzetti, G. P. Textor, and
L. B. Kelly

Technical Memorandum 33-523, Vol. III, May 15, 1973

For abstract, see Barnum, P. W.

THORPE, T. E.

T04 **Mariner 9 Star Photography**

T. E. Thorpe

Appl. Opt., Vol. 12, No. 2, pp. 359–363, February 1973

Successful photography of stars by the Mariner 9 spacecraft has confirmed both mathematical prediction of point source response by vidicons and preflight calibration results. Camera-B limiting magnitude and integrated image data are presented to provide information relevant to absolute photometric reduction. These data appear consistent to better than 15% and suggest a good calibration source. Decalibration of Mars picture information, however, requires precise knowledge of Mars spectral radiance and camera point spread function. The effect of image motion on star detection thresholds is also discussed.

TRAJMAR, S.

T05 **Electron Impact Excitation of H_2O**

S. Trajmar, W. Williams, and A. Kuppermann (California Institute of Technology)

J. Chem. Phys., Vol. 58, No. 6, pp. 2521–2531,
March 15, 1973

Relative differential cross sections for elastic scattering and for a number of inelastic processes corresponding to vibrational and vibronic excitation of H_2O have been determined at 53, 20, and 15 eV impact energies in the 0–90° angular range. The measurements were carried out with an instrumental resolution of about 80 meV for transitions corresponding to various energy losses. On the basis of the angular distribution of the scattered electrons, it is suggested that the 4.5 and 9.81 eV transitions are associated with excitations of triplet states, while the angular distribution of the scattered electrons at all other energy losses indicate predominantly singlet–singlet transitions. The sharpness of the 9.81 eV transition indicates that the corresponding state has an equilibrium geometry similar to that of the ground state.

T06 **Vibrational Excitation in CO by Electron Impact in the Energy Range 10–90 eV**

A. Chutjian, D. G. Truhlar (University of Minnesota), W. Williams, and S. Trajmar

Phys. Rev. Lett., Vol. 29, No. 24, pp. 1580–1583, December 11, 1972

For abstract, see Chutjian, A.

T07 **Excitation of the $W^3\Delta_u$, $w^1\Delta_u$, $B'^3\Sigma_u^-$, and $a'^1\Sigma_u^-$ States of N_2 by Electron Impact**

A. Chutjian, D. C. Cartwright (The Aerospace Corporation), and S. Trajmar

Phys. Rev. Lett., Vol. 30, No. 6, pp. 195–198, February 5, 1973

For abstract, see Chutjian, A.

TROMBKA, J. I.

T08 **Lunar Surface Radioactivity: Preliminary Results of the Apollo 15 and Apollo 16 Gamma-Ray Spectrometer Experiments**

A. E. Metzger, J. I. Trombka (Goddard Spaceflight Center), L. E. Peterson (University of California, San Diego), R. C. Reedy (University of California, San Diego), and J. R. Arnold (University of California, San Diego)

Science, Vol. 179, No. 4075, pp. 800–803, February 23, 1973

For abstract, see Metzger, A. E.

TRUHLAR, D. G.

T09 **Vibrational Excitation in CO by Electron Impact in the Energy Range 10–90 eV**

A. Chutjian, D. G. Truhlar (University of Minnesota), W. Williams, and S. Trajmar

Phys. Rev. Lett., Vol. 29, No. 24, pp. 1580–1583, December 11, 1972

For abstract, see Chutjian, A.

UCHIYAMA, A. A.

U01 **Leak Rates in Sealed Cells**

H. A. Frank and A. A. Uchiyama

J. Electrochem. Soc., Vol. 120, No. 3, pp. 313–317, March 1973

For abstract, see Frank, H. A.

UNTI, T. W. J.

U02 **Note on Asymptotically Flat Empty Spaces**

T. W. J. Unti

Gen. Relat. Grav., Vol. 3, No. 1, pp. 43–58, 1972

The algebraic programming system FORMAC is used to extend asymptotic solutions of spin coefficient equations reported earlier. The expansions are then applied to metrics with geodesic rays and to previously-conserved terms. It is shown how the expansion may prove useful in finding new solutions to the field equations.

VINCENT, N. L.

V01 **Error Analysis for Mariner Venus/Mercury 1973 Conducted at the JPL Mesa West Antenna Range**

N. L. Vincent, C. A. Smith, A. J. Brejcha, and H. A. Curtis

Technical Memorandum 33-625, June 1, 1973

Theoretical analysis and experimental data are combined to yield the errors to be used with antenna gain, antenna patterns, and RF-cable insertion loss measurements for the Mariner Venus/Mercury 1973 Flight Project. These errors apply to measurements conducted at the JPL Mesa West Antenna Range, on the high-gain antenna, low-gain antenna, and RF coaxial cables.

VON ROOS, O. H.

V02 **DSN Progress Report for March–April 1973: A Global Model of the Earth's Ionosphere: The Nighttime Ionosphere**

O. H. von Roos and P. R. Escobal

Technical Report 32-1526, Vol. XV, pp. 32–47, June 15, 1973

This article discusses the nighttime ionosphere and considers specifically the dawn and dusk situation in which a transition from electron production by the Sun's radiation to a cessation of this production gradually occurs. The strict-nighttime ionosphere is governed by electron attachment and diffusion. The transition period depends very much on the declination angle of the Sun and the latitude of the geographical location on Earth where knowledge of the ionospheric electron distribution is desired.

Simple and concise expressions for the electron distribution in the upper ionosphere are derived so that calibrations for range corrections on a global scale are possible. The ionospheric model presented contains six empirical parameters which are considered functions of geographical location and must be determined by measurement.

V03 A Problem in Classical Mechanics

O. H. von Roos

Am. J. Phys., Vol. 41, No. 3, pp. 435-436, March 1973

Two bodies having arbitrary mass distributions exert forces and torques on each other. Each mass distribution engenders a force field, derivable from a potential, which subjects the other body to forces and torques. It is possible to change the mass distribution without changing the external potential. This article develops proof that no matter what the mass distributions of the two bodies, as long as they lead to the same external potentials, the torques will be the same and can be stated in expressions containing only external potential fields.

WALLACE, R. A.

W01 Saturn Satellite Encounter Opportunities for Mariner Jupiter–Saturn 1977

R. A. Wallace

JPL Quarterly Technical Review, Vol. 3, No. 1, pp. 14–25, April 1973

The Mariner Jupiter–Saturn 1977 mission will allow scientists to collect data from a sophisticated spacecraft flying through the Saturn system some time between November 1980 and September 1981. This opportunity to explore one of our solar system's most complex planet and satellite systems must be planned and designed for, if the mission is to take full advantage of the science value return that is possible. Part of optimizing the Saturn-encounter design for science value return will be the search for close satellite encounters.

This article investigates the opportunities for close satellite encounters which meet the planetary constraints at Saturn that are imposed by science value return and environmental conditions. Since the satellites travel at various speeds in their orbits, Saturn arrival time is critical and has been chosen as the design parameter. Arrival times are recommended which afford close satellite encounters and also meet important mission constraints. A design chart illustrates the satellite opportunities as a function of Saturn arrival date. Potential applications are given to illustrate the use of the Saturn satellite opportunity chart in encounter design.

WANG, T. G.

W02 Temperature Dependence of the Accommodation Coefficient of Liquid-Helium Film

T. G. Wang, D. D. Elleman, E. E. Olli, and M. M. Saffren

Phys. Rev. Lett., Vol. 30, No. 11, pp. 485–487,
March 12, 1973

The accommodation coefficient γ of a helium film from 1.15 to 4°K is determined by measuring the time constant of a rotating superconducting Nb sphere levitated in vapor and covered with a saturated helium film. The conventional assumption of the phenomenological theory of superfluidity, that the order parameter ψ vanishes at the free surface of helium II, implies that γ is unity and independent of temperature. We find that γ is nearly unity above the λ point, suffers an abrupt drop close to T_λ, and gradually levels off to the value of $\cong 0.8$ at lower temperatures.

WELLS, I. D.

W03 DSN Progress Report for January–February 1973: The DSN Hydromechanical Equipment Service Program

I. D. Wells and R. M. Smith

Technical Report 32-1526, Vol. XIV, pp. 215–221,
April 15, 1973

Operational experience from the first 64-m-diameter antenna indicated that the increase in the quantity of spares required to support the system was becoming prohibitive. With additional antennas becoming operational, it was obvious that an efficient, controllable program was necessary to support the DSN. A study was conducted to determine the optimum method for providing repair, test, and calibration service in support of hydromechanical equipment.

Several possible sources of service were considered; the governing factors throughout the comparison phase of the study were cost and reliability. Major consideration was given to conservation of skilled personnel, control of service environment, turnaround time, and the adoption of an oil-sampling and contamination-control program. This article summarizes the results of the study and the present and future status of the program.

WEN, L. C.

W04 Ion Thruster Thermal Characteristics and Performance

L. C. Wen, J. D. Crotty, and E. V. Pawlik

J. Spacecraft Rockets, Vol. 10, No. 1, pp. 35–41, January 1973

Experimental and analytical results for a typical 20-cm-diam, hollow-cathode ion thruster are reported. The foundation of the investigation was the application of thermal model correction techniques. Pertinent thermal properties and plasma heating characteristics of the thruster were determined through correlation and integration of temperature measurement data with a single-state Wiener–Kalman filter. The thruster self-heating levels on various parts were realistically estimated. Analytically predicted temperatures were forced to agree with the measured values for the purpose of constructing a corrected thermal model, which could then be used to evaluate more realistic thruster circumstances and environments. The expected accuracy of the resultant analytical network model was demonstrated to be ±10 K. Thruster thermal performance data for a typical five-thruster array are presented as functions of environmental solar intensities. The thermal analyses are also extended to a 30-cm thruster system.

WHITEHEAD, P. B.

W05 The Mariner Venus Mercury Flight Data Subsystem

P. B. Whitehead

Proceedings of the National Telecommunications Conference, Houston, Texas, December 4–6, 1972, pp. 28B-1–28B-5

On previous Mariners the Flight Telemetry Subsystem and the Data Automation Subsystem shared responsibility for data handling on the spacecraft. The Flight Telemetry Subsystem handled engineering measurements and the Data Automation Subsystem handled scientific measurements. On Mariner Venus/Mercury 1973 the Flight Data Subsystem (FDS) will combine both these functions.

The FDS collects science and engineering data, formats it into serial data streams, and sends it to the Modulation/Demodulation Subsystem for transmission to the ground or to the Data Storage Subsystem for storage on a digital tape recorder. The FDS is controlled by serial digital words called coded commands received either from the Central Computer and Sequencer or from the ground via the Modulation/Demodulation Subsystem. The FDS is divided into eight major blocks: power converter, timing and control, engineering data, memory, memory input/output and control, nonimaging data, imaging data, and data output. The subsystem consists of some 4000 components. It weighs 17 kg (35 lb) and uses 35 W of power.

WHITTLESEY, A. C.

W06 Electromagnetic Interference of Power Conditioners for Solar Electric Propulsion

A. C. Whittlesey and T. W. Macie

Technical Memorandum 33-623, July 1, 1973

Electrical, multi-kilowatt power-conditioning (PC) equipment needed on board a spacecraft utilizing solar-electric propulsion creates an electromagnetic environment that is potentially detrimental to the science, navigation, and radio-communication hardware. Three lightweight, 2.5-kW PCs were evaluated in terms of their electromagnetic characteristics. It was found that the levels of radiated and conducted interference exceeded the levels anticipated for a solar-electric-propulsion mission. These noise emissions, however, were the result of deficient interference design in these models, rather than a basic inability of this type of PC to control interference.

It is essential that PC design specifications clearly define the electromagnetic-interference (EMI) and electromagnetic-compatibility requirements, that milestones of design evaluation be established, and that the quality assurance plan include provisions for satisfying the EMI requirements as well as an EMI test to verify adequacy of the design.

WILLIAMS, W.

W07 Electron Impact Excitation of H_2O

S. Trajmar, W. Williams, and A. Kuppermann (California Institute of Technology)

J. Chem. Phys., Vol. 58, No. 6, pp. 2521–2531, March 15, 1973

For abstract, see Trajmar, S.

W08 Vibrational Excitation in CO by Electron Impact in the Energy Range 10–90 eV

A. Chutjian, D. G. Truhlar (University of Minnesota), W. Williams, and S. Trajmar

Phys. Rev. Lett., Vol. 29, No. 24, pp. 1580–1583, December 11, 1972

For abstract, see Chutjian, A.

WILLSON, R. C.

W09 Active Cavity Radiometer

R. C. Willson

Appl. Opt., Vol. 12, No. 4, pp. 810–817, April 1973

The active cavity radiometer (ACR) is a pyrheliometer that accurately defines the absolute radiation scale. The physics of the pyrheliometric method and the ACR approach to this method are presented in detail. A mathematical abstraction of the method is generated through a quasi-equilibrium analysis of the power balance of the ACR's cavity detector. An error analysis is carried out on the quasi-equilibrium equation to determine the uncertainties of ACR measurements relative to the absolute radiation scale. The uncertainty of ACR measurements as a function of irradiance level is presented in graphical form.

W10 Experimental Comparisons of the International Pyrheliometric Scale With the Absolute Radiation Scale

R. C. Willson

Nature, Vol. 239, No. 5369, pp. 208–209, September 22, 1972

A series of radiometer comparison tests has been carried out at the JPL Table Mountain Observatory during the period May 1968 to August 1970. Solar irradiance measurements by instruments

(Eppley Angstrom Pyrheliometers) reproducing the International Pyrheliometric Scale (IPS) have been compared with measurements made simultaneously by a number of JPL active cavity radiometers (ACRs) and practical absolute cavity radiometers (PACRADs). This article presents the results of these tests which demonstrate a systematic difference between the absolute radiation scale, as defined by the ACR and PACRAD measurements, and the IPS. An IPS absolute error of 2.2 ± 0.5% is indicated.

W11 New Radiometric Techniques and Solar Constant Measurements

R. C. Willson

Solar Energy, Vol. 14, No. 2, pp. 203–211, January 1973

A series of absolute cavity radiometers, designed to measure solar irradiance, has been developed at JPL. Analysis indicates the absolute uncertainty of irradiance measurements made by the most recent devices to be less than ±0.5 mW/cm^2. In experiments the radiometric scale defined by the JPL instruments has been compared with the International Pyrheliometric Scale (IPS). A systematic 2.2% difference has been observed with the IPS producing consistently lower measurements.

The solar constant and spectral distribution have been derived from high-altitude balloon flight measurements made by two types of JPL cavity radiometers. Measurements at 25 km in 1968 produced a solar constant value of 137.0 mW/cm^2. From 1969 measurements at 36 km, a value of 136.6 mW/cm^2 was derived, with an estimated absolute uncertainty of ±0.5%.

WILSON, A. H.

W12 Furlable Spacecraft Antenna Development: Second Interim Report

R. E. Oliver and A. H. Wilson

Technical Memorandum 33-606, May 15, 1973

For abstract, see Oliver, R. E.

WOLLENHAUPT, W. R.

W13 Lunar Shape via the Apollo Laser Altimeter

W. L. Sjogren and W. R. Wollenhaupt

Science, Vol. 179, No. 4070, pp. 275-278, January 19, 1973

For abstract, see Sjogren, W. L.

WOO, R.

W14 **Remote Sensing of the Turbulence Characteristics of a Planetary Atmosphere by Radio Occultation of a Space Probe**

R. Woo and A. Ishimaru (University of Washington)

Radio Sci., Vol. 8, No. 2, pp. 103–108, February 1973

The purpose of this article is to analyze the effects of small-scale turbulence on radio waves propagating through a planetary atmosphere. The analysis provides a technique for inferring the turbulence characteristics of a planetary atmosphere from the radio signals received from a spacecraft as it is occulted by the planet. The planetary turbulence is assumed to be localized and smoothly varying with the structure constant varying exponentially with altitude. The variance of log-amplitude and phase fluctuations of a wave propagating through the atmosphere are derived. When the distance between the spacecraft and the planetary atmosphere exceeds L_0^2/λ, where L_0 is the outer scale of turbulence, the effects of inhomogeneity and finite size of the turbulent medium become important. A recent study, reported earlier, pointed out that the structure constant for the Venusian atmosphere inferred from the Mariner 5 occultation data was significantly lower than that inferred from the Venera 4 data. By applying the analysis developed in this article it is shown that the effects of inhomogeneity and finite size of the turbulence, which were excluded in the previous analysis, account for this difference. More important, however, is the fact that the new techniques are available for use in future radio-occultation missions.

YANG, J.-N.

Y01 **On the Normality and Accuracy of Simulated Random Processes**

J.-N. Yang

J. Sound Vibr., Vol. 26, No. 3, pp. 417-428, 1973

Efficient methods of simulating stationary and nonstationary random processes and envelopes, by using a series of sine or cosine functions or by using the fast Fourier transform, have been proposed previously. Without applying the central limit theorem, it is shown in this article that the simulated random processes are asymptotically gaussian processes as the number of terms, N, of sine or cosine functions approaches infinity. The accuracy of the first-order probability densities of the simulated random processes is investigated by using the fast Fourier transform. Numerical results are computed with respect to the variation of the number of terms, N, of sine or cosine functions used for simulation. It is shown that within the practical range of N, such as 500, the accuracy is remarkably satisfactory even outside the region of 3 standard deviations. The investigation of the accuracy of the second-order probability densities by applying the fast Fourier transform is also described in detail. The study of accuracy presented herein is of vital importance in determining the applicability and practicality of methods of simulation.

YASUI, R. K.

Y02 **Parametric Performance Characteristics and Treatment of Temperature Coefficients of Silicon Solar Cells for Space Application**

R. E. Patterson and R. K. Yasui

Technical Report 32-1582, May 15, 1973

For abstract, see Patterson, R. E.

YEN, T. F.

Y03 **Analyses of the Returned Lunar Surface Fines for Porphyrins**

J. H. Rho, A. J. Bauman, E. A. Cohen,
T. F. Yen (University of Southern California), and
J. Bonner (California Institute of Technology)

Space Life Sci., Vol. 3, No. 4, pp. 415–418, October 1972

For abstract, see Rho, J. H.

YODER, M. F.

Y04 **DSN Progress Report for January–February 1973: A Study of Varshamov Codes for Asymmetric Channels**

R. P. Stanley and M. F. Yoder

Technical Report 32-1526, Vol. XIV, pp. 117–123,
April 15, 1973

For abstract, see Stanley, R. P.

YOUNG, A. T.

Y05 **Comment on "The Composition of the Venus Cloud Tops in Light of Recent Spectroscopic Data"**

L. D. G. Young and A. T. Young

Astrophys. J., Vol. 179, No. 1, Pt. 2, pp. L39–L43, January 1, 1973

For abstract, see Young, L. D. G.

Y06 **The Planet Venus: A New Periodic Spectrum Variable**

L. D. G. Young, A. T. Young, J. W. Young, and J. T. Bergstralh

Astrophys. J., Vol. 181, No. 1, Pt. 2, pp. L5–L8, April 1, 1973

For abstract, see Young, L. D. G.

Y07 **Mariner 9—Image Processing and Products**

E. C. Levinthal (Stanford University), W. B. Green, J. A. Cutts, E. D. Jahelka, R. A. Johansen, M. J. Sander, J. B. Seidman, A. T. Young, and L. A. Soderblom (U.S. Geological Survey)

Icarus, Vol. 18, No. 1, pp. 75–101, January 1973

For abstract, see Levinthal, E. C.

YOUNG, J. W.

Y08 **The Planet Venus: A New Periodic Spectrum Variable**

L. D. G. Young, A. T. Young, J. W. Young, and J. T. Bergstralh

Astrophys. J., Vol. 181, No. 1, Pt. 2, pp. L5–L8, April 1, 1973

For abstract, see Young, L. D. G.

YOUNG, L. D. G.

Y09 **Comment on "The Composition of the Venus Cloud Tops in Light of Recent Spectroscopic Data"**

L. D. G. Young and A. T. Young

Astrophys. J., Vol. 179, No. 1, Pt. 2, pp. L39–L43, January 1, 1973

It has been suggested in previous reporting that the topmost clouds of Venus are composed of concentrated aqueous HCl solutions. This article compares laboratory spectra of aqueous HCl solutions with spectra of Venus and concludes that the composition of the clouds of Venus is in much better agreement with sulfuric than with hydrochloric acid solutions.

Y10 **The Planet Venus: A New Periodic Spectrum Variable**

L. D. G. Young, A. T. Young, J. W. Young, and J. T. Bergstralh

Astrophys. J., Vol. 181, No. 1, Pt. 2, pp. L5–L8, April 1, 1973

This article describes a study of the transparency variations in the atmosphere of Venus as well as their correlation (if any) with ultraviolet cloud features photographed cooperatively by the Paris, New Mexico State University, and Lowell observatories. The study has shown that the apparent strength of CO_2 absorptions in the spectrum of Venus varies by 20% in a period of 4 days. The variations are synchronous over the disk and thus represent a fundamental dynamical mode of the atmosphere.

Y11 **High Resolution Spectra of Venus—A Review**

L. D. G. Young

Icarus, Vol. 17, No. 3, pp. 632–658, December 1972

The existing high resolution spectra of Venus show considerable variations in the abundance of CO_2. As this is the major constituent of the atmosphere, these day-to-day variations indicate that the effective reflecting cloud layer is undergoing substantial vertical displacements over a relatively short time scale. The published observations indicate that CO is uniformly mixed with the CO_2, but that the lines of HF may be formed deeper in the atmosphere and HCl lines considerably deeper. These conclusions are based on extrapolations of laboratory measurements and could be considerably altered by new laboratory measurements made under conditions similar to those near the tropopause in Venus.

YOUNGER, H. C.

Y12 **DSN Progress Report for January–February 1973: Simulated Deep Space Station Control Console Study**

H. C. Younger

Technical Report 32-1526, Vol. XIV, pp. 222–225,
April 15, 1973

This article describes a study of deep-space-station operations with the aid of a simulated control console which is currently being used to evaluate operations at the Echo Deep Space Station. This study is intended to improve performance and reduce operating costs by allowing the station to be operated on a system basis by system-engineering personnel. Study approach and current status are presented.

ZAFONTE, L.

Z01 Hydrocarbons in Air Samples From Antarctic Dry Valley Drilling Sites

J. V. Behar (University of California, Riverside),
L. Zafonte (University of California, Riverside),
R. E. Cameron, and F. A. Morelli

Antarctic J. U.S., Vol. VII, No. 4, pp. 94–96, July-August 1972

For abstract, see Behar, J. V.

ZYGIELBAUM, A. I.

Z02 DSN Progress Report for January–February 1973: An Input/Output Processor for the XDS 930: An Exercise in Micro-Programmed Design

A. I. Zygielbaum

Technical Report 32-1526, Vol. XIV, pp. 131–140,
April 15, 1973

A micro-programmed, stored-logic, input/output (I/O) processor has been developed to evaluate micro-programming as a digital design technique. This I/O processor can be used for investigating DSN standard computer/computer interfaces as well as for experimentation with external control of the XDS 390 computer in emulation of multiple-computer systems.

Subject Index

Subject Categories

Antennas and Transmission Lines
Apollo Project

Bioengineering
Biology

Chemistry
Comets
Computer Applications and Equipment
Computer Programs
Control and Guidance
Cosmology

Earth Atmosphere
Earth Surface
Electricity and Magnetism
Electronic Components and Circuits
Energy Storage
Environmental Sciences

Facility Engineering
Fluid Mechanics

Gravitational Phenomena

Industrial Processes and Equipment
Information Distribution and Display
Information Theory
Interplanetary Exploration, Advanced

Lunar Exploration, Advanced
Lunar Interior
Lunar Spacecraft, Advanced
Lunar Surface

Management Systems
Mariner Jupiter/Saturn 1977 Project
Mariner Mars 1969 Project
Mariner Mars 1971 Project
Mariner Venus/Mercury 1973 Project
Mariner Venus 67 Project
Masers and Lasers
Materials, Nonmetallic
Mathematical Sciences
Mechanics
Mechanisms

Optics
Orbits and Trajectories

Packaging and Cabling
Particle Physics
Photography
Pioneer Project
Planetary Atmospheres
Planetary Exploration, Advanced
Planetary Interiors

Planetary Motion
Planetary Spacecraft, Advanced
Planetary Surfaces
Plasma Physics
Power Sources
Propulsion, Electric
Propulsion, Liquid
Pyrotechnics

Quality Assurance and Reliability

Radar
Radio Astronomy

Safety Engineering
Scientific Instruments
Soil Sciences
Solar Phenomena
Solid-State Physics
Spacecraft Environments and Shielding
Spectrometry
Standards, Reference
Stellar Phenomena
Structural Engineering

Telemetry and Command
Temperature Control
Test Facilities and Equipment
Thermodynamics
Thermoelectric Outer-Planet Spacecraft (TOPS)
Tracking

Viking Mars 1975 Project

Wave Propagation

Subjects

Publication Index

Technical Reports

DSN Progress Reports for January–April 1973 (Technical Report 32-1526, Vols. XIV and XV)

421	Network Operations (contd)	L15
422	DSN Facility Operations	W03 Y12
430	DSN Systems Engineering Office	D03 D04 M20 M29 M30

Technical Memorandums

Number	Entry
33-426, Vol. XI	R12
33-523, Vol. III	B04
33-603	P03
33-604	F02
33-606	O02
33-607	B02
33-608	G07
33-609	M10
33-610	S05
33-612	J09
33-613	L04
33-614	F06
33-615	S09
33-616	J10
33-619	R14
33-622	P09
33-623	W06
33-625	V01
33-627	L05

JPL Quarterly Technical Review, Vol. 3, No. 1

JPL Technical Division	Entry
290 Project Engineering	B03
340 Guidance and Control	B15
380 Propulsion	C10 F01
390 Mission Analysis	W01

Open Literature Reporting

Publication	Entry
AIAA J.	
Vol. 11, No. 1, pp. 12–13	P11
Vol. 11, No. 3, pp. 366–368	S02
AIAA/SAE Eighth Joint Propulsion Specialist Conference, New Orleans, Louisiana, November 29-December 1, 1972	
AIAA Preprint 72-1060	P05
AIAA Preprint 72-1185	C20
Am. J. Phys.	
Vol. 41, No. 3, pp. 435–436	V03
Anal. Chem.	
Vol. 45, No. 1, pp. 2–6	G10
Antarctic J. U.S.	
Vol. VII, No. 4, pp. 92–94	M23
Vol. VII, No. 4, pp. 94–96	B13
Vol. VII, No. 5, pp. 187–189	C05
Appl. Opt.	
Vol. 12, No. 2, pp. 359–363	T04
Vol. 12, No. 4, pp. 810–817	W09
Astronaut. Aeronaut.	
Vol. 10, No. 12, pp. 40–54	H09

Publication	Entry
Proceedings of the Third Lunar Science Conference (Supplement 3, Geochimica et Cosmochimica Acta)	
Vol. 2, pp. 2149–2155	R15
Progr. Astronaut. Aeronaut.	
Vol. 31, pp. 247–266	S23
Radio Sci.	
Vol. 8, No. 2, pp. 103–108	W14
Science	
Vol. 179, No. 4070, pp. 275–278	S12
Vol. 179, No. 4075, pp. 800–803	M19
Solar Energy	
Vol. 14, No. 2, pp. 203–211	W11
Space Life Sci.	
Vol. 3, No. 4, pp. 360–373	R16
Vol. 3, No. 4, pp. 415–418	R17
Space Sci. Rev.	
Vol. 14, No. 2, pp. 179–271	N01
Technometrics	
Vol. 15, No. 1, pp. 167–175	L26
The Moon	
Vol. 5, Nos. 3–4, pp. 348–367	J03
Trans. ASME, Ser. C: J. Heat Transf.	
Vol. 95, No. 1, pp. 85–92	B01

NASA — JPL — Coml., L.A., Calif.